ÇUKUROVA UNIVERSITY
INSTITUTE OF NATURAL AND APPLIED SCIENCES

PhD THESIS

Hudhaifa HAMZAH

INVESTIGATION OF NANOFLUID TRANSPORT IN A CORRUGATED CHANNEL UNDER PULSATING EFFECT

DEPARTMENT OF MECHANICAL ENGINEERING

ADANA-2021

ABSTRACT

PhD THESIS

INVESTIGATION OF NANOFLUID TRANSPORT IN A CORRUGATED CHANNEL UNDER PULSATING EFFECT

Hudhaifa HAMZAH

CUKUROVA UNIVERSITY
INSTITUTE OF NATURAL AND APPLIED SCIENCES
DEPARTMENT OF MECHANICAL ENGINEERING

Supervisor	: Prof. Dr. Beşir ŞAHİN
	Year: 2021, Pages: 135
Jury	: Prof. Dr. Beşir ŞAHİN
	: Prof. Dr. Hüseyin AKILLI
	: Prof. Dr. Ünal AKDAĞ
	: Prof. Dr. Coşkun ÖZALP
	: Assoc. Porf. Dr. Çetin CANPOLAT

The present research numerically illustrated the effect of pulsating turbulent flow and single-walled carbon nanotubes/water, SWCNT-H_2O nanofluid in a corrugated channel on hydrothermal characteristics and entropy production. Two various models for describing the flow of nanoparticles in a base fluid are applied. These models are homogeneous single-phase, SPM and Lagrangian-Eulerian model (or discrete phase model), DPM. This simulation covers the Reynolds number, pulsation frequency, phase shift, and nanoparticles concentration in the range of (for steady flow: $4000 \leq Re \leq 10000$ and for pulsating flow:$4000 \leq Re \leq 7000$), ($1 \leq f \leq 5$), ($0^o \leq \theta \leq 180^o$) and ($0\% \leq \varphi \leq 3\%$), respectively. CFD simulations show that the pulsation frequency, *f,* and phase shift, θ have a significant role in improving the heat transfer ratio and controlling the entropy generation through the wavy channel. Finally, it is recommended to use SWCNT/water nanofluid with a high volume fraction (φ=3%) as a working fluid in the considered channel due to its high heat transfer ratio and low thermal irreversibility.

Key Words: Entropy generation, Phase shifts, Phase models, Pulsating flow, SWCNT-water nanofluid, Wavy channel.

ÖZ

DOKTORA TEZİ

SALINIM ETKİSİ ALTINDA OLUKLU BİR KANALDA NANOAKIŞKAN TAŞINMASININ İNCELENMESİ

Hudhaifa HAMZAH

ÇUKUROVA UNİVERSİTESİ
FEN BİLİMLERİ ENSTİTÜSÜ
MAKİNA MÜHENDİSLİĞİ ANABİLİM DALI

Danışman : Prof. Dr. Beşir ŞAHİN
Yıl: 2021, Sayfa: 135
Jüri : Prof. Dr. Beşir ŞAHİN
: Prof. Dr. Hüseyin AKILLI
: Prof. Dr. Ünal AKDAĞ
: Prof. Dr. Coşkun ÖZALP
: Doç. Dr. Çetin CANPOLAT

Mevcut araştırma, sinüzoidal dalgalı bir kanalda türbülanslı salınmlı akışın ve tek duvarlı karbon-nanottüp-su (SWCNT-su) nanoakışkanının hidrotermal özellikler ve entropi üretimi üzerindeki etkisini sayısal olarak göstermiştir. Baz akışkan içerisindeki nano partiküllerin hareketini tanımlamak için iki farklı model uygulanmıştır. Bu modeller, Homojen tek-fazlı, TFM ve Lagrangian-Eulerian (veya ayrık faz model), AFM modellerdir. Bu simulsayon (sabit akış için: $4000 \leq Re \leq 10000$ ve salınımlı akış için: $4000 \leq Re \leq 7000$), ($1 \leq f \leq 5$), ($0^{o} \leq \theta \leq 180^{o}$) ve ($0\% \leq \varphi \leq 3\%$) aralığında sırsasıyla Reynolds sayısı, salınım frekansı, sinüzoidal duvarlar arasındaki faz açısı ve nanopartikül konsantrasyonunu kapsamaktadır. HAD simülasyonları, salınım frekansı, f ve fazaçısı, θ' nin, ısı transfer oranını iyileştirmede ve dalgalı kanal yoluyla entropi oluşumunu kontrol etmede önemli bir rolü olduğunu göstermektedir. Sonuç olarak, yüksek ısı transfer oranı ve düşük termal tersinmezliği nedeniyle, söz konusu kanalda çalışma akışkanı olarak yüksek hacim oranına (φ=%3) sahip SWCNT/su nanoakışkanının kullanılması tavsiye edilmektedir.

AnahtarKelimeler: Entropi üretimi, Faz modelleri, Salınımlı akış, SWCNT-su nano akışkanı, Dalgalı kanal.

EXTENDED ABSTRACT

Forced convection flow in a parallel-plate channel is a common configuration in the hydrothermal system due to its wide thermal engineering applications. Presently, energy management is an essential requirement for both environmental and economic reasons. Since most of the thermal energy in industrial processes passes through heated channels, their improvement has still needed. Researchers have employed a variety of methods to increase the rate of heat transfer in such channels. Among the different offered methods, channels with corrugated walls have confirmed their high performance. This is due to its ability to thin and destroy the thermal boundary layer adjacent to the walls and, consequently, improve thermal performance. On the other hand, pulsating flow is considered one of the efficient techniques for improving the flow mixing between the core flow and wake flow regions in these configurations. Further, replacing the traditional heat transfer fluid with nanofluids having a higher potential of thermophysical properties is another option for enhancing the heat transfer rate. These nanofluids are engineered colloidal dispersions of metallic or nonmetallic nano-scale particles in a host liquid. Moreover, the pulsating flow has the benefit of limiting the deposition of nanoparticles in the host liquid.

In the current thesis, combining these different strategies (wavy wall, nanofluid and pulsating flow) is applied to improve the heat transfer rate and reduce the entropy generation through the channel. Accordingly, the combination of wavy, nanofluid, and pulsating flow is expected to be a promising strategy for improving the heat transfer ratio and controlling the irreversibility production in compact heat exchangers. In particular, this thesis provides an overview of numerical studies in order to gain a clear understanding and detailed overview of the influence of several parameters, such as the type of solid-nanoparticle, working fluid particle, volume concentration, nanoparticle size, nanoparticle shape, Brownian diffusion and thermophoresis impact on heat transfer and fluid flow

characteristics of convective heat transfer using nanofluids. Additionally, the thesis provides detailed information on the most frequently used correlations that are used to predict the effective thermophysical properties of nanofluids. Therefore, this thesis was expanded for an extensive comparison between the homogenous phase model, SPM and discrete phase model, and DPM of nanofluid flow to find an appropriate CFD modeling that yields more precise outcomes. Since the two-phase approach takes the two-phase nature of the nanofluid flow into account, it can obtain more realistic results for modeling the convective heat transfer of nanofluids.

Numerical simulations were performed by solving nonlinear equations of the SPM and DPM that govern the flow domain through the wavy channel. The simulations are implemented to compute the influence of pulsation frequency, f, Reynolds number, Re and nanoparticles concentration, φ on heat transfer, fluid flow, and entropy production mechanisms for SWCNT-water nanofluid flow through a sinusoidal wavy channel having different phase shift, θ.

According to the literature survey, most of the published studies deal with the entropy generation analysis of pure fluid and/or nanofluid flow in thermal systems under constant inlet flow conditions. Also, CFD modeling of nanofluid as a single-phase is mainly associated with the pulsating flow in heated channels. Moreover, the combined influence of the pulsating inlet flow and wavy channel with different phase shifts on convective heat transfer has never been considered in the previous studies. In the current thesis, our goal is to investigate the impact of turbulent steady and pulsating flow on hydrothermal and entropy generation of SWCNT-water nanofluid in a wavy channel having different phase shifts using both homogenous single-phase, SPM and discrete phase model, DPM. Eventually, the combination of wavy, nanofluid, and pulsating flow is expected to be a hopeful strategy for improving the heat transfer ratio and controlling the irreversibility production in compact heat exchangers.

ACKNOWLEDGMENTS

Firstly, I would like to express my sincere gratitude to my supervisor Professor. Dr. Beşir ŞAHİN, for his support, encouragement, providing guidance and feedback throughout this research.

I would also like to express my thanks to all the Mechanical Engineering Department/ Çukurova University staff, especially the head of the department, Prof. Dr. Hüseyin AKILLI for their care and outstanding scientific performance during the period of my study.

Further, I would like to thank the following people who helped me with this research: Harun ZONTUL, Laith M. JASIM, Aboubaker Abdalla IBRAHIM and Fuad SARIGIGUZEL.

I am also grateful to the Research Projects Department of Cukurova University for funding under contract No: FDK-2018-6952.

Finally, I cannot forget to thank my family and friends for their unconditional support, patience and encouragement.

CONTENTS **PAGE**

LIST OF TABLESPAGE **PAGE**

LIST OF FIGURES PAGE **PAGE**

NOMENCLATURE

a	: Wave amplitude, m
A	: pulsation amplitude
Be	: Bejan number
C_p	: specific heat, J kg^{-1} K^{-1}
d	: nanoparticle diameter, m
D_H	: hydraulic diameter, m
E	: enhancement
f	: pulsation frequency
F	: body force, N
h	: heat transfer coefficient, W m^{-2} K^{-1}
G_κ	: creation of kinetic energy
G_ω	: creation of ω
H	: channel height, m
i, j	: components
k	: thermal conductivity, W m^{-1} K^{-1}
L_t	: total length of the heated test section, m
L_w	: wavelength, m
m	: mass, kg
n	: undulation number
N	: dimensionless of average entropy generation
N^*	: dimensionless of local entropy generation
Nu	: Nusselt number
p	: pressure, N m^{-2}
Pr	: Prandtl number
q''	: heat flux, W m^{-2}
Re	: Reynolds number

S : entropy generation, W K^{-1} m^{-3}

S_m, S_e : source and sink terms

S_T : dimensionless of total entropy generation

T : temperature, K

t : time, s

u, v : *x*-*y* velocity components, m s^{-1}

x, y : Cartesian coordinates, m

Greek symbols

α : thermal diffusivity, m^2 s^{-1}

δV : cell volume, m^3

Δp : pressure drop, N m^{-2}

θ : phase shift, degrees

κ : turbulent kinetic energy, m^2 s^{-2}

μ : dynamic viscosity, kg m^{-1} s^{-1}

μ_t : turbulent molecular viscosity

ν : kinematic viscosity, m^2 s^{-1}

ρ : density, kg m^{-3}

σ_κ : effective *Pr* for turbulent kinetic

σ_ω : effective *Pr* for the rate of dissipation

φ : particle volume fraction

ψ : non-dimensional stream function

ω : vorticity magnitude

ϖ : specific dissipation rate of turbulence kinetic energy, m^2 s^{-3}

Subscripts

avg : average

bf : base fluid

fr : *frictional*

nf : nanofluid

p : pulsating flow

P : nanoparticle

s : steady flow

th : thermal

XIX

1. INTRODUCTION

Energy and the environment have become issues of concern for the public industry. This is due to the rapid requirement in fossil fuel energy consumptions. For thise reason, more attention has been spent on improving energy-saving technologies to overcome the high energy demand in the past few decades. Heat exchangers are extensively utilized in many facilities in view of energy sustainability, recovery, generation, and transformation. Accordingly, it is evident that preparing more effective thermal exchanging systems can reduce energy anxieties appreciably. Since reducing energy consumption is a short-term solution, developed countries have developed some guidelines on energy saving and energy efficiency with the aim of saving energy both in industry and in local businesses.

Forced convection flow in a parallel-plate channel is a common configuration of the hydrothermal system due to its wide applications, e.g., heat exchangers, electronic equipment, domestic air conditioning systems, chemical reactors and so forth. Researches on thermal and hydrodynamic performance in channels that aim to provide better energy transport are one of the most common topics in terms of thermal applications. This issue has very substantially important from an energy conservation perspective. Presently, energy management is an essential requirement for both environmental and economic reasons. Since most of the thermal energy in industrial processes passes through heated channels, their improvement has still needed.

1.1. The increase of compact thermal systems

Enhancing the thermal transmission rate is the starting point for more compact heat exchangers, and thus is the key to successful thermal management for many industrial applications, e.g., power plants, solar heating systems, nuclear reactors and so on. Escalating the heat transfer coefficient of heat exchange units is essential for energy and material saving as well as space and size reductions. For these purposes, Numerous researchers (Shah & Sekuli, 2003; Webb, 1994) have suggested different approaches to increase the thermal transport rate and minimize component sizes of traditional heat exchangers. Basically, three different methods to improve the heat transfer coefficient have been identified: active, passive and compound. The active methods are complex and thus need an external source of power to improve the thermal-hydraulic performance. For example, applying magnetic source (Zontul et al.2021), rotating cylinder (Hudhaifa Hamzah et al., 2021; Jasim et al., 2021), rotary wheel (Nóbregaand Brum2009), pulsating flow (Akdag et al., 2014; Elshafei et al., 2008) and vibration pipe flow (Mitsuishi et al.2020) are common types of active methods utilized to increase the efficiency of thermal systems. Due to the extra costs included, active methods have attracted comparatively little concern in researches and practices. Regardless of the active technique, many investigators utilized passive methods to improve the efficiency of thermal systems. The passive method needs less effort toward improving the thermal-hydraulic performance, but it needs an extra small amount of energy to cover the pressure drop due to the geometrical modifies, leading to an increase in the required pumping power only. Consequently, passive methods in terms of energy-saving are more effective than active methods. The most prevalent examples of passive methods are inserting obstacles (Al-Kouz et al., 2018; Siavashi et al., 2018), swirl generators (Jafari et al. 2017), rough surfaces (A. Albojamal et al., 2017; H. Hamzah et al., 2020), porous structures (Feng et al., 2020; P. Hu & Li, 2020), coiled tubes (Janssen and Hoogendoorn, 1978; Naphon and Wongwises, 2006), change cross-section or direction of flow (Darr et al. 2016), and so forth. For instance, surface modification leads to enhance flow mixing between the thermal boundary layer adjacent to the surfaces and the core flow region and, accordingly, a high thermal transmission rate. Also, the enhancement of energy transport is accomplished by inserting extended baffles and/or fins due to increasing the turbulence within the flow domain. In spite of many investigations have shown the worthy impact of passive methods on heat transfer augmentation in previous years, but, this method has almost attained its limit. The compound method includes incorporations of active and passive methods with each other in the same system. A wall configuration with a magnetic source (Tashtoushand Al-Odat2004) or pulsating flow with a helically corrugated rib (Naphonand Wiriyasart 2018) is a simple example of this method.

Currently, accessible working liquids, including water, ethylene glycol (EG), and engine oil, are extensively utilized in several practical applications. These traditional thermal liquids have immanently low thermal conductivity as contrasted with solids. Consequently, there is an obvious requirement to modify substitutional thermal liquids with better cooling or heating capacity which leads to enhance efficiency and compactness of thermal systems.

1.2. Nanofluids

Many types of heat exchanging systems offering various levels of thermal efficiency; their primary function is to transfer heat at a low financial cost. To achieve the optimum operation of these systems, a working fluid with higher thermal conductivity is needed. Due to the high thermal conductivity of solid particles, energy transport can passively be improved by suspending these particles into the working fluids, which results in increasing the thermal conductivity of the entire mixture. Based on this concept, the suspension of metallic particles with micrometer dimensions into the liquids was coined by Maxwell J.C. (1873), theoretically to show the capability of improving the thermal conductivity of the entire mixture. Subsequently, the addition of polystyrene spheres with micrometer dimensions to the glycerine (as the host liquid) was experimentally investigated by (Ahuja, 1975). He detected that the thermal conductivity of the mixture increased by 300% as compared to glycerine. Despite this, issues like quick deposition, plugging, erosion, as well as high-pressure drop due to the existence of these micrometer-scale particles have restrained this technique far from workable usage.

Over the past two decades, nanotechnology is progressively viewed as a feasible strategy to eliminate the risk of energy shortage. In this regard, researchers have been actively pursuing many ways in which nanotechnology can significantly improve the efficiency of standing heat transfer systems. Therefore, developments of nanotechnology in the heat transfer field showed that the suspension of nano-sized particles (usually <100 nm) in a base fluid leads to generating a stable mixture defined as nanofluids. The phenomenon of nanofluids was first prepared by (Choi, 1995). Nanofluid is a promising strategy for all systems contained heat transfer fluid and is also the key to successful thermal management due to the following properties:

- Large heat transfer area between nano-scale particles and base fluid and thus remarkably increases the thermal capacity of nanofluid.
- High suspension stability with prevalent Brownian motion of nanoparticles.
- High optical properties as compared to base fluid and thus appear low emission and high absorption in solar systems.
- Various kinds of including metallic or non-metallic nanoparticles can be suspended in base fluids to compose nanofluids.
- Adaptable characteristics, such as thermal conductivity, density, surface wettability and viscosity, by changing solid volume fractions of nanoparticles to adjust various applications.
- Generally, nanofluids have high thermal conductivity, high density as well as high viscosity with low thermal expansion coefficient and low specific heat, thus increasing efficiency and also the pressure drop of thermal systems.
- Micro-sized particles resort to aggregate and settle quickly, while nano-sized particles can stay dispersed in host liquids for a longer period of time.

- Minimizing clogging and erosion as compared with micro-sized particles, so proper for utilizing in micro-channels.

Nanofluid usage was made great progress in improving the heat transfer rates for many engineering applications, e.g., reactor-heat exchanger (Fan et al., 2008), cooling and heating devices (Kulkarni et al., 2009), solar collectors (Taylor et al., 2011), solar stills (Gnanadason et al., 2012), energy storage tank (Thirugnanasambandam et al., 2010), refrigerator devices (Bi et al., 2008), engine cooling system (Bai et al., 2008), automobile radiator (Zafar Said et al., 2019), hydraulic braking system (Popa et al., 2010), cooling of automatic transmission (Tzeng et al., 2005), microelectronic components (Tsai et al., 2004), magnetic sealing (Kim & Kim, 2003), optical filters (Philip et al., 2003), medical applications (Jalal et al., 2010), nuclear reactors (Boungiorno et al., 2008), plasma charging arc system (Kao et al., 2007), lubricating mechanism (J. Zhou et al., 2000), grinding process of cast iron (Shen et al., 2008) and so forth. For more detailed information on nanofluid applications, see the following references (Devendiran & Amirtham, 2016; Saidur et al., 2011).

1.3. Nanofluid models

1.3.1. Single-phase model

The single-phase model is considered that the nano-scale particles can be simply diluted, and accordingly, the numerical simulations of this model are; generally based on the assumed effective thermophysical properties. Moreover, this approach supposes that both the host liquid and solid nanoparticles are in a thermal equilibrium state and they have equal velocities. This model is modest and demands less computational time. For this reason, it has been extensively employed in various numerical investigations for forced convective heat transfer of nanofluids.

1.3.2. Two-phase model

In general, nanofluids are inherently biphasic fluids; thus, they can be expected to have specific characteristics of a solid-liquid mixture. Therefore, the classic two-phase flow theory has been carried out for various types of nanofluids. For the two-phase method, the solid particles and the host liquid are assumed to be two various phases with various thermal characteristics and velocities. In other words, it cannot be assumed that the slip velocity between the liquid and nanoparticles is equal to zero. This is due to the set of forces acting on solid particles by the host fluids, particle deposition and suspension. Such forces include drag, lift, gravity, Brownian, friction and thermophoretic. Since the two-phase model takes into account the motion between particle and liquid molecules, it can obtain real results. In spite, this model explains the conception of the roles of each phase within the thermal operation, but it requires longer computational time than the single-phase model.

2. LITERATURE SURVEY

2.1. Effective factors of nanofluid

According to the publications, there are various factors that can directly affect the thermal properties of nanofluids. The most important of these factors are the kind of nano-scale particle and base fluid, nanoparticle volume concentration as well as nanoparticle size and geometry. This section provides detailed information about the impact of these factors on the thermophysical properties of nanofluids.

2.1.1. Effect of nanoparticle type and base fluid

As mentioned earlier, nanofluids exhibited higher thermal properties than conventional fluids. This is due to the high thermal conductivity of the suspended nanoparticles and also the relatively low thermal conductivity of conventional fluids. Figure 2.1 and Figure 2.2 show different kinds of base fluids and nanoparticles, respectively, which are often used by researchers in preparing nanofluids. Sivakumar et al., (2016) experimentally modeled the forced convection flow for two different water nanofluids through the serpentine microchannel heat sink. They considered Al_2O_3 and CuO as the nanoparticles. The results show that homogeneously suspended and stabilized nano-sized particles remarkably increase the heat transfer performance of the host liquid. Further, the experimental data deduced that CuO-water nanofluid has a higher forced convective thermal coefficient than Al_2O_3-water nanofluid. Roslan et al., (2012) numerically studied the hydrothermal representation of different types of water nanofluids comprising Ag, Cu, Al_2O_3 or TiO_2 nano-sized particles in a container with a rotating cylinder. They resulted that the Ag-water nanofluid with higher thermal conductivity has the maximum thermal performance between all nano-sized particles examined in this work. Natural convection hydrothermal of nanofluids within the trapezoidal enclosure was numerically investigated by Saleh et al., (2011). Al_2O_3 and Cu nano-scale particles mixed with pure water were utilized as flowing fluids. They reported that the mixing of nanoparticles with conventional liquids was successfully used as a passive control technique of heat transfer increment. Moreover, they found that using nanofluids greatly effects both flow and temperature distributions, especially for high Rayleigh numbers.

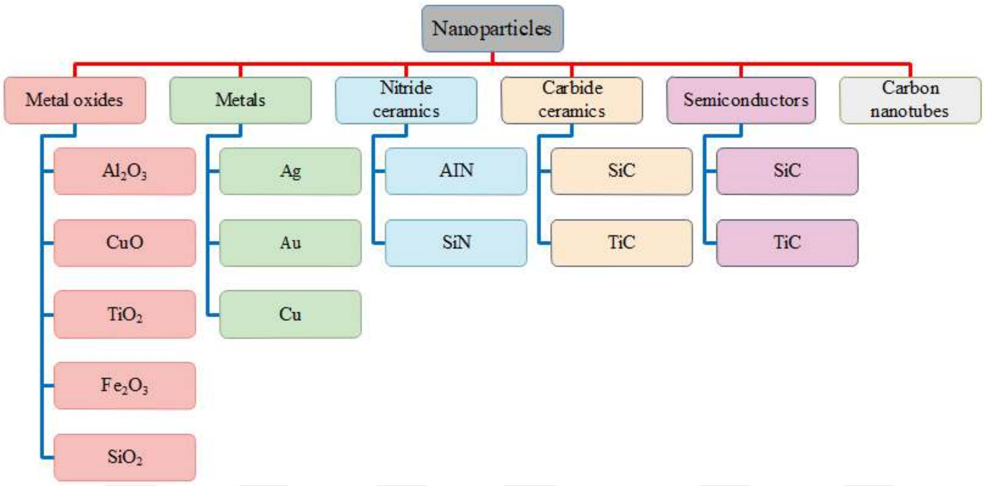

Figure 2.1. Common types of nanofluids.

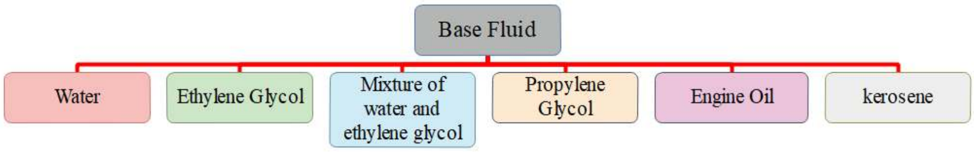

Figure 2.2. Common types of base fluids.

On the other hand, many researchers reported that the heat transfer capacity of nanofluids is also dependent on the type of host liquid due to their different thermal conductivity. Hwang et al., (2006) declared that the thermal conductivity enhancement of nanofluids containing CuO nanoparticles suspended in distilled water and ethylene glycol are 3% and 9%, respectively. The theoretical and numerical investigation has been accomplished to estimate the forced convection heat flow of nanofluids through a uniform heated tube by Maïga et al., (2004). The numerical simulations were implemented for both laminar and turbulent flow regions. Two different types of base fluids, water and ethylene glycol, which containing Al_2O_3 nanoparticles with various volume concentrations within the range of (1-10%) were considered as flowing fluids. The researchers detected better heat transfer enhancements by using ethylene glycol as a host fluid rather than distilled water. This enhancement was more declared with the increment of the volume concentration of Al_2O_3 nanoparticles as well as Reynolds's number. In addition, for both laminar and turbulent regions, each of the considered nanofluids has a higher forced convective thermal coefficient than their host liquids.

Moreover, it has been declared that the utilize of nanofluids with two or three different types of nanoparticle provides a considerable increase in heat transfer over their host liquids, mainly due to the high thermal conductivity of nanoparticles, as outlined in (Dhinesh Kumar & Valan Arasu, 2018; Leong et al., 2017). This new concept of preparing nanofluids is known as hybrid nanofluids. Minea, (2017) numerically analyzed turbulent forced convection flow in a three-dimensional tube under a uniform heat flux of thermal condition. Considering the homogenous single-phase approach, the comparison between the nanofluids and their hybrids as well as base fluid was executed based on three different types of solid oxide nanoparticles (Al_2O_3, TiO_2 and SiO_2). Among 18 different concentration of studied nanofluids, the results declared that the suspending of 2.5% Al_2O_3 and 1.5% SiO_2 in a host fluid gives the maximum heat transfer augmentation of 241% as compared with pure water, while the minimum augmentation in heat transfer was recorded as 4% for 3% Al_2O_3.

2.1.2. Effect of nanoparticle volume fraction

Among the other parameters, volume fraction, also known as volume concentration, is classified as the most effective parameter on the thermal properties of nanofluid. It can be explained as the volume ratio of solid particles to that of the whole mixture, and it is expressed as follows:

$$\varphi = \frac{m_p/\rho_p}{m_p/\rho_p + m_{bf}/\rho_{bf}} \times 100 \qquad (2.1)$$

Generally, studies have acknowledged that as the nano-scale particle volume concentration increases, the heat transfer performance increase. When the solid volume fraction is increased, the whole thermal properties of the mixture were enhanced, Brownian motion and transmigration of nano-scale particles related to the higher volume concentration are the essential causes behind the heat transfer enhancement M'hamed et al., (2016). Anoop et al., (2009)andWen et al., (2004) have both proposed an experimental investigation to analyze the laminar forced convection flow of Al_2O_3-water nanofluid in a heated tube. Overall, they declared that the enhancement of thermal transmission always coincides with using nanofluids. Distinctively, the reinforcement impact of the thermal transmission is improved with rising the volume fraction of nanoparticles, particularly at the inlet zone. The energy transport enhancement of circular heated tubes loaded with Al_2O_3-water nanofluids was examined numerically for both laminar and turbulent flow by the same authors in (V. Bianco et al., 2009) and (Vincenzo Bianco et al., 2011), respectively. The coupling between solid and liquid phases was performed for the homogeneous single-phase model and different two-phase models, namely mixture and discrete phase. Their outcomes declared that the increment in volume fraction is an essential source for improving the heat transfer coefficient; however, it is escorted by growing the magnitudes of wall shear stress. Demir et al., (2011) numerically evaluated the forced convective flow for two types of water nanofluids including TiO_2 and Al_2O_3 nano-scale particles in a heated double-tube. Their numerical results demonstrated that suspend nanoparticles improved the forced convective flow of the pure water remarkably, even for comparatively small concentrations of nanoparticles. Further, they concluded that higher particle concentrations in the base fluid result in higher thermal transmission rate and also result in a higher pressure drop. Consequently, a wise determination should be possessed when choosing a nanoparticle concentration that makes balances between enhanced thermal transmission and the side effect of pressure drop.

Influences of volume concentration on the surface tension of nanofluids were reviewed by Khaleduzzaman et al., (2013). Despite some contrasting findings, they concluded that the surface tension of most nanofluids increases proportionally as volume concentration increases. Also, they found that there is no available model or correlation that can predict the accurate surface tension improvement or deviation relative to volume concentrations. A numerical simulation to investigate the impacts of Al_2O_3 nanoparticles volume fraction which mixed with water on the hydrothermal of developed mixed convection flow through a turned tube was proposed in (Akbarinia and Behzadmehr, 2007). For the same operating condition, they reported that the increase in nanoparticle concentration has no obvious influence on velocity vectors and isothermal lines.

The thermal performance of TiO_2-water nanofluid in a circular tube was experimentally examined by Sajadi and Kazemi, (2011). They realized that an increase in the volume fraction of solid particles did not affect the enhancement of heat transfer over the turbulent flow range. In addition, they provided a new correlation for predicting the Nusselt number in terms of Reynolds and Prandtl numbers for all the considered concentrations of TiO_2 rely on the experimental results.

For the free convection flow, the effects of nanofluid concentrations on the thermal-hydraulic performance in square and non-square cavities have been profusely studied by many investigators numerically (Abu-Nada et al., 2010; Abu-Nada & Oztop, 2009; Haddad et al., 2012; Khanafer et al., 2003; Oztop & Abu-Nada, 2008; M. Sheikholeslami & Ellahi, 2015). As a common result of these works, it was found that the heat transfer enhancement occurs with the presence of solid nano-scale particles and this enhancement rises with increasing particle concentrations. On the contrary, some experimental studies have observed that there is no increase in free convection flow by increasing nanoparticle concentrations (Ho et al., 2010; Wen & Ding, 2005, 2006). Ignoring the slip velocity among liquids and solid particles in numerical simulations is the main source for this discrepancy between experiment and numerical investigations.

It is worth mentioning that both viscosity and density are the corresponding parameters of nanofluids to the nanoparticle concentration. As a result, large amounts of nanoparticle concentration can significantly affect the pressure drop and limits their use in thermal devices that are operating under restricted pumping energy conditions.

2.1.3. Effect of nanoparticle size

Nanoparticle size is another crucial factor affecting the flow and thermal mechanisms of nanofluids. Experimental findings showed an increase in thermal conductivity, typically with a reduction in nanoparticle size (Beck et al., 2009; Chon et al., 2005; Mintsa et al., 2009). Hemmat Esfe and Saedodin, (2015) investigated the impact of various nanoparticles size of Mgo–water nanofluid in a smooth circular pipe under a turbulent flow regime empirically. It was revealed that the smallest nanoparticles size has the highest thermal conductivity and, accordingly, the Nusselt number. In another empirical examination, Y. Hu et al., (2017) implemented experiments on the boiling heat transfer coefficient of SiO_2 nanofluid considering different nanoparticle diameters. It was found that the boiling performance of nanofluid was enhanced by reducing the nanoparticle diameter. The same flow regime was experimentally implemented by Abbasian Arani and Amani, (2013) through the double tube heat exchanger using TiO_2–water nanofluid. They examined the influence of the average diameter of TiO_2 particles ranging from 10 nm to 50 nm. The experimental results detected that the nanofluid with a nanoparticle diameter of 20 nm gives a higher heat transfer rate than other tested dimensions. For Reynolds number greater than $12x10^3$, they found that the pressure drop alters by varying the particle size, But it does not change notably for a lower Reynolds number.

Numerous numerical simulations have been done to analyze nanofluids hydrothermal behaviors where the influence of nanoparticles size is considered. Moraveji et al., (2011) acquired good conformity between the numerical simulation and experimental results under the laminar regime ranges for Al_2O_3-water nanofluid with various concentrations and two mean particle diameters of 45 nm and 150 nm. Based on the CFD analysis, Ebrahimnia-Bajestan et al., (2011) confirmed the relevance between nanoparticle size and thermal performance which was experimentally achieved in Anoop et al., (2009). Kalteh et al., (2012) reported that the improvement in energy transport as a result of the reduction in nanoparticle diameter is not clearly declared particularly for low solid volume fractions. As mentioned in the work of (Tahir and Mital, 2012) by considering the nanoparticle size, nanoparticle concentration, and the Reynolds number revealed that the Nusselt number has a non-linear relationship with the particle diameter. The CFD simulation by Mirmasoumi and Behzadmehr, (2008) solved the mixed convection problem of alumina-water nanofluid through a straight tube taking into account nanoparticle size influence. It has been found that the changing of the average nanoparticle diameter does not remarkably alter the hydrodynamics mechanisms. Fani et al., (2013) presented a numerical analysis on a microchannel-heat-sink with trapezoidal shape for electronic cooling applications considering the impact of the nanoparticle diameter. They observed that by raising solid volume fraction, the impact of nanoparticle diameter becomes more pronounced. In addition, it was determined that the augmentation in the pressure drop rate was concentrated for nanoparticles diameter greater than 150 nm. Contrary to the pressure drop, energy transport diminishes with an increment in nanoparticle size. Additionally, it was stated that by detecting the optimum diameter of nanoparticles, the highest heat transfer coefficient and lowest pumping power could be achieved. Shariat et al., (2014) studied the transport of alumina nanoparticles dispersed in water with four various values of diameter from 13 nm to 72 nm in laminar mixed convection through the elliptical duct numerically. Their numerical predictions reported that the diameter of particles has a great impact on the Nusselt number but slightly affecting the friction coefficient.

2.1.4. Effect of nanoparticle shape

Although the most commonly used geometric shape of particles is spherical, many investigators have announced the significant impact of the alternative types of nanoparticle shape. As elucidated in refs. (S M S Murshed et al., 2005; Xie et al., 2002), the cylindrical shape of nanoparticles provides the higher thermal conductivity of nanofluids because of the extended surface area of this shape. Timofeeva et al., (2009) declared that the most affected properties of nanofluid with its nanoparticle shape is viscosity. Furthermore, to obtain the low viscosity of nanofluid, it has been recommended to utilize nanoparticles with a minimum aspect ratio (surface area to volume).

In accordance with the reality that the shape of nanoparticles can have a profound effect on the properties of nanofluids, various studies have been looked at the influences of this factor on the thermal behavior in systems using nanofluids. Vanaki et al., (2014) examined the impact of the different SiO_2 nanoparticle shapes and host fluids on the thermal transmission rate and skin friction coefficient in a wavy channel based on the 2-D numerical simulation. The results revealed that the SiO_2-Ethylene glycol nanofluid with platelet nanoparticles shape has the highest thermal transmission rate compared to water-based fluid and other examined nanoparticle shapes while the skin fraction coefficient is independent of nanoparticle shapes. Bahiraei et al., (2020) examined the thermal entropy production characteristics of nanofluid through the hexagonal microchannel cooler, taking into account the various nano-scale particle shapes. It was concluded that the nanofluids containing nanoparticles with oblate spheroid and platelet shapes indicate the largest and smallest quantities of entropy production, respectively. Further, the nanofluid with cylindrical nanoparticles is not effective in reducing frictional entropy production. Abdelmalek et al., (2020) evaluated the impacts of

Cu-water nanofluid with different shape factors of the particle within a cold cavity where a hot wavy circular was located in its center. They declared that the effect of particle volume fractions on the Nusselt number has been shown to be more important than their shapes. Sheikholeslami, (2017) inspected the augmentation in the heat transfer coefficient within a porous container in view of varied nanoparticle shapes. The results revealed that the nanoparticle having the platelet shape had the highest augmentation in heat transfer. Ooi and Popov, (2013) analyzed the impact of copper nanoparticle's shape on the convective thermal transmission rate within the square enclosure numerically. They adapted the radial basis integral equation approach to find the numerical solution. Their findings indicated that the changing nanoparticle shapes clearly impact the magnitude of the thermal transmission rate of the nanofluid.

2.2. Thermophysical properties of nanofluid

Generally, the main goal of studying the properties of nanofluids is to improve their overall or individual properties as much as conceivable, taking into account the requirements of the system. Moreover, the thermophysical properties of nanofluids have an essential role in modeling since they strongly influence the simulation results. The most common properties are density, ρ, specific heat, C_p, dynamic viscosity, μ and thermal conductivity, k. In numerical modeling, it is difficult to specify the convenient model for each property of nanofluids, which can exactly match the available experimental data. Numerous theoretical investigations and experimental measurements have been performed and introduced by investigators for the prediction of nanofluids models. Yet, the physical parameters of nanofluids are still a subject of controversy due to their variety and complexity.

2.2.1. Density

In most researches, the density of nanofluid is specified by employing the classical mixing relationship between host liquids and solid materials (Drew, 1973; Pak and Cho, 1998) which can be expressed theoretically as:

$$\rho_{nf} = (1-\varphi)\rho_{bf} + \varphi\rho_{np} \tag{2.2}$$

As a result of the shortage of experimental information, the density of nanofluids in the open literature was assumed to be a linear function of solid particle concentration with the exception of its temperature dependence.

One of the initial studies that used Eq. (2.2) for predicting the density of nanofluids was offered by Pak and Cho, (1998). Their experimental measurements were conducted in a circular pipe under the room temperature condition for Al_2O_3 and TiO_2-water nanofluids with particle weight fractions changed up to 4.5%. Pastoriza-Gallego et al., (2009) experimentally examined the density of Al_2O_3 nano-scale particles suspended in distilled water with solid volume fractions of 0.5-7% for various particle sizes. Three different temperatures ranging from 283.15 to 313.15 K were applied for measuring this property of nanofluid. They showed that smaller nanoparticles have a more pronounced effect on the volumetric manner. The effective density augments proportionally with the nanoparticle weight fractions. Moreover, the deviation of the measured nanofluid density from the Eq. (2.2) was increased as the particle load increased. Teng & Hung, (2014) declared the same notifications of a decrease in the effective density of nanofluids with volume fraction. Andrew and Kirk, (2009) tested the density for Al_2O_3 particles dispersed in water at 25 ^{o}C utilizing two different techniques. In the first technique, a mass balance concept was used to evaluate the effective density of the mixture. In the second technique, a hydrometer device was employed. Measured data from these techniques were compared and an approximately linear relationship was detected between the effective density and solid volume fraction.

Wong et al., (2018) offered a crucial compilation for the thermophysical characteristics of nanofluids. They derived a correlation for the evaluation of alumina nanofluid density using the experimental results provided by Ho et al., (2010). Both particle concentration and temperature impacts were taking into account. The developed correlation can be represented as:

$$\rho_{nf} = 1001.064 + 2738.6191\varphi_{np} - 0.2095T_{nf} \tag{2.3}$$

The validity of the above correlation is varied for the volume fraction from 0% to 4% over a temperature range of 5 ^{o}C ≤ T_{nf}≤ 40 ^{o}C. Eq. (2.3) was in excellent agreement with the reported experimental data in Ref. (Said et al., 2013). In comparison with Eq. (2.2), a maximum deviation of 0.6% was observed. Therefore, Eq. (2.2) can be employed to estimate the density of different types of nanofluids.

According to the authors' knowledge, there is no correlation for the nanofluid density taking into account the effects of nanofluids type, particle shape and particle diameter. Therefore, it is necessary to develop a new correlation based on these factors to obtain an accurate density value.

2.2.2. Specific heat

The specific heat capacity of nanofluid is considered to be a proportional function of the solid particle concentration when mixtures of host liquids and solid materials are in a state of thermal equilibrium. Therefore, it can be represented by the following classical mixture equation as announced in Refs. (Das et al., 2007; Maïga et al., 2004; Pak and Cho, 1998; Palm et al., 2006):

$$\left(C_p\right)_{nf} = (1-\varphi)\left(C_p\right)_{bf} + \varphi\left(C_p\right)_{np} \tag{2.4}$$

Other researchers propose a substitutional model based on the theory of heat capacity (Eastman et al., 1999; Xuan and Roetzel, 2000):

$$\left(\rho C_p\right)_{nf} = (1-\varphi)\left(\rho C_p\right)_{bf} + \varphi\left(\rho C_p\right)_{np} \tag{2.5}$$

The above two equations can, of course, have different outcomes for the specific heat of nanofluid. Very limited works are existence on the experimental measurements of nanofluids specific heat. Therefore, both equations have been considered equivalently and used excessively in nanofluid researches. Wong et al., (2018) compared the specific heat values of alumina- water nanofluid utilizing both models with experimental results presented by Zhou and Ni, (2008) for different particle concentrations range 0-21.6%. They found that the model given in Eq. (2.5) shows more consistency with the experimental data than the other model given in Eq. (2.4). Further, the variation in the specific heat determination utilizing these models is less than 10% for alumina-water nanofluid flowing through a heated pipe as reported by Bianco et al., (2009). Some empirical models for nanofluids specific heat are available in open literature published by Refs.(Sekhar and Sharma, 2015; Vajjha and Das, 2009; Yiamsawasd et al., 2012).

Wang et al., (2006) theoretically studied the influence of particle size and temperature on the specific heat for CuO nanoparticles. Their results showed that the proposed theoretical model was compatible with the corresponding experimental data. Yang et al., (2008) applied the mechanic's molecular technique for examining the specific heat capacity of carbon nanotubes(CNTs). They found that the measured specific heat capacity has a fixed value for the specified temperature and approximately independent of the particle geometry of the (CNTs).

Robertis et al., (2012) applied the temperature Modulated DSC (TM-DSC) mechanism for determining the specific heat of their prepared nanofluids (Cu-EG).

Their findings revealed that the mixing of Cu particles with pure ethylene glycol minimizes the specific heat and changes the melting and crystallization features of the nanofluids. Further, the (TM-DSC) method showed an excellent agreement between experimental data and calculated values from Eq. (2.5) for Cu-EG nanofluids within the entire investigated temperature limit, indicating that the Eq.(2.5) is an accurate model for determining the specific heat of nanofluids. Saeedinia et al., (2012) experimentally examined the specific heat values of oil-based CuO nanofluid with the augmentation in copper oxide nanoparticles concentration from 0.2 to 2% at various temperatures. In their experiment, the specific heat of nanofluid is lower than the host liquid values, and it reduces as the particle weight fraction increases. The finding revealed that the decrement in specific heat value of CuO-oil nanofluid with the solid particles concentration of 2% at 40 ^{o}C was up to 22%. Another experimental data of Al_2O_3-water revealed a reduction in the specific heat value of 14% in the volume fraction range between 0 and 3.6% at room temperature as reported by Barbés et al., (2014). As declared by Hanley et al., (2011) the values of specific heat of Al_2O_3-water, CuO-water, and SiO_2-water nanofluids with the particle size of 50, 30 and 32 nm, respectively increased with the temperature of nanofluids. More details for estimating specific heat of nanofluids can be realized in a comparative review paper of Shahrul et al., (2014).

Although the specific heat of nanofluids depends on the particle morphology, nanofluid temperature and nanoparticle concentration, virtually no general correlation combined these influencing factors. In addition, it is necessary to establish standardized correlations for computing the specific heat capacity of nanofluids by considering all possible factors affecting the hydrothermal mechanisms of nanofluids.

2.2.3. Thermal conductivity

Thermal conductivity plays a vital role in calculating the thermal performance of nanofluids. In contrast to density and specific heat, several studies on nanofluid thermal conductivity considered the influences of multiple factors such as nanoparticle morphology, weight fraction, particles and host liquids properties and mixture temperature. Numerous studies have explained that nanofluids thermal conductivity increases linearly with nanoparticle concentration (Beck et al., 2009; Kleinstreuer and Feng, 2011; Mintsa et al., 2009; Oh et al., 2008) as well as temperature (Abdolbaqi et al., 2016; Mintsa et al., 2009; Murshed et al., 2008), while some investigations have announced an asymmetric relationship between them (Bobbo et al., 2011; Wang et al., 2002). In addition, studies that take into account the effect of particle morphology (shape and diameter) and host liquid characteristics on the thermal conductivity of nanofluids have shown that there is a nonlinear relationship between them (Ambreen and Kim, 2018; Chon et al., 2005; Prasher et al., 2006; Wang et al., 2002).

The earliest model of thermal conductivity arose by Maxwell's (James Clerk, 2010) where it was suggested for solid-liquid suspensions. This model is limited to the spherical shape of particles, and it has been widely applied by investigators in published literature (Hassani et al., 2015; Minea, 2014; Nada, 2009; Yarmand et al., 2014). Maxwell's model can be represented as:

$$k_{nf} = \frac{k_{np}+2k_{bf}+2\varphi(k_{np}-k_{bf})}{k_{np}+2k_{bf}-\varphi(k_{np}-k_{bf})} k_{bf} \tag{2.6}$$

It is worthy of mentioning that the validity of the aforesaid models is limited to micro and milli-scale suspensions. Moreover, these classical models lead to underestimating the thermal conductivity value in comparison with experimental results, probably because these models involve only the influence of nano-scale particle concentration. To overcome these differences, many efforts have been made to expand or update the classical models, taking into account the factors that have the greatest impact on solid-liquid dispersions. Figure2.3 summarizes the effects of certain factors proposed by various researchers on the thermal conductivity of nanofluids. Therefore, researchers have been encouraged to modify additional theoretical models to evaluate the thermal conductivity of nanofluids by including these factors. For example, the developed models by Yu and Choi., (2009), Xuan et al., (2011), and Wang et al., (2012) considered the influence of the following factors: nanolayer formation around the nanoparticle surface, aggregation and Brownian motion, temperature, and particle diameter as well as Brownian motion, adsorption and particle size, respectively. Most authors have modified their models based on their experimental results. A summary of the models used by several researchers to characterize the thermal conductivity of nanofluids in numerical modeling is introduced in a review article published by Vanaki et al., (2016). Moreover, it is worth mentioning that several empirical correlations to evaluate thermal conductivity have been derived by many authors based on their experimental results, but these are related to certain types of nanofluid examined.

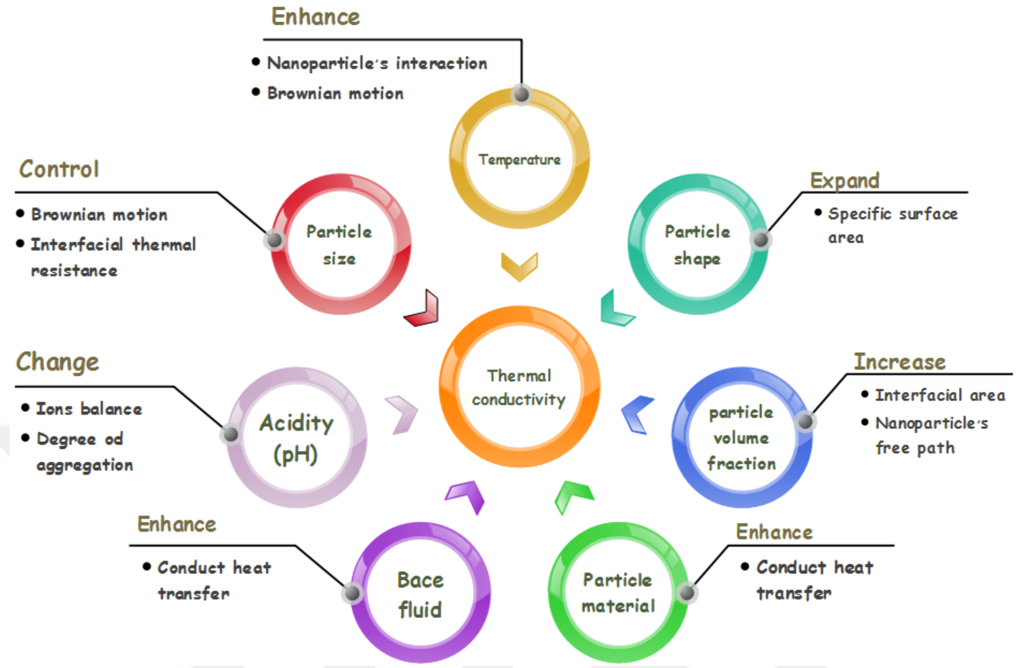

Figure 2.3. Effective factors on thermal conductivity.

Minea, (2017) numerically simulated the influence of utilizing three various models for estimating the thermal conductivity of Al_2O_3-water nanofluid on forced convection flow through heated tubes. These models are presented by Maxwell, (1981), Maïga et al., (2005) and Yu and Choi, (2003). In comparison between these three correlation models, the author's results revealed that the proposed correlation in Ref. (Labib et al., 2013) showed the largest augment in heat transfer coefficient values, while the other two correlations provide similar outcomes. Bianco et al., (2009) performed a numerical investigation to test forced convection of nanofluids containing alumina particles in circular tubes utilizing two different correlations for determining thermal conductivity. The first correlation considered the experimental data given by Maiga et al., (2005). The second correlation involved the experimental data available in Bianco et al., (2009) by considering temperature-dependent properties. It was reported that the second correlation gives a higher rate of thermal transport in comparison with the first correlation that is independent of temperature. Thermal conductivity models of Khanafer and Vafai, (2008) with constant and variable properties were adapted by Albojamal et al., (2017) to study the numerical simulation of Al_2O_3-H_2O and CuO-H_2O nanofluids flowing in a wavy channel. It was observed that the variation between the dependent and independent temperature models becomes insubstantial within the wavy channel as a result of the existence of prominent mixing regions adjacent to the wavy wall.

So far, researchers are far from realizing a universal model of thermal conductivity that can take into account all the relevant influencing factors to predict this property of nanofluids accurately.

2.2.4. Viscosity

Viscosity is another potential property that characterizing the thermal-hydraulic performance of nanofluids. The viscosity of base liquids generally increases with a suspension of solid particles. Within the past two decades, numerous studies on nanofluid viscosity have shown inconsistencies and dissipating of data. Like thermal conductivity, the earliest considered models are based on the dispersion theory of larger than nano-scale particles with a spherical shape.

In the numerical simulation of nanofluid convective heat transfer within a triangular cavity having corrugated walls, Nasrın et al., (2004), employed two models for predicting nanofluid viscosity. With changing nanoparticle concentrations, the Nusselt number value utilizing the proposed model by Pak and Cho, (2007) was always greater than the other model presented by Brinkman, (1981). The same models were implemented in the numerical study conducted by Chamkha et al., (2007) for mixed convective flow within a container using another type of nanofluids.

2.3. Comparison between single- and two-phase models

Two approaches (single and two-phase models) can be used to model the flow of nanofluids. Homogeneous (SPM) and thermal dispersion are the main types of single-phase approach, whereas mixture, Eulerian, the volume of fluid (VOF), and discrete phase model (DPM) are the main types of two-phase approach. The SPM is one of the most commonly utilized approaches in most CFD simulations. Nevertheless, the CFD predictions produced by this approach may lead to some discrepancies in comparison with the experimental data as stated by Mahian et al., (2019). These discrepancies are associated with ignoring the slip conditions between solid nanoparticles and the host liquid. The use of two-phase models in investigations of forced convection could enhance the results mainly by taking into account the influence of forces acting on the motion of nanoparticles in a host liquid (Albojamal and Vafai, 2017).

In comparison with the experimental data, Behzadmehr et al., (2007) performed a numerical simulation of nanofluid flowing in a heated tube under turbulent flow regimes. They confirmed that the outcomes of the two-phase mixture approach versus the single-phase are more credible and nearer to the experimental data published by Li & Xuan, (2003). Bianco et al., (2009) carried out a CFD simulation of water-alumina nanofluid flow through a circular heated tube under developed laminar forced convection (Re<1200). They employed SPM and DPM for modeling nanofluids with either dependent- or independent-temperature properties. The researchers detected that the maximum deviation of the average heat transfer rate between these models is about 11% for high nanoparticle concentrations and variable thermal properties. A CFD simulation on fully developed laminar and turbulent forced convection of water-alumina nanofluid inside a straight heated tube was implemented by Onyiriuka et al., (2018). SPM, mixture, DPM and combined of DPM and mixture were used to model the nanofluid in their research. Their numerical predictions showed that the average deviation between DPM and SPM was less than 2% for turbulent flow, while about

4.25% for laminar flow. Lotfi et al., (2010) tested the reliability of homogenous single-phase, SPM and two different types of two-phase approaches to evaluate the experimental results for nanofluid flow subjected to the laminar regime. They detected significant variances when employing a single-phase model against two-phase models. Albojamal et al., (2017) simulated and compared the forced convection of alumina-water nanofluids inside a channel having sinusoidal walls under laminar flow conditions. Four modeling concepts were used: (homogeneous and dispersion) as single-phase approaches and (DPM and mixture) as two-phase approaches. The results stated by the authors showed that both the homogeneous and DPM approaches could be counted as accurate methods and more reliable when modeling nanofluids as compared with other approaches.

Table 2.1 summarizes the comparison between single-phase and two-phase models, providing the author's name, geometry configuration, flow regime, phase model, nanofluid type, problem parameters, and findings. Further, a comprehensive comparison study by Vanaki et al., (2016) Provides more details about the forced convection flow of nanofluids in heated channels.

Table 2.1. Comparison between single-phase and two-phase models

Authors	Geometry and Flow regime	Nanofluid model	Variable parameters	Results
Behzadmehr et al., (2007)	Turbulent, Circular tube	SPM and Mixture	Cu-water φ=1% 10515≤Re≤22540	Their CFD simulation revealed that the mixture approach is more accurate than the SPM approach compared to the available experimental data.
V. Bianco et al., (2009)	Laminar, Circular tube	SPM and DPM	Al_2O_3-water 0≤φ≤4% 250≤Re≤1050 d_{np}=100nm	The maximum differences between models in terms of an average heat transfer coefficient I s reported as 11% at Re=1050 and φ=1%.
He et al., (2009)	Laminar, Straight tube	SPM and Euler-DPM	TiO_2-γ 0.24≤φ≤1.18% 900≤Re≤1500 d_{np}=21nm	Along with the considered range of Reynolds number, the heat transfer rate of an Euler-DPM model is slightly higher than that of a SPM model.
Haghshenas Fard et al., (2010)	Laminar, Circular tube	SPM and Eulerian	Cu-water 0.2≤φ≤3% 700≤Re≤2050	The Eulerian approach presents preferable agreement with experimental measurements. For example, the average relative error between numerical predictions and experimental results is 16% for the SPM approach and 8% for the Eulerian approach.
Lotfi et al., (2010)	Laminar, Horizontal tube	SPM, Mixture and Eulerian	Al_2O_3-water 1≤φ≤7% 700≤Re≤1800 d_{np}=42nm	In comparison with the accessible experimental data, their numerical predictions exhibit that the mixture approach is more accurate than SPM and Eulerian approaches, where both of these approaches show an underestimated result of the Nusselt number.
Vincenzo Bianco et al., (2011)	Turbulent, Circular tube	SPM and Mixture	Al_2O_3-water 0≤φ≤6% 10×10^3≤Re≤10×10^4 d_{np}=38nm	At φ=1%, a significant convergence is observed between the phases, but with an increase in nanoparticle concentration, a significant deviation is observed.

Table 2.1. devamı

Kalteh et al., (2011)	Laminar, Straight microchannel	SPM and Eulerian	Cu-water $0 \leq \varphi \leq 5\%$ $200 \leq Re \leq 1600$ $d_{np}=100nm$	Eulerian results always show a higher heat transfer improvement compared to the SPM results.
Moraveji and Esmaeili, (2012)	Laminar, Circular tube	SPM and DPM	Al_2O_3-water $0 \leq \varphi \leq 4\%$ $250 \leq Re \leq 1050$ $d_{np}=100nm$	The maximum deviation between presented models in an average value of heat transfer coefficient is detected as 11% at Re=500 and φ=1%.
Mojarrad et al., (2013)	Laminar, Horizontal tube	SPM, Mixture, and Eulerian	Al_2O_3-water $1 \leq \varphi \leq 7\%$ $700 \leq Re \leq 1800$ $d_{np}=42nm$	In comparison with the accessible experimental data, their numerical predictions exhibit that the mixture approach is more accurate than SPM and Eulerian approaches, where both of these approaches show an underestimated result of the Nusselt number.
Moraveji and Ardehali, (2013)	Laminar, Rectangular mini-channel heat sink	SPM, VOF, Mixture, and Eulerian	Al_2O_3-water $0.5 \leq \varphi \leq 6\%$ $130 \leq Re \leq 1600$ $d_{np}=33nm$	The deviation between the results of two-phase approaches was negligible, and they were more accurate than the single-phase approach when compared to experimental reference data.
Hejazian and Moraveji, (2013)	Laminar, Circular tube	SPM and Mixture	TiO_2-water $0.05 \leq \varphi \leq 0.25\%$ $4800 \leq Re \leq 30500$ $d_{np}=30nm$	The mixture approach with a maximum deviation of approx. 20% agrees better with the corresponding experimental data than the SPM approach.
Peng et al., (2014)	Turbulent, Circular tube	SPM, Mixture, and Eulerian	TiO_2-water $0.5 \leq \varphi \leq 1.5\%$ Re=5330	The Eulerian model has the highest accuracy while the mixture model has the lower accuracy, and the accuracy of the SPM approach lies between them.

Table 2.1. devamı

Behroyan et al., (2015)	Turbulent, Cylindrical tube	SPM, Mixture, Eulerian, and DPM	Cu-water $0 \leq \varphi \leq 2\%$ $10000 \leq Re \leq 25000$	Their predicted results reveal that the SPM approach and the DPM approach as a whole are the recommended approaches. The Eulerian approach gives imprecise results except for φ=0.5%, and the mixture approach has a maximum error of 15%.
Ganesan et al., (2016)	Turbulent, Circular tube	SPM and Eulerian	Cu-water $0 \leq \varphi \leq 1.5\%$ $10000 \leq Re \leq 25000$	The differences in an average Nusselt number compared to the experimental data range from 10-18% for the SPM model and 18-23% for the Eulerian model.
Bahiraei, (2016)	Laminar, Straight tube	SPM and DPM	CuO-water $0.3 \leq \varphi \leq 3\%$ Re=1350	The maximum deviation of the local heat transfer coefficient with the corresponding experimental results is given as 2% for the DPM model and 10% for the SPM model.
Ghasemi et al., (2017)	Laminar, Rectangular and circular heat sinks	SPM and Eulerian	CuO-water $0.25 \leq \varphi \leq 0.75\%$ $210 \leq Re \leq 490$ $d_{np}=29nm$	Comparison of the CFD predictions with the related experimental reference data exhibits that the Eulerian approach is more precise than that of the SPM approach.
Albojamal and Vafai, (2017)	Laminar, Circular tube	SPM, DPM, and Mixture	Al_2O_3-water $1 \leq \varphi \leq 4\%$ $250 \leq Re \leq 1050$ $d_{np}=100nm$	The maximum deviation between SPM and DPM in terms of an average heat transfer coefficient is 5.9% at Re=1050 and φ=1%. The mixture model deviates significantly over the entire range of the laminar flow regime.

Table 2.1. devamı

Onyiriuka et al., (2018)	Laminar and Turbulent, Circular tube	SPM, DPM, Mixture, and Combined of DPM and Mixture	Al_2O_3-water $1 \leq \varphi \leq 3\%$ $1050 \leq Re \leq 6020$ $d_{np} \leq 100 nm$	For laminar flow, the maximum deviation between SPM and DPM was 4.25% at Re=1420 and φ=3%. For turbulent flow, the maximum deviation between SPM and DPM was 2% at Re=6020 and φ=3%. Both mixture and combined of DPM and mixture give overpredict results.
Wang et al., (2018)	Laminar, Microscale trapezoidal channel	SPM, Mixture, Eulerian, and DPM	Al_2O_3-water φ=0.15 and 0.26% $300 \leq Re \leq 1200$	The numerical simulations showed that the accuracy of the implemented models with regard to the heat transfer coefficient could be ordered as DPM > Mixture > Eulerian > SPM.
Hazeri-Mahmel et al., (2021)	Laminar, Horizontal pipe	SPM and Mixture	Al_2O_3-water $1 \leq \varphi \leq 5\%$ $250 \leq Re \leq 1050$	The maximum deviation between the SPM and mixture was 52.5% at Re=250 and φ=3%.

2.4. Carbon nanotubes (CNTs)

In consequence of their extraordinary thermal and mechanical properties, carbon nanotubes (CNTs) have drawn attentiveness for suspending as nano-sized particles in liquids. Therefore, compared to other nanofluids, CNT nanofluids are a suitable selection to increase the heat exchange capacity in various thermal processes. After detecting carbon nanotubes in the past three decades (Iijima and Ichihashi, 1993), CNTs have received great concern from many investigators due to their wide range of interesting thermal properties. CNTs are tubes with long-chained molecules of carbon having a hexagonal structure of hybridized atoms. Depending on the rolling up of sheet structure, CNTs can be classified into single-walled carbon nanotubes (SWCNT) and double-walled carbon nanotubes (DWCNT). Among various types of nanoparticles, even those with a high thermal conductivity value, CNTs claim to have higher thermal conductivity than other spherical nanoparticles (Thostenson et al., 2001). From this point of view, the use of CNTs in thermal systems is a credible and effective approach to increasing their performance. Many investigators have announced the supremacy of CNT nanofluids over convective thermal transport in comparison with the available types of nanofluids (Chougule and Sahu, 2015; Sun et al., 2015).

Moreover, they indicate that the improvement of convective thermal transport in a smooth pipe utilizing nanofluids of CNT is noticeably more significant than the improvement in thermal conductivity (Chougule & Sahu, 2013; J. Wang et al., 2013). For instance, in an earlier experimental work by Ding et al., (2007), they revealed that the maximum increment in thermal transmission was 350% for CNT nanofluids flow in a smooth tube. Also, the volume fraction of CNT was detected to be the dominant factor that influences the heat transfer coefficient compared to other factors. Selimefendigil and Öztop, (2018) conducted a numerical simulation to test the mixed convection flow of CNT nanofluid inside the bifurcation channel with an annulus having an inner rotating wall at the connection section. They detected that the value of the Nusselt number, *Nu* is higher for high concentrations of carbon nanotubes. Sarafraz and Hormozi, (2016) implemented experimental research to examine the thermal efficiency and pressure drop, Δp of the plate heat exchanger by utilizing MWCNT nanofluid under different flow rates and inlet temperatures. They found that the suspension of the aforementioned nanoparticles in water improved the thermal efficiency with a slight increment in pressure drop, Δp.

One of the main problems arising from the use of CNT nanofluids as a working fluid in convective heat transfer systems is the increase in pressure drop, Δp. Nevertheless, this increase in pressure drop, Δp is negligible as demonstrated in many studies if the CNT volume fraction, φ is low. Interestingly, several investigations have confirmed that the mixing of CNT with the traditional liquids causes less pressure drop, Δp as compared with other types of nanofluids (Huang et al., 2016; V. Kumar et al., 2016; Yazid et al., 2017). However, Ebrahimnia-Bajestan et al., (2011) inspected numerically the influences of CNT nanofluid versus different aqueous nanofluids consisting of (alumina, copper oxide and TNT) nanoparticles on the pressure drop, Δp of a straight pipe. They deduced that CNT-H_2O nanofluid, with 9620 Pa, has the highest value of pressure drop, Δp among the other considered nanofluids. An experimental study conducted by Amiri et al., (2015) has focused on the pressure drop, Δp of MWCNT-nanofluids flowing through the smooth pipe within the limit of the laminar regime. The findings declared by the authors revealed that the maximum augmentation in pressure drop, Δp was 17% in comparison with traditional liquids at the solid concentration up to φ=1% at *Re*=1050.

2.5. Steady flow

2.5.1. Corrugated channel

Researches on thermal and hydrodynamic performance in channels that aim to provide better energy transport are one of the most common topics in terms of thermal applications. This issue has very substantially crucial from an energy conservation perspective (Abdelaziz et al., 2011). Various strategies have been used to obtain a more effective process in thermal systems (Kurtulmuş and Sahin, 2020). These strategies can be categorized into two categories, such as active and passive flow control. In the second category, modifying surfaces or geometries are the most commonly used strategies to improve the performance of thermal devices. The mentioned method provides better mixing processes and disturbing the laminar boundary layer by forming local turbulence; and thus, decreasing thermal resistance and enhancing energy transport. It is worth mentioning that the wavy channels are widely utilized as effective passive methods for increasing thermal transmission in heat exchange systems (Kurtulmuş et al., 2020). Such systems include the radiator of automotive vehicles, electronic packaging, heat exchangers, solar water heating, geothermal energy, and so forth.

Generally, chamfering the right edge of the corrugated surfaces can reduce the friction factor coefficient to approximately 60% (Sparrow and Hossfeld, 1984). Due to this reason, investigators usually studied the augmentation of the heat transfer coefficient through the channels with wavy walls instead of sharp-cornered walls. According to the published literature survey by Kurtulmuş and Sahin, (2019), the most studied corrugated channels have wavy or sinusoidal walls, sharp walls, rectangular walls, arc walls and trapezoidal walls, respectively.

The wavelength, L_w amplitude, a space between the surfaces, H undulation number, n and phase shift, θ are the dominant characteristics of a corrugated channel which have an essential role on the thermal transmission within the corrugated channels. A methodical collection of simulation and experiment investigations have been performed to state the impact of these parameters on the forced convection flow through the channels (Akbarzadeh et al., 2016; Ghani, Kamaruzaman, et al., 2017; Ghani, Sidik, et al., 2017; H. Hamzah et al., 2020; Islamoglu & Parmaksizoglu, 2003; Miroshnichenko et al., 2017; Ramgadia and Saha, 2014; Sidik et al., 2017; Yang et al., 2016). Circulation zones were detected adjacent to the top and bottom surfaces of the corrugated channel when its corrugations are large enough. According to the numerical modeling of forced convection flow inside a sinusoidal wall channel which is done in ref. (Wang and Chen, 2002), it was reported that varying the amplitude-wavelength, a/L_w ratio has a directing impact on these zones and subsequently thermal transmission along the channel surfaces. The influence of channel spacing expansion/contraction ratio on the thermal-hydraulic performance was experimentally and numerically performed by Kurtulmuş et al., (2020) in a sinusoidal wavy channel for a turbulent flow regime. They figured out that the smaller channel spacing has the highest thermal transmission rate with a higher friction factor, f even for relatively low Reynolds numbers, Re. Yang et al., (2014) implemented a numerical optimization of thermal transport through the wavy channel for the laminar flow regime by taking the influence of different wavy-wall parameters into account. They reported that for a given Reynolds number, Re and whatsoever is the wave amplitude, a, the performance factor, TPF is reduced by rising the undulation number, n. The influence of the height to width ratio of the triangular corrugated channel was numerically examined in Ref. (Comini et al., 2003) over a low range of Reynolds numbers (Re=100-600). They stated that any reduction in the aspect ratio gives an augmentation in Nusselt numbers, Nu friction factor, f, and accordingly, an increase of the global performance, TPF. The effect of the phase difference, θ between the confined corrugated walls was numerically analyzed for airflow by Yin et al., (2012). It was realized that both friction factor, f and Nusselt number, Nu grow by reducing the phase difference value, θ.

The augmentation in thermal efficiency of corrugated channels compared to smooth configurations has been reported in previous studies (Kurtulmuş et al., 2020; G. Wang and Vanka, 1995). As mentioned earlier, adjusting surfaces or instilling ribs gives well-decided passive tools to dominate the heat flow through the channels without expending extra power, which has decisive crucial in a wide range of thermal processes. Otherwise, the corrugation of the walls creates obstructions to the fluid flow; therefore, the pressure drop increases and then energy consumption (Y. T. Yang et al., 2014). Therefore, it is important to optimize the configuration of walls. Many investigators have conducted extensive research on corrugated walls by developing their relevant parameters such as wavelength, L_w amplitude, a space between the surfaces, H undulation number, n and phase shift, θ (Kurtulmuş and Sahin, 2019). Further, the transverse corrugated channels with different corrugation walls of triangle, curve, rectangle, and trapezium were compared by Kumar et al., (2021). They announced that channel configuration and flow rate have a significant impact on the rate of heat transfer.

2.5.2. Corrugated channel and nanofluids

Nanotechnology is one of the most exciting and fast-progressing areas of science today. Developments in nanotechnology have progressively led to an increase in the thermal conductivity of traditional liquids by impregnating solid nano-sized particles (usually <100nm) in these liquids (Choi and Eastman, 1995). Nanofluids show many right sets of circumstances to enhance the performance of thermal processes by enhancing the thermal parameters of the conventional fluids. The combination of corrugated walls and using nanofluids instead of traditional fluids are two common passive methods for improving the rate of energy transport. Therefore, the influences of two different passive strategies, including wavy walls and utilizing nanofluids on the turbulent flow, heat transfer, and entropy production, were studied together in the present work.

Many investigations in various regimes were carried out on thermo-hydraulic mechanisms using nanofluids through different shapes of corrugated channels. Pandey and Nema, (2012) implemented an experimental study of Al_2O_3-water nanofluid flowing inside a counter-flow heat exchanger having a corrugated plate test section. Their outcomes revealed that the thermal performance of the heat exchanger notably enhanced due to the presence of the nanoparticles, where this enhancement increases with rising Reynolds, Re and Peclet, Pe numbers. Additionally, power consumption increases with an increase in the alumina particle concentrations, φ. A numerical analysis of Hatami and Jing, (2017) on the possibilities of alumina nanofluid demonstrated its impact on improving the efficiency of a solar collector with a wavy absorber plate. Heidary and Kermani, (2010) offered a numerical investigation on hydrodynamic flow and energy transport of pure water containing Copper nanoparticles inside a sinusoidal-wall channel. Their results have shown an enhancement in heat transfer with increasing solid particle concentrations, φ and flow rate. The same findings were achieved by Ajeel et al., (2019) in numerical research through a heated channel having trapezoidal configuration surfaces using SiO_2-H_2O nanofluid. Ahmed et al., (2011) introduced a numerical work for the flow of Cu-H_2O nanofluid in a channel with triangular surfaces. They declared an increment in thermal transmission rate and pressure drop, Δp with an augmentation in the solid structure concentration, φ of nanofluid. In another study by the same authors (Ahmed et al., 2014), they examined the effect of the phase shift, θ between the channel walls. Their outcomes indicated that for low Reynolds number, Re the phase shift with θ=0°

provides the highest pressure drop, Δp within the tested range of the nanoparticle concentration, φ, while for the high Reynolds number, *Re* the phase shift of θ=180° records the highest value of pressure drop, Δp. Vanaki et al., (2014) examined the impacts of the different SiO_2 nanoparticle shapes, host fluids, phase shifts, θ and wavy amplitudes, a on the thermal transmission rate, skin friction coefficient and performance evaluation criterion, *PEC* of the wavy channel based on the 2-D numerical simulation. They selected a homogeneous single-phase model, SPM to represent the thermo-physical properties of nanofluid. The authors revealed that the SiO_2-Ethylene glycol nanofluid with platelet nanoparticles shape affords the greatest thermal transmission rate in comparison with water-based fluid and other considered nanoparticle shapes, while the skin friction coefficient, C_f does not depend on the shape of nanoparticles. Further, it turns out that the *PEC* reduces with augmentation of the Reynolds number, *Re* and the optimum shape of the channel was found for the phase shift of θ=30° with an amplitude of a=0.5.

Albojamal et al., (2017) conducted a numerical simulation to predict the thermal transmission of Al_2O_3 and CuO/water nanofluids in a transverse channel having wavy walls. They implemented three different models (SPM, dispersion and DPM) for modeling the flow of nanofluids. Their numerical predictions declared that these combinations increase the rate of thermal transmission by about 20% over the base liquid, but this is accompanied by an increase in pressure drop values. From this point of view, these methods also have a negative effect on pressure drop and energy cost Ahmed et al., (2011). Therefore, analysis of such methods is essential from an energy-saving perspective to decide how much changes in relevant parameters will affect pressure drop and thermal transmission rate. The outcomes of this analysis can provide useful guidance to the designer of thermal systems.

2.6. Pulsating flow

Pulsating flow consists of a periodic oscillating flow induced by a steady flow, which is considered laminar, transient, or turbulent flow regimes. Many differences are perceived between the characteristics of steady and pulsating flows, such as the separation and disturbance of the boundary layer in the internal flows in addition to the state of transition to the turbulent regime. Due to the variety of applications, pulsating flow can potentially be investigated in many areas in the near future.

Thermal performance can be actively improved by using pulsating flow within the channel. Many published studies have shown that powerful mixing of the working fluid was the major reason for improving heat transport through the use of pulsatile flow (Rahgoshay et al., 2012; Zhang et al., 2018). Two factors must be taken into account when introducing pulsed flows without a continuous term. These factors are the frequency of pulsation, f and amplitude of pulsation, *A*. Nield and Kuznetsov, (2007) examined laminar pulsating flow in a heated tube or channel. Their outcomes revealed that in pulsed flows, the average rate of heat transfer periodically fluctuates around its values in a steady-state flow. Akdag, (2010) numerically simulated forced convection heat transfer in a discretely heated channel exposed to a laminar pulsating flow. Simulations are performed for different Womersley numbers $(3.5 \leq W_o \leq 44)$ and pulsation amplitude $(1 \leq A_o \leq 5)$ at a fixed value of Reynolds number $(Re = 125)$. It was observed that the thermal transmission from the heated section is strongly influenced by both amplitude and frequency of the pulsating flow. While, the mechanisms of turbulent pulsating flow inside a uniformly heated pipe were experimentally tested by Elshafei et al., (2008). Reynolds number and pulsation frequency are considered in the range of $10^4 \leq Re \leq 4 \times 10^4$ and $6.6 \leq f \leq 68$ Hz. The researchers reported that the maximum improvement over the steady-state case was achieved for the parameter of $Re = 3.7 \times 10^4$ and f=13.3 Hz. In addition, the problems of pulsating flow and some suggestions for future work are pointed out and introduced in a critical review of Esfe et al., (2021).

A limited number of studies have considered the flow of pure fluid and/or nanofluid in a corrugated channel under inlet conditions of pulsating flow. Most of these studies have focused on the characteristics of pulsating flow under a constant configuration of the corrugated channels (Esfe et al., 2021). For example, Jin et al., (2007) experimentally studied the improvement of thermal transmission by inserting laminar pulsating flow of water inside a channel with triangular grooves. They detected that the improvement in heat transfer was about 350% in comparison with the steady flow conditions. Kurtulmuş and Sahin, (2020) experimentally examined turbulent pulsating water flow in sinusoidal heated channels using the particle image velocimetry method. It was found that the heat transfer of the pulsating velocity profile was stated to be 1.5 times that of the steady-state velocity profile. Hoang et al., (2021) implemented CFD simulations to test the thermal performance of water flow through a 3D V-shaped undulating channel exposed to turbulent pulsating conditions at the inlet section. They announced that the thermal performance factor under pulsating flow conditions varied from 1.3 to 1.4, while they ranged from 0.9 to 1.17 under constant flow conditions. Akdag et al., (2014) modeled the laminar pulsating flow of Al_2O_3-H_2O nanofluid within a wavy mini-channel using the SPM approach. The authors stated that the combined impact of pulsating and nanofluid through a sinusoidal channel significantly improves the thermal transition rate compared to that of a constant flow. Jafari et al., (2015) numerically analyzed the pulsating flow of SWCNT-H_2O nanofluid flowing through the convergent-divergent channel utilizing the lattice Boltzmann technique. As they reported, both frequency and amplitude of pulsating flow are critical factors in enhancing the rate of thermal transmission.

2.7. Entropy generation

From a thermodynamics point of view, energy can be dissipated due to an irreversible process. The irreversibility process (or entropy generation) mainly comes from fluid friction and heat transfer. Taking entropy analysis into account in investigating thermal processes leads to improve the research work. Indeed, the analysis of entropy generation has been a powerful tool for optimizing, designing and evaluating an extensive range of engineering applications. Several investigators have performed this analysis on various solar collectors and heat exchanger systems. For example, Rashidi et al., (2017) investigated entropy production in a permeable solar collector within the laminar regime range. They found that the rate of entropy production increases due to the reduction in the permeability of porous structures. Bahaidarah and Sahin, (2013) examined the entropy generation features of the pure fluid flow inside a corrugated channel. They stated that the channel configuration has a significant influence on irreversibility distribution. Akbarzadeh et al., (2017) have numerically tested the entropy production and thermal characteristics of water flow in a converging-diverging channel, taking the effect of corrugation profiles into account. They asserted that the sinusoidal profile gives higher performance and relatively low entropy generation rather than other tested profiles. Turbulent forced convection flow of Cu-water nanofluid in a solar heater having a corrugated absorber plate was numerically examined by Akbarzadeh et al., (2018). The SST k-ω model was utilized and the two-phase mixture approach was employed to simulate the turbulent flow of nanofluid. It has been detected that entropy production reduces by utilizing nanofluid as compared with pure water. To better understand this topic, readers are encouraged to read these studies (Bahiraei et al., 2017; Esfahani et al., 2017; Rashidi et al., 2018).

Analysis of entropy production (or generation) can be employed as a tool to evaluate the efficiency of a thermal process. Adrian, (1984) defined a systematic methodology for calculating entropy generation from thermal and friction impacts in various thermal systems. Since then, many studies were proposed on the optimal design of thermal applications depending on the principle of minimum entropy production (Zontul et al., 2021). Some typical examples involve: the optimization of porous locations inserted in a double-pipe heat exchanger investigated by Akbarzadeh et al., (2020); thermodynamic optimization in a combustion chamber of gas turbine under turbulent flame conditions examined by Arjmandi and Amani, (2015); the entropy analysis of five different types of nanofluids flow between two parallel sheets tested by Ahmad et al., (2018); as well as the optimization studies of forced convection nanofluids flow in corrugated channels under both laminar and turbulent flow regimes implemented by(M. Akbarzadeh et al., 2016; Dormohammadi et al., 2018; Esfahani et al., 2017; Shahsavar et al., 2021). It should be noted that all of these studies in this section were performed under steady-flow structures (Jasim et al., 2021).

2.8. Novelty of the current study

According to the literature survey, most of the published studies deal with the irreversibility analysis of pure liquid and/or nanofluid flow in thermal systems under constant inlet flow conditions.Also, CFD modeling of nanofluid as a single-phase is mainly associated with the pulsating flow in heated channels. Moreover, the combined influence of the pulsating inlet flow and wavy channel with different phase shifts, θ on convective heat transfer has never been considered in the previous studies. In this regard, our goal is to investigate the impact of turbulent pulsating flow on hydrothermal and entropy generation of SWCNT-water nanofluid in a wavy channel having different phase shifts using both SPM and DPM. Impacts of key variables such as Reynolds number, *Re*, pulsating frequency, *f*, the concentration of SWCNT, φ, phase shift, θ, and phase approach on convective thermal performance and thermodynamic irreversibility have been examined. From this point of view, researchers increasingly need to understand the physical mechanism of combining these techniques in different applications like pulse engines, sterling engines, industrial pulse tube coolers and identification of water reserves.

3. MATERIALS AND METHODS

3.1. Problem representation, assumptions and boundary conditions

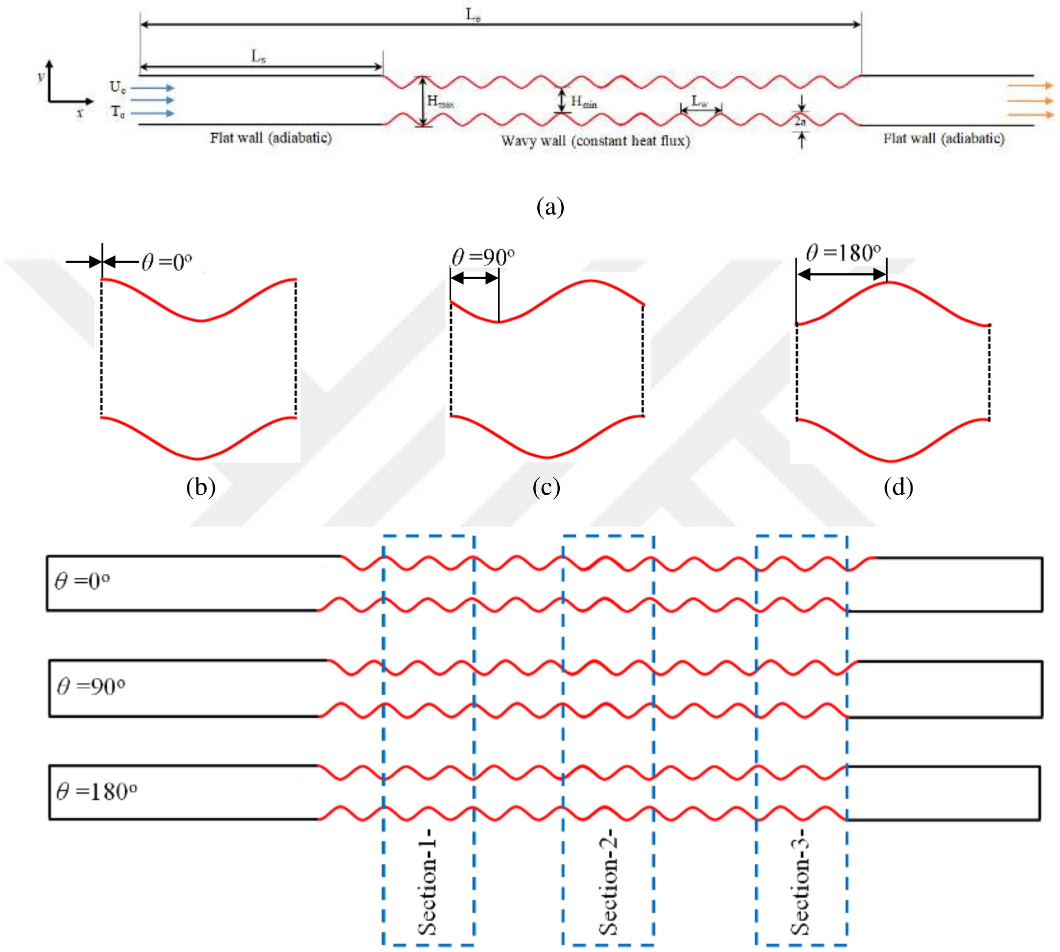

Figure 3.1. (a) Schematic representation of the tested model with constant amplitude, undulation, wavelength and channel height, (b) θ=0°, (c) θ=90°, (d) θ=180°, and (e) sections of contour view for considered corrugated channels.

The 2D graphical representation of the various configurations in this research is displayed in Figure3.1. As shown, this channel includes three sections : inlet and exit sections with straight walls and a middle section with sinusoidal walls. These straight ducts were employed as upstream and downstream sections for the test section (sinusoidal walls) to generate appropriate flow conditions. The length of these sections are as follows: upstream section=293 mm, test section=336 mm and downstream section=200 mm. The channel height ratio has a fixed value of $M=H_{min}/H_{max}=0.5$. Further, both the upper and lower walls of the sinusoidal test section are composed of twelve wavy units. The profile of each wavy unit was given as follows: wavelength, L_w=28 mm; and wave amplitude, a=3.5 mm. These parameters are similar to those presented in the experimental work of Kurtulmuş et al., (2020).

During this CFD modeling, three varying phase shift magnitudes of θ=0°, θ=90° and θ=180° were examined and compared. Both pure water and SWCNT-water nanofluid are chosen as the working fluid. In the case of steady flow, the flow at the entrance of the upstream straight channel was subjected to a constant temperature and uniform velocity profile with the turbulent range of Reynolds number ($4000 \leq Re \leq 10000$) and the exit was used to release the pressure with the atmospheric condition. For the pulsating flow, the cold working fluid entered with an unsteady pulsating velocity profile with the turbulent range of Reynolds number ($4000 \leq Re \leq 7000$). This profile is given as follows:

$$U_{in} = U_{avg}[1 + A\sin(2\pi f t)] \tag{3.1}$$

where U_{avg} is the average velocity of inlet flow, A is the pulsation amplitude and f is the pulsation frequency. This study covers pulsation amplitude in the range of $(1 \leq f \leq 5)$ and fixed the value of pulsation amplitude as $(A = 0.3)$.

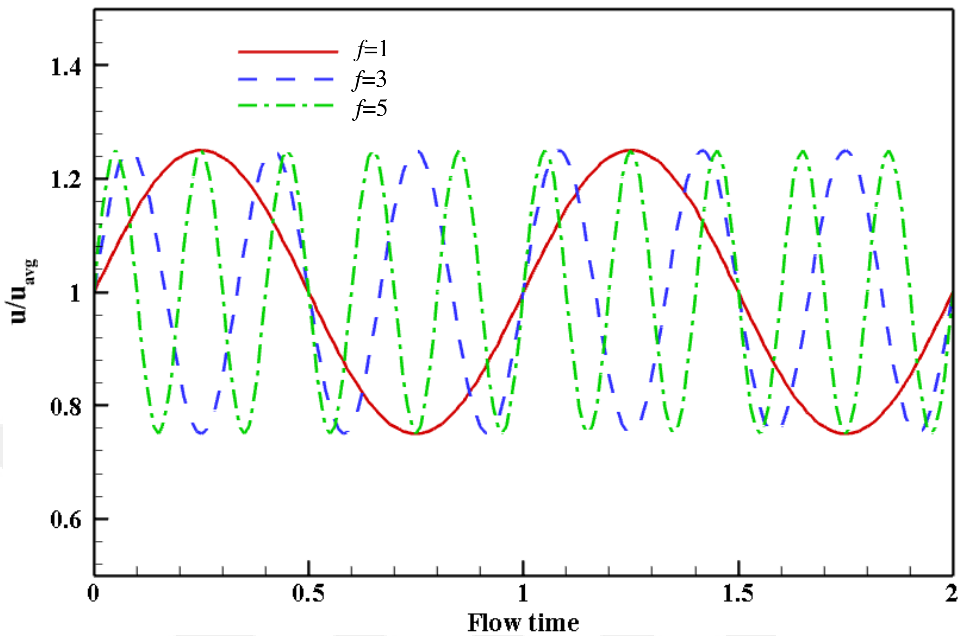

Figure 3.2. Schematic of pulsating velocity profile with non-dimensional flow time at different frequencies, *f*.

Figure 3.2 displays the dimensionless velocity profile with flow time for three different pulsating frequencies, *f*. In case of the DPM, the nanoparticles are injected in steady velocity $(U_{in} = U_{avg})$. A no-slip boundary condition was defined for the solid walls of the channel. The constant heat flux sources of q''=4553W/m^2 are exposed to the walls of the test section, while the walls of each straight section are ensured in accordance with adiabatic conditions. Finally, the hydrothermal flow is supposed to be 2D, incompressible, unsteady and turbulent.

3.2. Nanofluid properties for single-phase approach

Traditional heat transfer liquids like water have a low thermal conductivity in comparison with those of solids. Therefore, the suspension of SWCNT nanoparticles in pure water can improve their effective thermal conductivity. Table 3.1 lists the detailed physical properties of the SWCNT particles and host liquid applied in this work (Selimefendigil et al., 2019). Researchers have offered several related formulas for calculating the thermophysical properties of nanofluids. For the homogenous single-phase, SPM approach, the following correlations were adopted to determine these properties of SWCNT-water nanofluid.

Table 3.1. Thermo-physical properties of water and SWCNT nanoparticles (Selimefendigil et al., 2019).

	$\rho(kg/m^3)$	C_p(J / kg K)	k(W / m K)
water	997.1	4179	0.613
SWCNT	2600	425	6600

Since there is no experimental data for densities and specific heat capacities of nanofluid, linear correlations of the solid-liquid mixture in terms of nanoparticle concentration are utilized (Hamzah et al., 2020):

$$\rho_{nf} = (1-\varphi)\rho_{bf} + \varphi\rho_P \tag{3.2}$$

$$\left(\rho C_p\right)_{nf} = (1-\varphi)\left(\rho C_p\right)_{bf} + \varphi\left(\rho C_p\right)_P \tag{3.3}$$

Brinkman correlation (Brinkman, 1952) was adapted to predict the dynamic viscosity of SWCNT-water nanofluid:

$$\mu_{nf} = \frac{\mu_{bf}}{(1-\varphi)^{2.5}} \tag{3.4}$$

The thermal conductivity of SWCNT-water nanofluid, which depends on the composition of carbon nanotubes, can be determined as (Xue, 2005):

$$\frac{k_{nf}}{k_{bf}} = \frac{(1-\varphi)+2\varphi\frac{k_P}{k_P-k_{bf}}\ln\frac{k_P+k_{bf}}{2k_{bf}}}{(1-\varphi)+2\varphi\frac{k_{bf}}{k_P-k_{bf}}\ln\frac{k_P+k_{bf}}{2k_{bf}}} \tag{3.5}$$

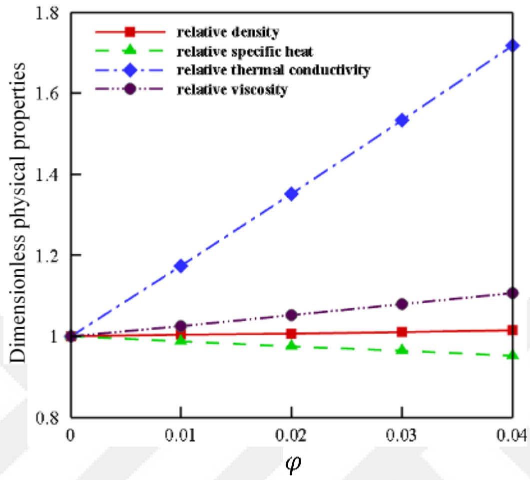

Figure 3.3. Variations of the relative physical properties versus volume concentration, φ for SWCNT-water nanofluid.

Moreover, Figure 3.3 shows the change in the relative thermophysical properties (ρ_{nf}/ρ_{bf}, $(\rho C_p)_{nf}/(\rho C_p)_{bf}$, μ_{nf}/μ_{bf}, k_{nf}/k_{bf}) defined by Equations (3.2)-(3.5) with respect to the concentration of nanoparticles for SWCNT-water nanofluid. In this research, the results were taken for solid nanoparticle concentrations, φ ranging from 0 to 3%.

3.3. Governing equations of Homogeneous single-phase model (SPM)

As mentioned earlier, this model implies that the nano-scale particles can be simply diluted to achieve the velocity of the working fluid. Consequently, the nanofluid is regarded as a homogeneous fluid with improved thermal properties, and these properties were determined by Equations (3.2)-(3.5). It is also assumed that the dispersed nanoparticles in the host liquid have a uniform morphology, and both phases (solid and liquid) are in a thermal equilibrium condition. Thus, in the current thesis, the introduced numerical results by this model depend on the following governing equations (Albojamal and Vafai, 2020; Bianco et al., 2009):

Continuity equation:

$$\nabla.\left(\rho_{nf}\vec{V}\right) = 0 \tag{3.6}$$

Momentum equation:

$$\nabla.\left(\rho_{nf}\vec{V}\vec{V}\right) = -\nabla p + \nabla\left(\mu_{nf}\nabla\vec{V}\right) \tag{3.7}$$

Energy equation:

$$\nabla.\left(\rho_{nf}\vec{V}CpT\right) = \nabla.\left(k_{nf}\nabla T\right) \tag{3.8}$$

3.4. Governing equations of discrete-phase model (DPM)

This approach analyzes the continuous (liquid) and discrete (dispersed) phases using Eulerian's and Lagrangian's assumptions, respectively. The coupling of these phases is achieved by alternately solving their equations until the solutions in both phases reach the stopped condition. By considering the momentum and heat exchanges between phases, the sink/source terms are combined with Equations (3.6)-(3.8).Therefore, the mathematical formulation of this approach can be presented as below (Albojamal and Vafai, 2017; Vanaki et al., 2016):

Continuity equation:

$$\nabla.\left(\rho_{nf}\vec{V}\right) = 0 \tag{3.9}$$

Momentum equation:

$$\nabla.\left(\rho_{nf}\vec{V}\vec{V}\right) = -\nabla p + \nabla\left(\mu_{nf}\nabla\vec{V}\right) + S_m \tag{3.10}$$

Energy equation:

$$\nabla.\left(\rho_{nf}\vec{V}CpT\right) = \nabla.\left(k_{nf}\nabla T\right) + S_e \tag{3.11}$$

where S_m describes the momentum transfer between phases which is calculated as:

$$S_m = \frac{1}{\delta V}\sum_{b=1}^{n}\vec{F}_b \tag{3.12}$$

In the discrete Lagrangian model, the current numerical code foretells the path of the dispersed phase by integrating the balance of the acting force on the nanoparticles. Therefore, the equation of particle motion is expressed by the below formula as (Mirzaei et al., 2014):

$$m_P\frac{d\vec{V}_P}{dt} = F_D + F_g + F_L + F_{Br} + F_T + F_P + F_v \tag{3.13}$$

On the left-hand side of the above equation, m_p is the particle mass, $\vec{V}_P$ is the particle velocity vector, and the right-hand side symbolizes the forces acting on the particle which are resistance, gravity, lift, Brownian, Thermophoresis, pressure gradient and virtual mass forces, respectively. More detailed information and correlations of these forces are provided in Refs. (Albojamal and Vafai, 2017; Vanaki et al., 2016).

The term of the energy source that expresses energy exchange between phases can be written as:

$$S_e = \frac{1}{\delta V} \sum_{nP} Nu_P \pi d_P k_P (T - T_P) \tag{3.14}$$

where Nu_p is computed from the Ranz-Marshall formula (Oosthuizen and Carscallen, 2013):

$$Nu = \frac{h.d}{k} = 2 + 0.6 Re_d^{1/2} Pr^{1/3} \tag{3.15}$$

3.5. Turbulence modeling

Many researchers conducted the shear stress transfer (SST) model to simulate flow in roughened channels since this model presents compatible results with those of experimental data (Akbarzadeh et al., 2018; Kurtulmuş et al., 2020). Therefore, the current simulation uses this model for wavy channel. The standard κ-ω turbulence model has the following equations (Menter, 1994):

$$\frac{\partial}{\partial x_i}\left(\rho_{nf} \kappa V_i\right) = \frac{\partial}{\partial x_j}\left\{\left(\mu_{nf} + \frac{\mu_t}{\sigma_\kappa}\right)\frac{\partial \kappa}{\partial x_j}\right\} + G_\kappa - \rho_{nf} \kappa \omega \beta_1 \tag{3.16}$$

$$\frac{\partial}{\partial x_i}\left(\rho_{nf} \omega V_i\right) = \frac{\partial}{\partial x_j}\left\{\left(\mu_{nf} + \frac{\mu_t}{\sigma_\omega}\right)\frac{\partial \omega}{\partial x_j}\right\} + G_\omega - \rho_{nf} \omega^2 \beta_2 + (1 - F_1)\rho_{nf} \sigma_{\omega,2} \frac{1}{\omega}\frac{\partial \kappa}{\partial x_i}\frac{\partial \omega}{\partial x_i} \tag{3.17}$$

where G_κ is the generation of the kinetic energy of turbulence due to the averaged velocity gradients, and G_ω represents the generation of ω.

The turbulent viscosity, $\mu_t$is represented as:

$$\mu_t = \frac{\rho_{nf}\kappa}{\omega} \frac{1}{max\left(\frac{1}{\alpha^*}, \frac{SF_2}{\alpha_1 \omega}\right)} \tag{3.18}$$

where F_1 and F_2 are the blending functions and S is the value of strain rate. In Equations (3.16) and (3.17), σ_κ and σ_ω are resemble the turbulent Prandtl numbers, *Pr*, which are determined as follows:

$$\sigma_\kappa = \frac{1}{\frac{F_1}{\sigma_{\kappa,1}}+\frac{(1-F_1)}{\sigma_{\kappa,2}}} \tag{3.19}$$

$$\sigma_\omega = \frac{1}{\frac{F_1}{\sigma_{\omega,1}}+\frac{(1-F_1)}{\sigma_{\omega,2}}} \tag{3.20}$$

The blending functions are defined by:

$$F_1 = \tanh(\emptyset_1^4) \tag{3.21}$$

$$F_2 = \tanh(\emptyset_2^2) \tag{3.22}$$

where,

$$\emptyset_1 = \min\left[\max\left(\frac{\sqrt{\kappa}}{0.09\omega y},\frac{500\mu}{\rho y^2\omega}\right),\frac{4\rho\kappa}{\sigma_{\omega,2}D_\omega^+ y^2}\right] \tag{3.23}$$

$$D_\omega^+ = \max\left[2\rho\frac{1}{\sigma_{\omega,2}\omega}\frac{\partial\kappa}{\partial x_j}\frac{\partial\omega}{\partial x_j}10^{-20}\right] \tag{3.24}$$

$$\emptyset_2 = \max\left[\left(\frac{2\sqrt{\kappa}}{0.09\omega y},\frac{500\mu}{\rho y^2\omega}\right)\right] \tag{3.25}$$

where y is the near-surface spacing and D_ω^+ is the positive portion of the cross diffusion term. The constants of this model are $\sigma_{\kappa,1} = 1.176$, $\sigma_{\omega,1} = 2$, $\beta_1 = 0.075$, $\beta_2 = 0.0828$, $\alpha_1 = 0.31$, $\sigma_{\kappa,2} = 1$ and $\sigma_{\omega,2} = 1.168$.

3.6. Parameters definition

To present and compare the hydrothermal index and entropy generation for the considered geometries inside wavy channels, some expressions are stated as (Kurtulmuş et al., 2020):

The Reynolds number, Re is given as:

$$Re = \frac{U_{avg} D_H}{\upsilon} \tag{3.26}$$

where U_{avg} is the average velocity of the working fluid over the cross-sectional area, υ is the kinematic viscosity of the base fluid and D_H is the hydraulic diameter ($D_H = 2H_{avg}$).

To determine the strength of energy transfer, the average Nusselt number, Nu_{avg} is exposed as:

$$Nu_{avg} = \frac{h_{avg,bf} D_H}{k_{bf}} \tag{3.27}$$

where $h_{avg,bf}$ and k_{bf} are the average heat transfer coefficient and thermal conductivity of the base fluid, respectively.

In the case of pulsating flow, the time average Nusselt number is defined as:

$$< Nu_{avg} >= \frac{<h_{avg}> D_H}{k_{bf}} \tag{3.28}$$

where $< h_{avg} >$ and k_{bf} are the time-averaged heat transfer coefficient and thermal conductivity of the base fluid, respectively.

The pressure drop, Δp among entrance and exit of the heated wavy walls is expressed as:

$$\Delta p = p_{avg,in} - p_{avg,out} \tag{3.29}$$

The friction factor, f is determined as;

$$f = 2\frac{\Delta p D_H}{\rho L_t U_{avg}^2} \tag{3.30}$$

Where L_t is the total length of the heated wavy surface.

The relative friction factor, f^* is expressed as the ratio of friction factor of the wavy channel, f to that of the straight channel, f_o:

$$f^* = \frac{f}{f_o} \tag{3.31}$$

The enhancement factor, E is computed as the ratio of average *Nu* of the wavy channel, $Nu_{avg}$to that of the straight channel, $Nu_{avg,o}$:

$$E = \frac{Nu_{avg}}{Nu_{avg,o}} \tag{3.32}$$

On the other hand, for calculating the enhancement factor, E with respect to the type of working fluid, the E_{nf} is described as:

$$E_{nf} = \frac{Nu_{avg,nf}}{Nu_{avg,bf}} \tag{3.33}$$

In addition, the thermal performance factor, *TPF* is introduced to calculate the E with an agreeable rise in f within the flow domain (Yang et al., 2020). The corresponding equations are presented below:

$$TPF = \frac{E}{f^{*(1/3)}} \tag{3.34}$$

To determine the *TPF* for the wavy channel depending on the type of working fluid, the corresponding equations are given below:

$$TPF_{nf} = \frac{E_{nf}}{f_{nf}^{*\,(1/3)}} \tag{3.35}$$

where f_{nf}^{*} is the relative friction factor according to the type of working fluid and it is defined as follows:

$$f_{nf}^{*} = \frac{f_{nf}}{f_{bf}} \tag{3.36}$$

In the present thesis, the heat transfer ratio, η is realized as:

$$\eta = \frac{<Nu_{avg,p}>}{<Nu_{avg,s}>} \tag{3.37}$$

where $<Nu_{avg,p}>$ is the time-averaged Nusselt number for pulsating inlet profile and $<Nu_{avg,s}>$ is the time-averaged Nusselt number for steady profile.

Finally, for computing the heat transfer ratio, $\eta$with respect to the type of working fluid, the η_{nf} is given as:

$$\eta_{nf} = \frac{<Nu_{avg,nf}>}{<Nu_{avg,bf}>} \tag{3.38}$$

3.7. Analysis of entropy generation

The entropy production analysis is performed to evaluate the thermal capacity in any irreversible process. Thus, in this research, the entropy analysis was implemented as a criterion for evaluating the thermal capacity through the wavy channel. In our case study, only the main sources were considered for entropy production. These sources are thermal, S_{th} and friction, S_{fr} impacts. The local entropy generations due to thermal and friction impacts in the dimensional form are respectively expressed as (Akbarzadeh, et al., 2017):

$$S_{th} = \frac{k}{T_m^2}\left[\left(\frac{\partial T}{\partial x}\right)^2 + \left(\frac{\partial T}{\partial y}\right)^2\right] \tag{3.39}$$

$$S_{fr} = \frac{\mu}{T_m}\left[2\left(\frac{\partial u}{\partial x}\right)^2 + 2\left(\frac{\partial v}{\partial y}\right)^2 + \left(\frac{\partial u}{\partial y} + \frac{\partial v}{\partial x}\right)^2\right] \tag{3.40}$$

where $T_m = \frac{T_h+T_c}{2}$

The above equations are converted to non-dimensional form as follows:

$$N_{th}^* = \frac{S_{th}D_H^2}{k} \tag{3.41}$$

$$N_{fr}^* = \frac{S_{fr}D_H^2}{k} \tag{3.42}$$

The local of total entropy generation, S_T and Bejan number, Be in non-dimensional form are respectively represented as:

$$S_T = N_{th}^* + N_{fr}^* \tag{3.43}$$

$$Be = \frac{N_{th}^*}{N_{th}^* + N_{fr}^*} \tag{3.44}$$

The average of N_{th}^* and N_{fr}^* within the wavy channel is obtained by integrating their equations (Equations (3.41) and (3.42)) over the entire flow domain:

$$N_{th} = \frac{\int_A N^*_{th} dA}{A} \tag{3.45}$$

$$N_{fr} = \frac{\int_A N^*_{fr} dA}{A} \tag{3.46}$$

3.8. Numerical procedure

Numerical computations were performed by solving nonlinear equations of the homogeneous single-phase model, SPM (Equations (3.6)-(3.8)) and discrete-phase model, DPM (Equations (3.9)-(3.11)) that govern the flow domain through the wavy channel with considering boundary conditions. ANSYS FLUENT (R17.2 Academic) computer program was adopted for calculations in the present thesis. To discretize the nonlinear governing equations, the control volume scheme is applied. The PRESTO, QUICK and SECOND ORDER UPWIND schemes were utilized to discretize pressure, volume fraction, and remaining variables, respectively. The pressure-velocity fields were linked together utilizing the SIMPLE algorithm. The simulation takes the two-way connection between the liquid and solid phases into account for the discrete phase model, DPM. Thus, the fluid can influence the motion of the solid particle by drag, and the particles can exchange momentum and energy with the continuous fluid. Since the present algorithm is based on coupling nonlinear governing equations, the iterative procedure was repeated until the final result converged. At every iteration, appropriate under-relaxation factors were adopted for each dependent variable to solve the equations easily. The precision of the convergence solution was controlled at a level of 10^{-6} for the set of governing equations. Finally, a user-defined function, UDF is utilized to insert the sinusoidal pulsating velocity profile (Equation (3.1)) at the inlet section of the wavy channel.

3.9. Mesh reliability

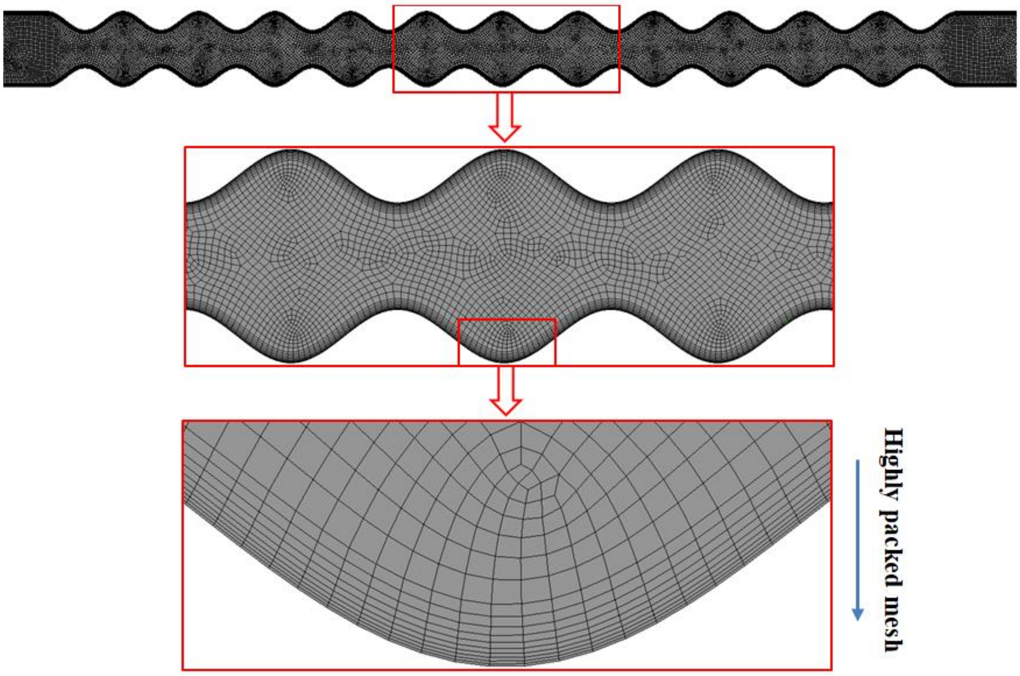

Figure 3.4. The utilized mesh topology with an enlarged view of the wavy wall.

As depicted in Figure 3.4, an unstructured triangular grid was adapted to mesh the flow domain of the corrugated channel. As shown from the zoomed view of Figure 3.4, the mesh was inflated with several uniform layers adjacent to the solid-liquid interfaces of the corrugated channel in order to meet the requirement of the boundary layer thickness (y+ < 1).

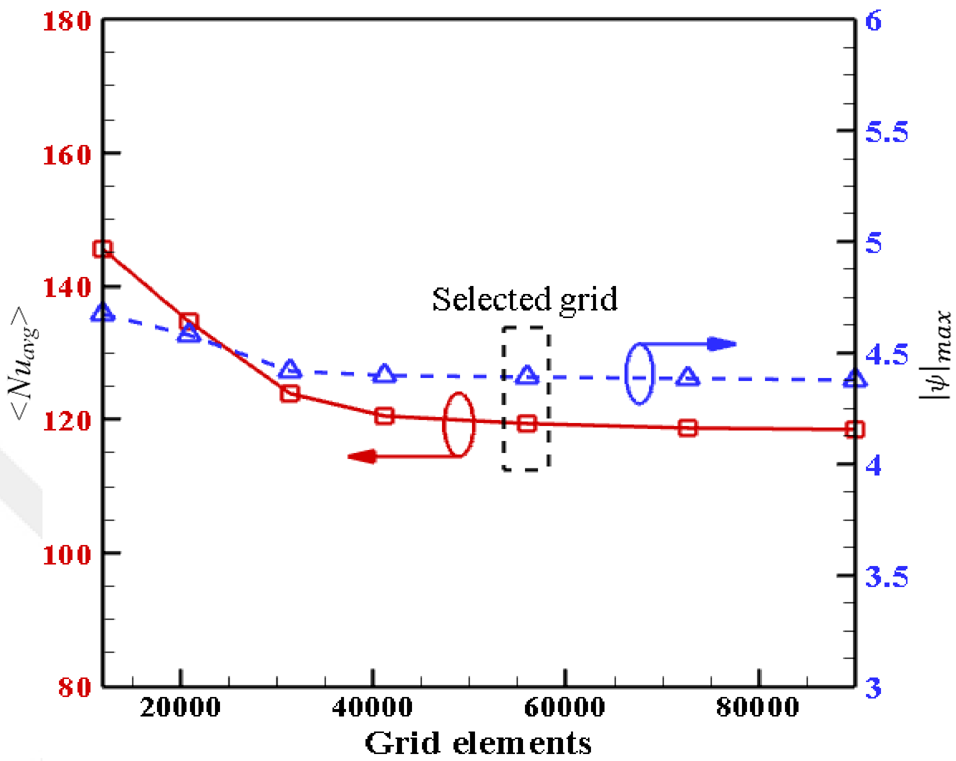

Figure 3.5. Grid reliability test for SWCNT-water nanofluid flow at an inlet steady flow, *Re*=7000, φ=3% and θ=0^o using DPM.

A mesh reliability check is conducted to ensure that the numerical outcomes are not affected by the element number of the grid. Six different meshes with growing elements from 11858 to 90083 are considered to conduct this check. Figure 3.5 displays the Nusselt number for each mesh size with a percentage error in between. Results of average Nusselt number were tested for *Re*=7000, φ=3% and θ=0^o using SPM. The obtained data in Figure 3.5 exhibited that the percentage error between the mesh elements of 55884 and 72672 is barely 0.2%. As such, the mesh with 55884 elements is taken into account for the remainder of the simulations in this article. It should be mentioned that the mesh is also examined with all considered phase shifts for various parameters of the turbulent flow regime, but their data are not involved in the current section for brevity.

3.10. Code validation

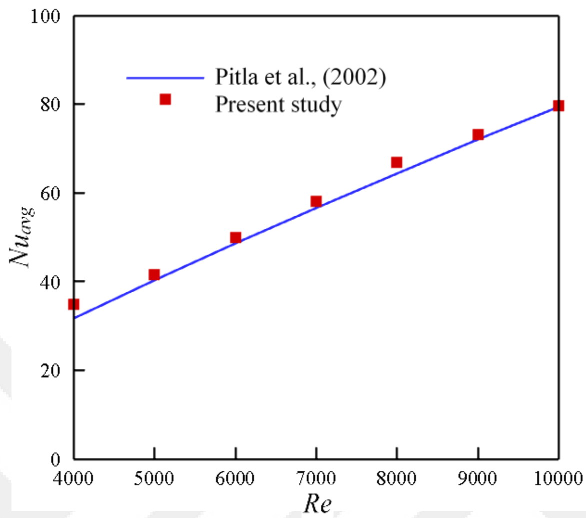

Figure 3.6. Comparison of the average Nusselt number, $Nu_{avg}$of the current numerical simulation with that obtained from the Gnielinsky correlation in a smooth heated channel.

To verify the dependability of the used numerical code and the above-mentioned solution procedure, forced convection water flow inside a smooth heated channel was examined. Figure 3.6 exhibits a comparison of the average Nusselt number, Nu_{avg} of the present code against an available correlation of Gnielinsky (Pitla et al., 2002). This figure reveals that the numerical outcomes of this work are consistent with those taken from the experimental data. Another verification test was carried out for turbulent flows of water in a corrugated channel. Figure 3.7 lists a comparison of the average Nusselt number, Nu_{avg} and friction factor, f of the current code with the experimental and numerical investigations of Kurtulmuş et al., (2020) in a sinusoidal channel. Also, this figure exhibits good accordance with experimental and numerical outcomes.

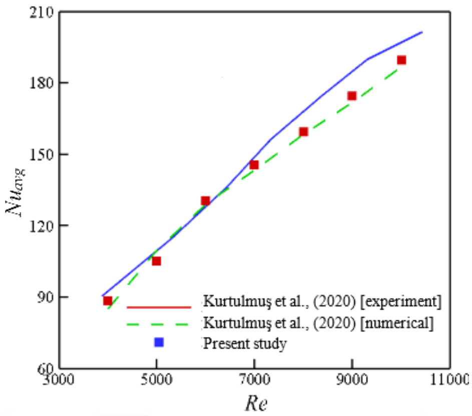

(a)

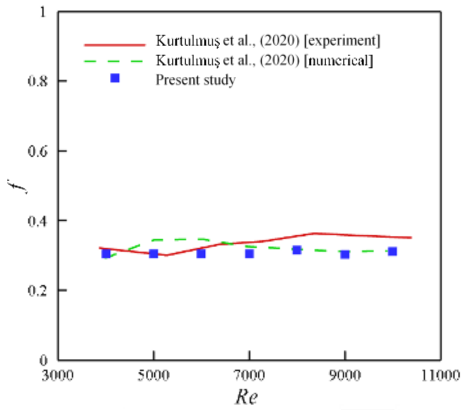

(b)

Figure 3.7. Verification of the current code for water flow in a sinusoidal channel with that obtained from the investigation of Kurtulmuş et al., (2020), (a) average Nusselt number, Nu_{avg} and (b) friction factor, f.

For the pulsating flow, the time-averaged Nusselt number, $<Nu_{avg}>$ of pulsating flow structures for pure water through a heated sinusoidal channel has been determined and compared with the experimental investigation of Kurtulmuş and Sahin, (2020). As documented in Figure 3.8, there is an acceptable consistency between the compared data. Further, the average Nusselt number, Nu_{avg} for Al_2O_3-water flow in a circular heated tube using both SPM and DPM was also determined and compared with CFD codes of Bianco et al., (2009) and Maïga et al., (2005). As illustrated in Figure 3.9, the presented data are in good agreement. In conclusion, the detected acceptable consensus between the results of the implemented numerical code and available numerical and experimental data confirms the trust in the current numerical analysis. Therefore, we can safely utilize the current CFD model.

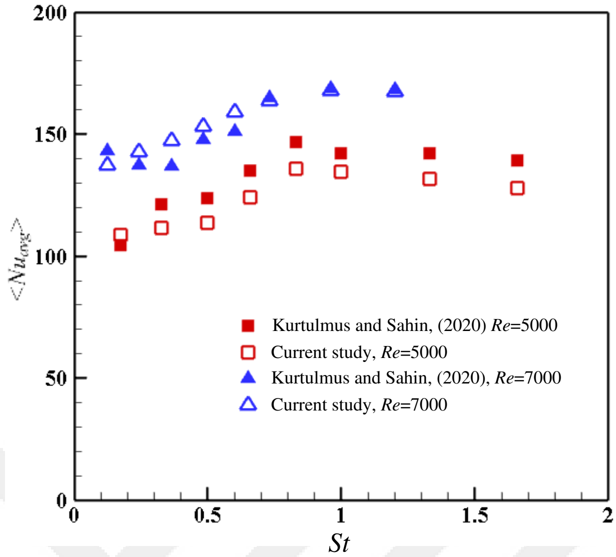

Figure 3.8. Numerical results of the average Nusselt numbers, Nu_{avg} together with the Strouhal numbers, *St* compared with the available data given from the experimental work ofKurtulmuş and Sahin, (2020).

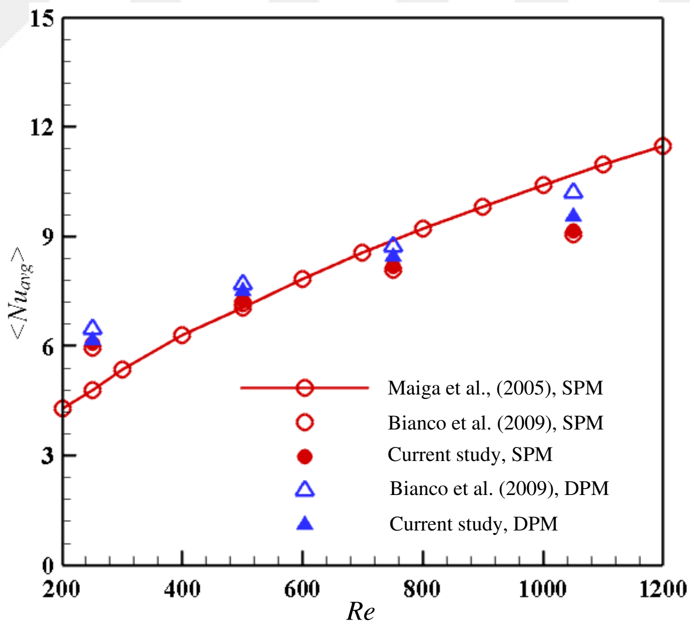

Figure 3.9. Comparison of the current CFD code for both SPM and DPM with regard to average Nusselt number with those obtained from investigations of Maïga et al., (2005)and Bianco et al., (2009).

4. RESULTS AND DISCUSSION

The simulations are implemented to compute the influence of steady flow, pulsation frequency, f, Reynolds number, Re and SWCNT concentration, φ on thermal-hydrodynamic and entropy production mechanisms for SWCNT-water nanofluid flow through a sinusoidal wavy channel having different phase shift, θ. In this regard, the CFD calculations are performed for a wide range of these parameters as follows: ($1 \leq f \leq 5$), (for steady flow: $4000 \leq Re \leq 10000$ and for pulsating flow: $4000 \leq Re \leq 7000$), ($0\% \leq \varphi \leq 3\%$), ($0^{o} \leq \theta \leq 180^{o}$) as well as steady flow conditions. SPM and DPM were considered for nanofluid flow. Since there are twelve waves on the heated walls of a wavy channel, it is not easy to show the flow mechanisms over the entire channel. Therefore, for the purposes of presentation and comparison, the numerical results obtained from the current CFD code for contour lines are presented at three observation locations of the wavy channel (i.e., sec-1, sec-2 and sec-3) as shown in Figure 3.1 (e).

4.1. Steady flow results

First, the simulations for pure water flow in a wavy channel were presented and analyzed to evaluate the influence of phase shifts on thermo-hydraulic performance and entropy generation. This is followed by comparing the performance and irreversible processes according to the considered phase models of nanofluid. Hence, in this section, the presented findings will be divided into two subsections in accordance with the effects of the geometric structure with Reynolds number and phase model with nanoparticle concentrations of nanofluid.

4.1.1. Effect of phase shifts and Reynolds number

Inside channel-limited flows, surface corrugations produce longitudinal and transversal circulation zones that induce the thermal boundary layer to become unstable and improve the flow mixing. These corrugations act as motivators of instability and can cause flow turbulence. Therefore, the effects of phase shift variations (i.e.,θ=0°, θ=90° and θ=180°) on hydrothermal indexes and entropy generations are depicted by means of contour plots in this section.

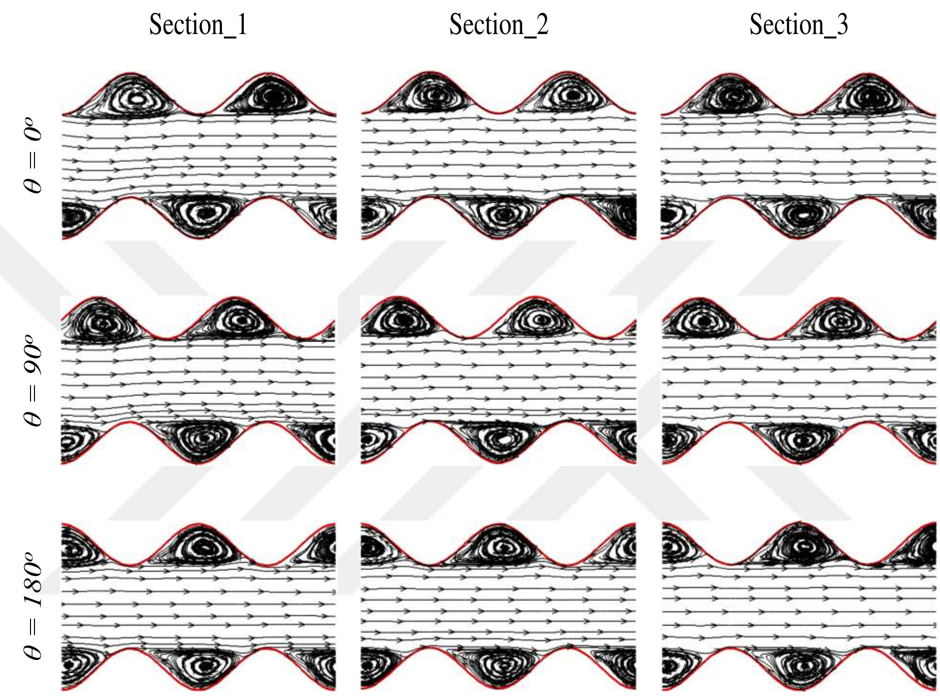

Figure 4.1. Contour lines of stream function, ψ for SWCNT-water nanofluid and various phase shifts, θ at Re=7000 and φ=3%.

Figure 4.1 displays the distribution of stream function, ψ under the above-mentioned parameters.After the water flow exceeds the upstream section, the reversal flow appears adjacent to the upper and lower walls of the channel due to the high-pressure drop penalty in the diverging part of the wave. This results in the formation of secondary flow regions in each diverging part along the test section. The structure of these regions comprises a viscous interaction between the primary recirculation zone and the wavy walls. For all phase shifts, θ, the topology of the stream function, ψ declares that the upper circulation zones rotate anticlockwise while the lower circulation zones rotate clockwise. For θ=180°, all circulation zones with their saddle points are symmetric relative to the axial direction of the wavy channel since the walls of this phase have the same sinusoidal profile. Although there is no clear difference between the centers of these circulation zones within the waves along the channel, but, there is slight alteration with the phase shift, θ configurations. Where the central positions of θ=0^{o} are slightly lower than that of θ=90^{o} and θ=180^{o}.

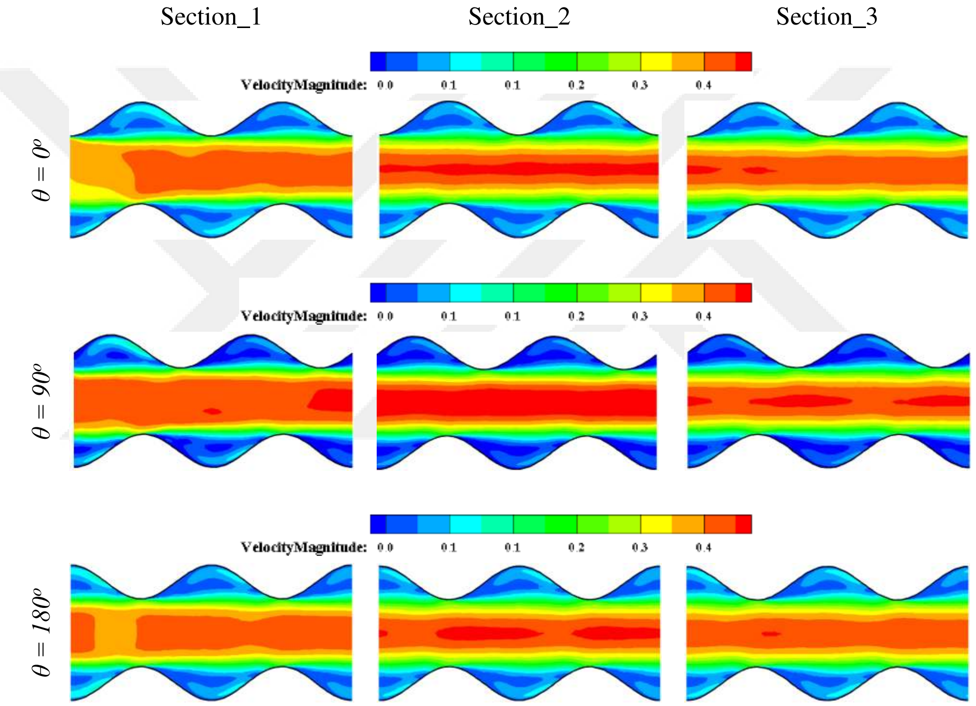

Figure 4.2. Contour lines of velocity vector, $\vec{V}$for SWCNT-water nanofluid and various phase shifts, θ at *Re*=7000 and φ=3%.

From the distribution of velocity vector, $\vec{V}$in Figure 4.2, it is distinctly observed that the water flow cannot maintain the uniform profile of the boundary layer as a result of the gradual convergent-divergent walls of the channel. Namely, velocity distributions within the wavy channel are not uniform like the straight channel. The deep blue color in both the top and bottom regions of the expansion section represents negative velocity magnitudes, as shown from the labels attached above their contours. In contrast, the flow with red color along the core region of the channel has positive high-velocity magnitudes. As will be illustrated in the next figures, these differences in velocity magnitudes contribute to an increment in heat transfer and frictional entropy generation. Despite there is no remarkable distinction between the velocity distributions of the 2nd and 3rd sections for all the presented phase shifts, θ. However, there is a considerable change in the velocity contours of the 1st section compared to other sections.

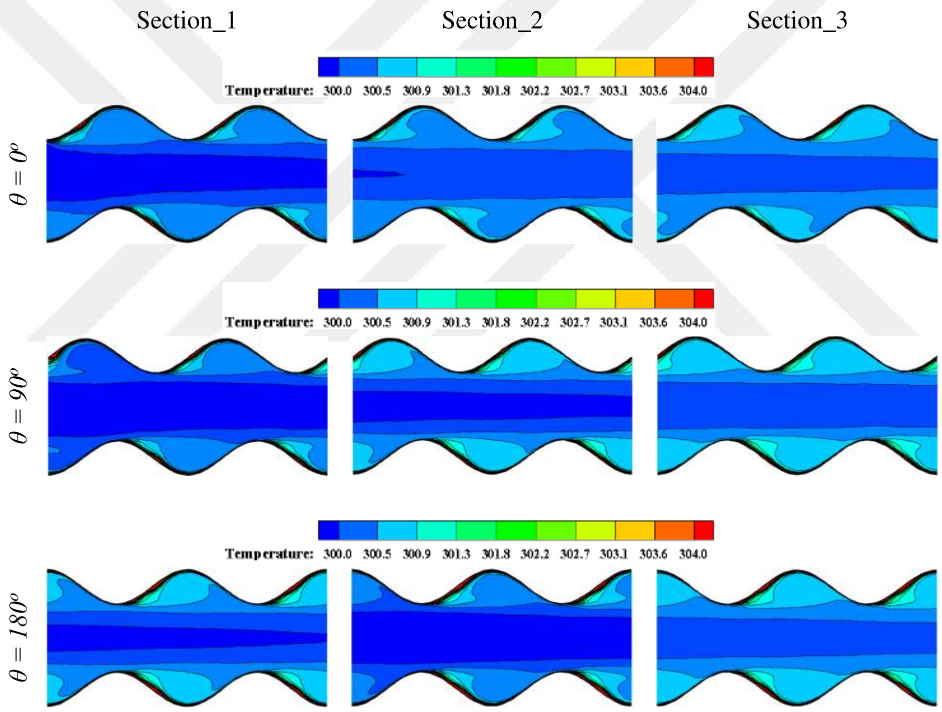

Figure 4.3. Contour lines of temperature, T for SWCNT-water nanofluid and various phase shifts, θ at Re=7000 and φ=3%.

From the temperature distributions, T in Figure 4.3, it was observed that the temperature gradients adjacent to the wavy walls are higher than the other regions of the channel for each configuration of θ. This is due to the effects of circulation zones within the waves that enhance the water mixing between the cold central region and the heated test section. Moreover, the influence of these zones on the temperature contours of θ=0^{o} is more obvious compared to θ=90^{o} and θ=180^{o}. The thinnest region of the thermal boundary layer places adjacent to the contraction portion of the groove. Like the stream function, ψ distributions, temperature distributions, T also have a symmetric structure relative to the central axis of the wavy channel for θ=0^{o}. Further, the thermal boundary layer in the 1st section is thinner than in any sections along the wavy channel.

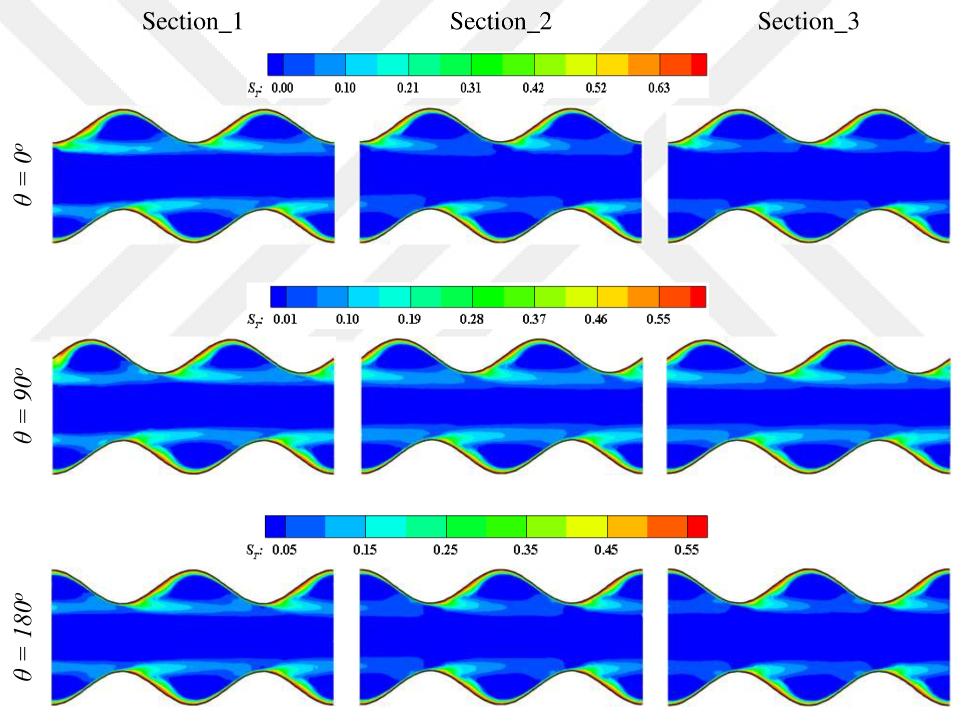

Figure 4.4. Contour lines of total entropy generation S_T for SWCNT-water nanofluid and various phase shifts, θ at Re=7000 and φ=3%.

From the total entropy generation, S_T lines in Figure 4.4, it is seen that the high values of S_T occur noticeably adjacent to the top and bottom heated walls of the channel. This is due to the high intensity of temperature and velocity gradients in these areas, as illustrated in Figures 4.1 and 4.2. As these walls are exposed to the uniform heat flux, entropy generation due to the thermal irreversibility is more than the frictional irreversibility for all configurations of θ. As expected, the values of entropy production in the central region of the channel are close to zero. Each wave has a zone with a low entropy production value. As displayed in Figure 4.1, a secondary flow region is formed in each wave of the channel. This limits the touch between the water and the heated wall and therefore reduces the temperature gradient. Accordingly, the thermal entropy generation drops remarkably in this region. Frictional irreversibility usually accumulates in narrow sections of the wavy channel. As previously explained, these areas create strong resistance to the fluid flow and induce larger viscous irreversibility. Finally, it can be observed that the maximum value of the total entropy generation is ordered as $\theta = 0^o > \theta = 90^o > \theta = 180^o$, respectively.

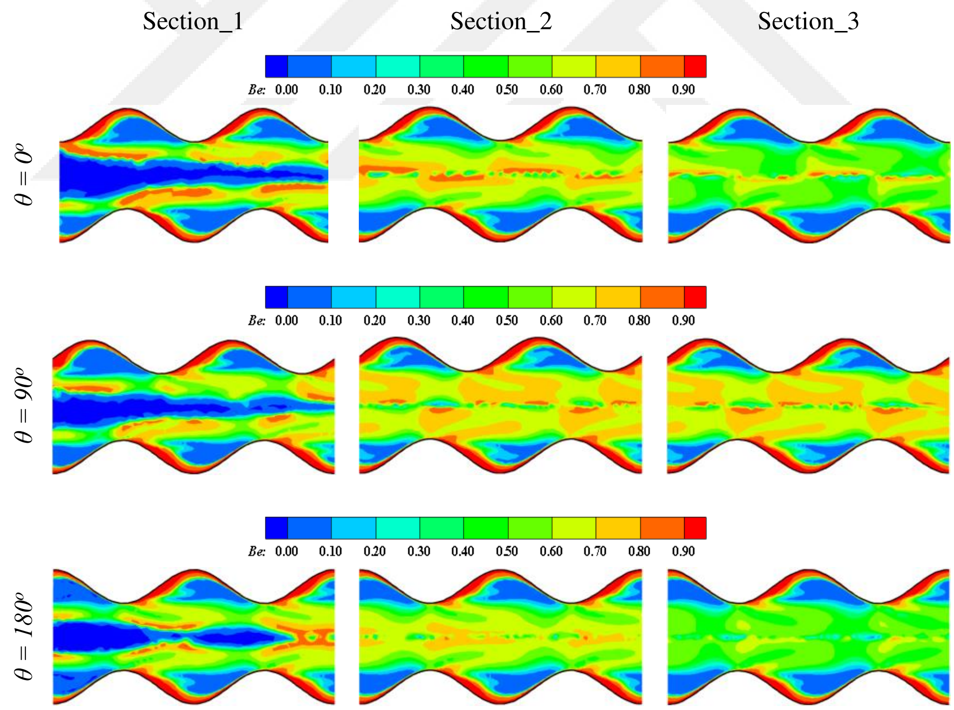

Figure 4.5. Contour lines of Bejan number, *Be*for SWCNT-water nanofluid and various phase shifts, θ at *Re*=7000 and φ=3%.

Figure 4.5 depicts the Bejan number, *Be* contours for different configurations of θ. It is worth mentioning that the Bejan number, *Be* is represented as a percentage of thermal irreversibility to the total irreversibility process during the flow domain. Therefore, this percentage ranges from 0 to 1. Thermal entropy generation predominates for the *Be* close to one, while friction entropy generation is dominated for the *Be* close to zero. As exhibited from *Be* plots, thermal entropy generation is predominant along the heated wavy walls due to high-temperature gradients in this channel region. The high value of the *Be* contour relatively presents a thickening of the thermal boundary layer. This develops toward the downstream direction and occupies most regions of the 3rd section. The high-temperature gradient within this layer confirms the thermal entropy and accordingly increases the value of the *Be*. Nevertheless, viscous irreversibility predominates only at the channel entrance as a result of high-velocity gradients within the developing flow region.

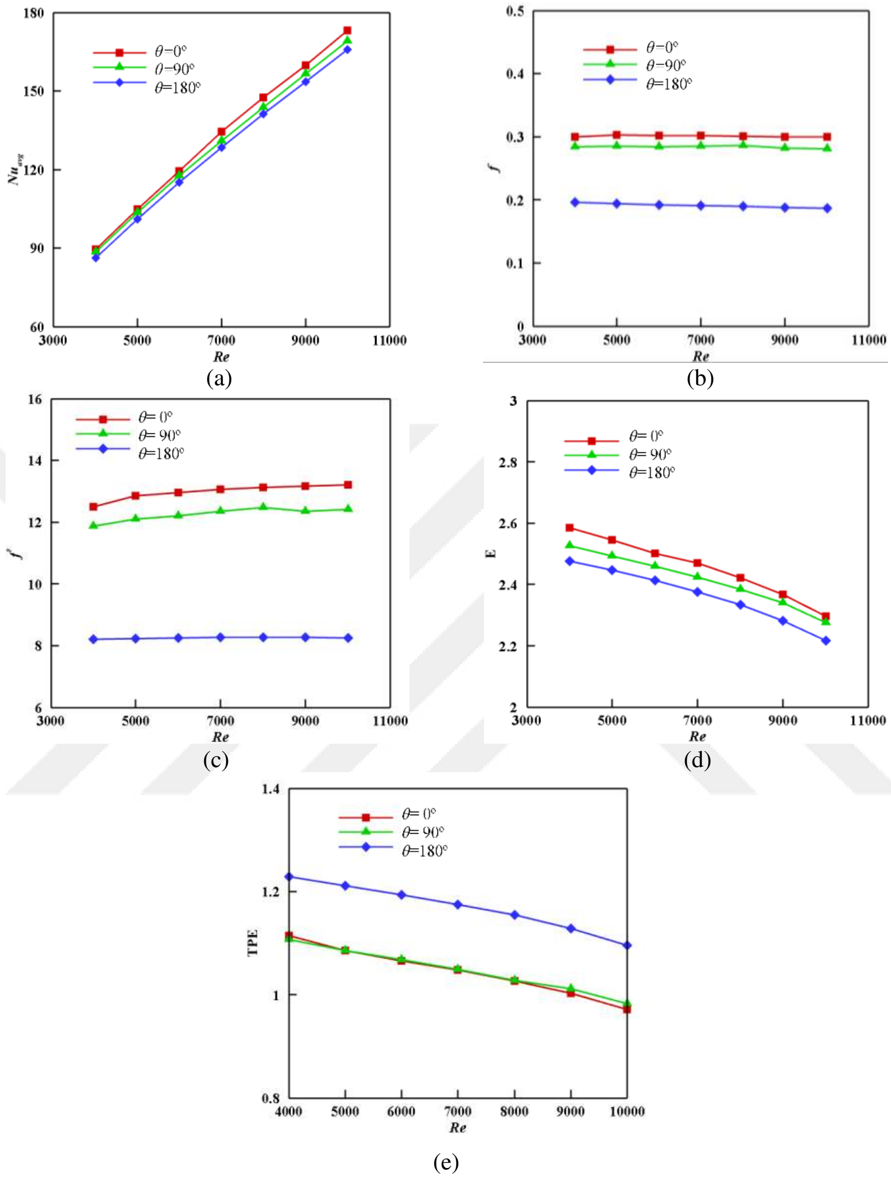

Figure 4.6 Different phase shifts, θ influence of corrugated channel for water flow at various Reynolds number, *Re* on: (a) average Nusselt number, Nu_{avg}, (b) friction factor, *f*, (c) relative friction factor variation, *f**(d) thermal enhancement, *E* and (e) thermal performance factor, *TPF*.

Figure 4.6 explores the effect of various phase shifts, θ on thermal-hydraulic behaviors for pure water (φ=0) using quantitative results. For this purpose, three different configurations (i.e., θ=0^o, θ=90^o and θ=180^o) and smooth channels in turbulent flow regimes were compared. The variations of the average Nusselt number, Nu_{avg} versus the considered limitations of the Reynolds number, *Re* is manifested in Figure 4.6 (a). As expected, this figure shows that Nu_{avg} grows with an increase in flow velocity for all configurations. This is because the turbulent intensity and, accordingly, convection heat transfer augments with an increment in *Re*. At *Re* = 4000, the Nu_{avg} values are approximately the same for all configurations, while with an increase in *Re*, some variations are noticeable. However, among the phase shifts, θ=0^o has a relatively high Nu_{avg} value, while θ=180^o has the lowest Nu_{avg} value. This is because the recirculation zones of θ=0^o are stronger than other configurations, as illustrated in Figure 4.1, so they can provide better flow mixing with the heated walls. The variations of friction factor, f versus the turbulent flow regime of the Reynolds number, *Re* is reported in Figure 4.6(b). According to this figure, the friction coefficient, f is almost stable with varying *Re* for all cases of θ, which shows that common inertial losses are efficient. Nevertheless, this coefficient is quite sensitive to the alteration of the channel configuration. As it is evident that the wavy channel with θ=180^o represents the lowest pressure drop penalty among other configurations. This occurs because the wavy walls of θ=180^o interrupt the flow of water less than the other geometries. Changes in these values of friction coefficients, f are important for designing thermal systems and estimating the operating costs. According to Figure 4.6(c), the trends of the relative friction factor, $f^*$with the variation in *Re* are quite close to those data displayed in Figure 4.6 (b) for all configurations. As clearly seen, the relative friction factor, $f^*$is slightly influenced by changing the flow velocity at θ=180^o. For θ=0^o, the wavy configuration causes a noticeable increase in the friction coefficient compared to the straight channel, by about 13% for *Re* = 10000. The profile of the heat transfer enhancement, E is depicted in Figure 4.6 (d). It can be stated that wavy channels are an active tool for improving thermal transport with a boundary layer destruction mechanism. The numerical result revealed that for all phase shifts, θ the magnitudes of E have a fairly same tendency in the investigated turbulent flow regime. The channel with zero phase shift, θ provides a marginally higher heat transfer enhancement compared to other channels. In addition, the E is reduced gradually by increasing Re. As it is seen, the best heat transfer enhancements are achieved at the low Re. For instance, 2.58%, 2.52%, and 2.47% improvements are seen for θ=0^o, θ=90^o and θ=180^o, respectively, at Re=4000 in comparison with the smooth channel. Figure 4.6 (e) reports the thermal performance factor, TPF profile. The figure obviously indicates that the TPF decreases with increasing the Re; this indicates that the optimal Re is related to the maximum TPF for each channel. The optimum flow velocity corresponds to the Re = 4000 for all examined geometries. For θ=180^o, the high values of TPF are due to the low relative friction factor, f^*, as shown in Figure 4.6 (c).

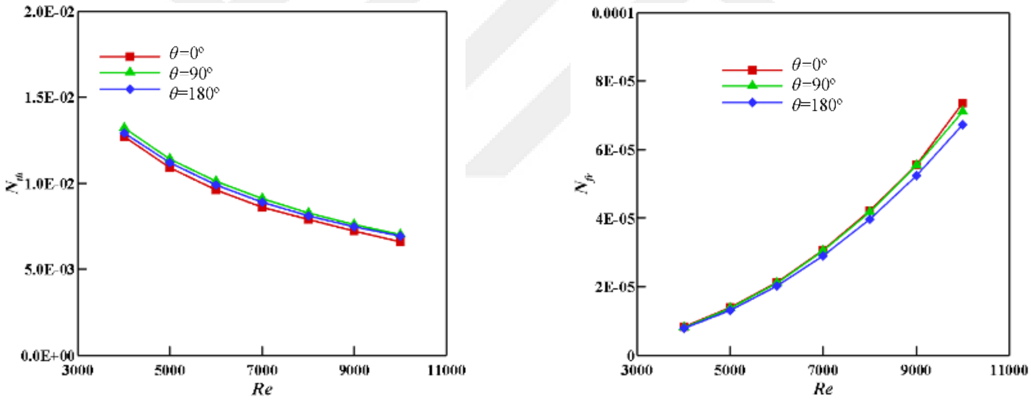

(a) (b)

Figure 4.7. Different phase shifts, θ influence of corrugated channel for water flow at various Reynolds number, Re on: (a) dimensionless thermal entropy generation, N_{th}, (b) dimensionless frictional entropy generation, N_{fr}.

Figure 4.7 (a) reports the changes of the integrated thermal entropy generation, N_{th} with the Reynolds number, Re for various configurations at φ=0. The numerical results indicate that increased Re remarkably reduces the N_{th} for all configurations. For example, a decreases in N_{th} by 93%, 88% and 86% is found for θ=0^o, θ=90^o and θ=180^o, respectively, at Reynold numbers between 4000 and

10000. As mentioned earlier in Figure 4.6(a), this increase in the *Re* leads to an increase in heat transfer rate. This situation changes the gradients of temperature within the flow domain and, as a result, causes a reduction in heat transfer irreversibility. In addition, the results revealed that the corrugated channel with θ=0^o produces marginally the highest N_{th} compared to other channels. Figure 4.7 (b) displays the changes of the integrated frictional entropy generation, N_{fr} with the Reynolds number, *Re* for various configurations at φ=0. In contrast to the trend of N_{th} indicated in Figure 4.7 (a), the N_{fr} significantly augments with an increment in the *Re*. For instance, an increase in N_{fr} values by 90%, 88% and 87% is obtained for θ=0^o, θ=90^o and θ=180^o, respectively, in between *Re*=4000 and *Re*=10000. As illustrated in Figure4.3, this increment in *Re* causes an increase in velocity gradient within the flow domain and, accordingly, generates extra frictional irreversibility. Moreover, it can be stated that the wavy channel with θ=180^o possesses the lowest N_{fr} among the other configurations.

4.1.2. Effect of phase model and nanoparticle concentration

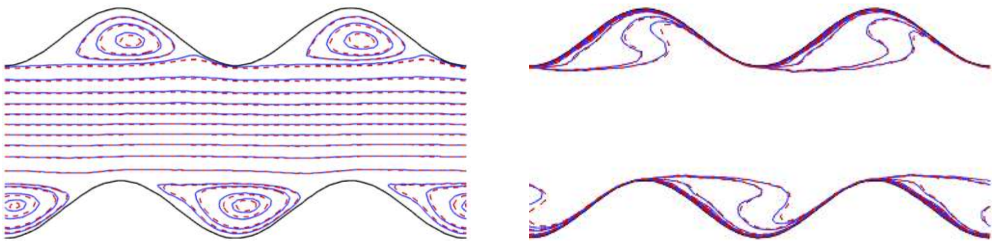

(a) (b)

Figure 4.8. Comparison between base fluid φ = 0 (—) and SWCNT-water nanofluid φ = 3%(---), from the point of view of (a) stream function, ψ, and (b) temperature lines, *T* at *Re* = 7000 and θ= 0^o.

The thermal-hydraulic indexes of the pure water (φ=0) and two-phase flow (*DPM*) of CNT-water nanofluid (φ=3%) in terms of stream function, ψ and temperature, *T* lines are exposed in Figure 4.8 at *Re*=7000 and θ=0. Fluid flow for pure water and nanofluid is represented by blue solid lines and red dashed lines, respectively. As displayed in this figure, the flow and thermal behaviors of the pure water are very close to the prophecy of the nanofluid. This is because the impacts of boundary conditions and geometric shapes are bigger than the variation between their thermo-physical properties. On the other hand, the variations between them are more obvious according to their rate of heat transfer, as well explained in the coming figures.

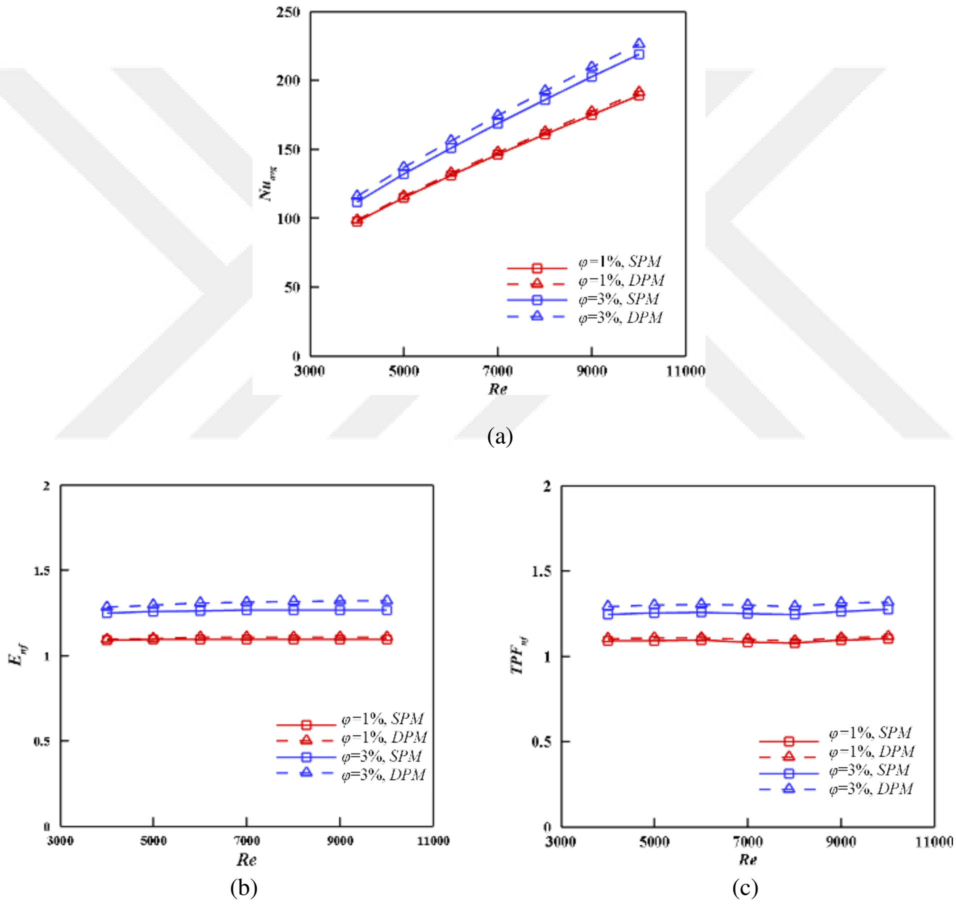

Figure 4.9. The influence of various nanofluid models and volume fractions at various Reynolds number, *Re* in a corrugated channel with a phase shift of $\theta = 0^{o}$on (a) average Nusselt number, Nu_{avg}, (b) thermal enhancement, E_{nf} and (c) thermal performance factor, TPF_{nf}.

Figure 4.9 demonstrates the impact of the nanoparticle concentrations with various phase models on the average Nusselt number, Nu_{avg}, thermal enhancement, E_{nf} and the thermal performance factor, TPF_{nf} at $\theta = 0^o$. In general, the values of Nu_{avg}, E_{nf} and TPF_{nf} are improved for both presented models by suspending nanoparticles and increasing their concentration. With the help of Figure 3.3, this can be clarified by observing that the thermophysical of base fluid enhances due to the dispersing solid particles having high thermal conductivity. In the case of the two-phase approach (DPM), where the effects of forces acting on nanoparticles are considered, there is a higher increment in these magnitudes compared to the single-phase approach (SPM), particularly at high nanoparticle concentration, φ=3%. For example, a difference of 12.3% is found in Nu_{avg} between homogenous (SPM) and discrete (DFM) phases when φ=3%. According to Figure 4.9(a), the Nu_{avg} is significantly affected by increasing *Re*. As illustrated previously, this is due to a reduction in the thickness of the thermal boundary layer, as a result, the temperature gradient near the heated walls increments. It is also recognized that the discrepancy in Nu_{avg} between φ=1% and φ=3% is more evident at high Reynolds numbers, *Re*. For the two-phase model (DPM), the Nu_{avg} augments by about 16% at the *Re*= 4000 when the volume fraction, φ augments from 1% to 3%, while this augmentation is about 20% for the *Re*= 10000. In Figure 4.9 (b) and (c), the values of $E_{nf}$and TPF_{nf} have similar trends within the studied range of *Re*. Moreover, they are slightly affected by changing the *Re*.

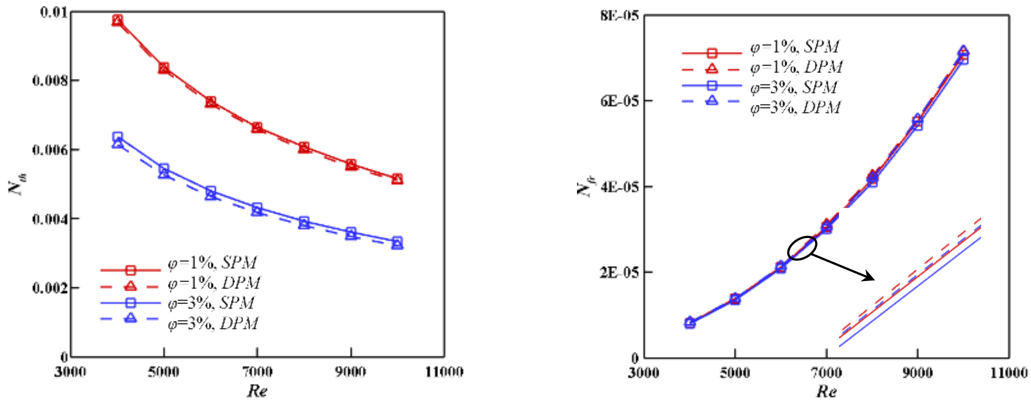

(a) (b)

Figure 4.10. The influence of various nanofluid models and volume fractions at various Reynolds number, *Re* in a corrugated channel with a phase shift of θ= 0°on: (a) dimensionless thermal entropy generation, N_{th}, (b) dimensionless frictional entropy generation, N_{fr}.

Impacts of phase model and nanoparticles concentration of SWCNT-water nanofluids on thermal, N_{th} and frictional, N_{fr} entropy productions are given in Figure 4.10 for turbulent flow regime at θ=0°. Figure 4.10 (a) states that the N_{th} decreases with increasing particle concentrations, φ for all phase models along with the considered turbulent regime. The differences between them are more noticeable for low *Re* compared to high *Re*. The improvements in thermal transmission caused by the use of nanofluids, especially those with a high φ, are responsible for this reduction in thermal irreversibility. In addition, this decrement is more dependent on the concentration of particles in the nanofluid than on the phase model. In Figure 4.10 (b), the change in the N_{fr} is much more detectable with an increase in the *Re* than with an increase in φ. This is due to the stronger influence of *Re* on the velocity gradient compared to the parameters of nanofluid.

4.2. Pulsating flow results

4.2.1. Effect of pulsation frequency and Reynolds number

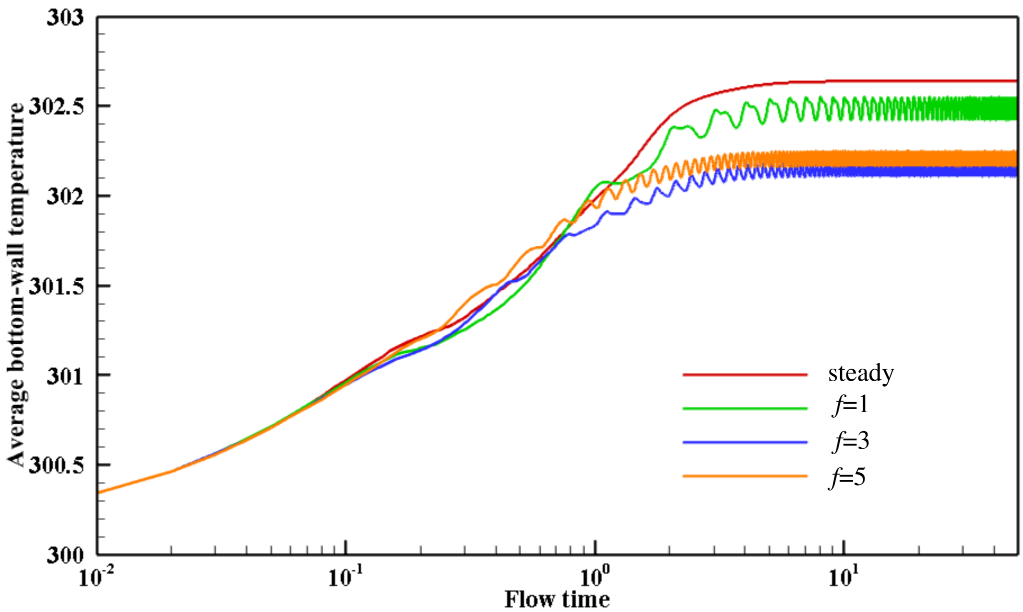

Figure 4.11. Variation of the average bottom-wall temperature with flow time at steady flow and different pulsation frequencies for *Re*=6000, φ=0 and θ=180°.

Figure 4.11 presents the average bottom-wall temperature variation and flow time for three different pulsation frequencies and steady flow. For all cases, it can be noted that the average values of temperature gradually increase with time until it reaches a stable state at about *t*=10. The figure shows that the inlet velocity profile has clear influence on the average temperature values. Similar to the inlet pulsating flow, the temperature decreases during the deceleration phase and increases during the acceleration phase. Moreover, it is obvious that even the highest value of the average temperature for the inlet pulsating flow is lower than that of the inlet steady-state flow. Thus, the time-averaged temperature for steady flow is always higher than that of pulsating flow. During the simulations, a time step size of $\Delta t = 0.001$ is utilized. It was verified that all phase models and channel configurations accomplished steady-state conditions between t= 50-100; thus, all current results have been presented within this period. After this time, at least the average of 2-4 pulse periods was calculated to obtain accurate data for time-averaged quantities.

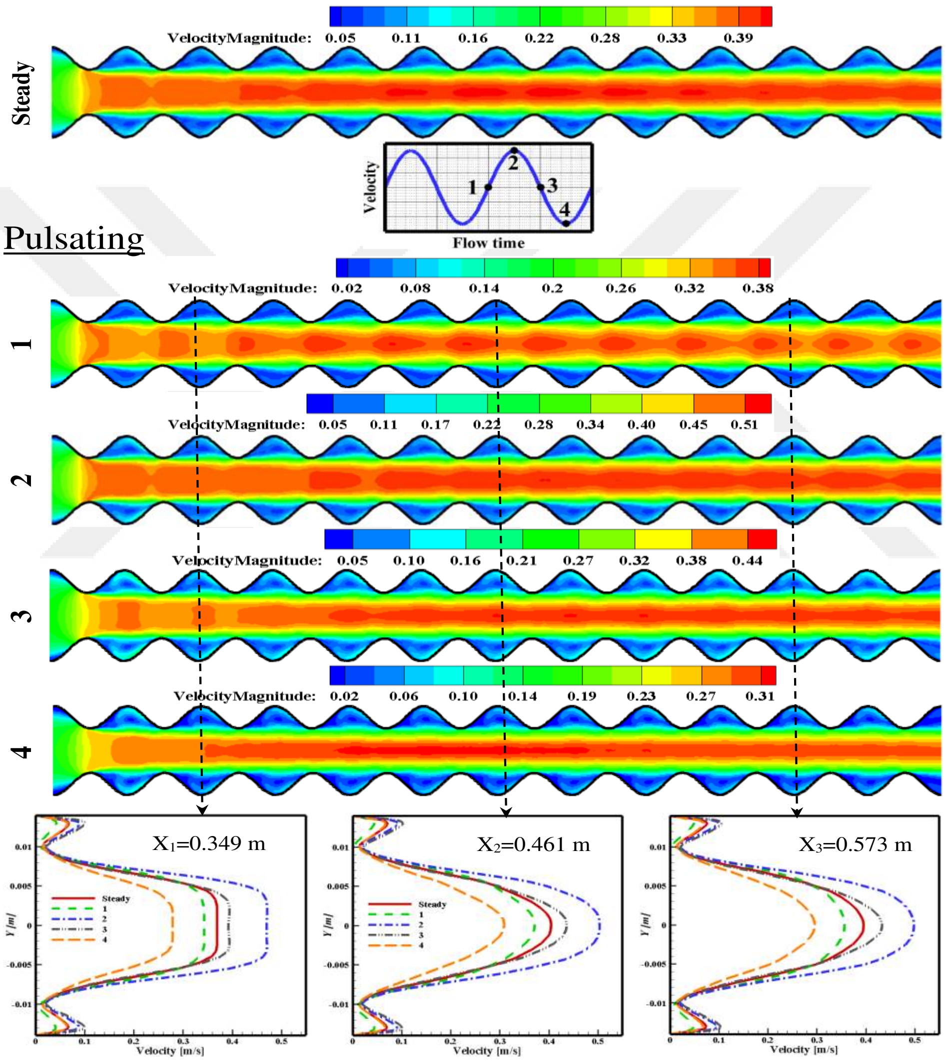

Figure 4.12. Contour lines of instantaneous velocity magnitude, $\vec{V}$ in terms of steady flow conditions and four various time steps within one period of pulsating flow for SPM of SWCNT-water nanofluid atRe=7000, f=1, φ=3% and θ=180°.

To illustrate the overall flow structures under inlet pulsating profile, Figure 4.12 depicts the contour lines of the instantaneous velocity magnitude, $\vec{V}$at four various time steps for Re=7000, f=1, φ=3% and θ=180°. These steps (i.e. 1, 2, 3 and 4) correspond to four different phase angles in one period of pulsating flow. Further, the result of steady inlet flow was introduced in the first row of this figure as a reference case for comparison. In the case of steady flow, velocity distribution provides similar behavior after the 4th wave of the channel. In contrast to this behavior, the velocity distribution of the pulsating flow detects more unsteady behavior with acceleration zones. The velocity values of the 2nd and 3rd-time steps are always higher than the reference case, while these values for the 1st and 4th-time steps are always lower than the reference case. Therefore, the impacts of the pulsating profile on the flow field within the wavy channel are perceptible in this figure. Taking into account the geometric peculiarities of corrugated channels, it is credible that the oscillating input velocity creates various flow structures within these types of channels, resulting in observable changes in the thickness of the thermal boundary layer. It can be seen from the low values of the velocity that there are vortices restricted inside the waves. In the case of an inlet pulsating flow, the exchange between these vortices and the core of streamflow is stronger than that of the steady inlet flow. In addition, the flow patterns for a specific time step within one period of pulsating flow are quite different from another time step.

When the flow inters to the corrugated channel, the boundary layer breaks from the channel walls as a result of the unfavorable pressure drop. Namely, the momentum of flow layers adjacent to the channel walls can not exceed the pressure recovery inside these grooves. Afterward, the momentum of the flow predominates to restore the pressure in converging parts, which leads the boundary layer to reattach with channel walls. As a result, the vortexes create in each wave along the channel. In addition, the pulsating flow adds additional flow resistance to the main streamflow, which improves the flow mixing between the core and the heated walls. This resistance mainly depends on the pulsation frequency. Therefore, pulsating frequency's effect on hydrothermal and entropy production is presented and compared with the inlet steady flow using contour lines in Figures (4.13)-(4.18). All these figures are offered for SWCNT-water nanofluid flow (φ=1%) at three observation sections (i.e., sec-1, sec-2 and sec-3) along the channel for Re=5000 and θ=180^o.

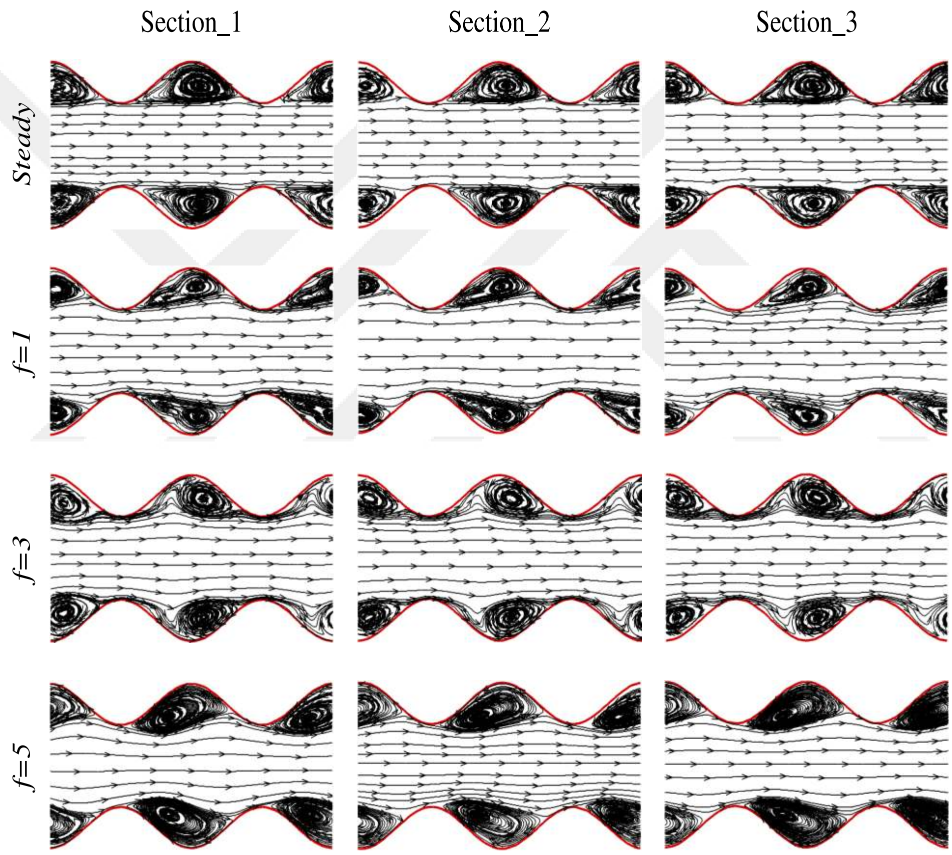

Figure 4.13. Contour lines of time-averaged stream function, <ψ> for SPM of SWCNT-water nanofluid at steady inlet flow and various pulsating frequencies, f under fixed values of Re=5000,φ=1% and θ=180^o.

Figure 4.13 shows the patterns of the time-averaged stream function, $<\psi>$ for the aforementioned parameters. For all flow conditions, the time-averaged stream function, $<\psi>$ graph shows that there are two vortices rotating in opposite directions within each wave. The upper one rotates counterclockwise while the lower one rotates clockwise. The size, position and morphology of these vortices are different for each flow condition. However, the distribution of $<\psi>$ has an almost symmetric behavior along the central axis of the wavy channel for both steady and pulsating flow. Despite the fact that there is no obvious variation in the saddle points and centers of these vortexes between waves along the channel, but, there is a clear variation with changing the value of pulsation frequency, f. In the case of inlet steady flow, the vortex occupies most of the diverging area of the wave for all the presented sections. For f = 1, the size of the vortex decreases and its center moves to the channel surface. In other words, it covers the upper left side of the wave. While for f=3, the center point of the vortex moves downstream, and its size covers the right half of the wave. At a high pulsation frequency (f = 5), this vortex moves upstream, and its center approaches from the axis of the channel. Further, the maximum absolute value of $<\psi>$ is detected at f = 3.

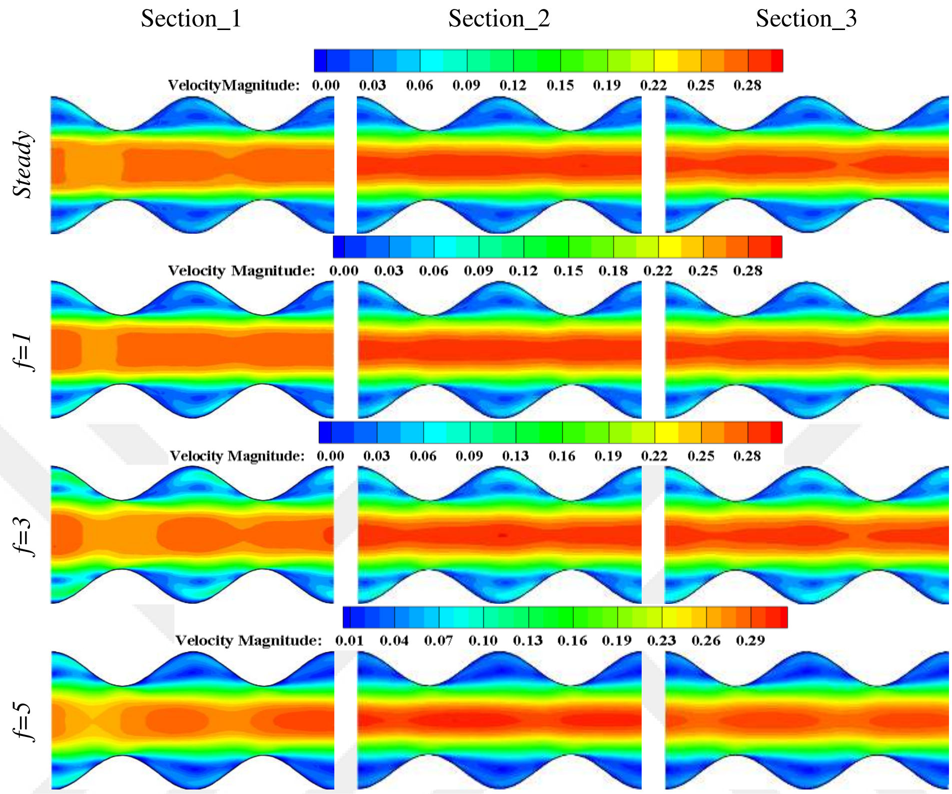

Figure 4.14. Contour lines of time-averaged velocity magnitude, $<\vec{V}>$ for SPM of SWCNT-water nanofluid at steady inlet flow and various pulsating frequencies, f under fixed values of Re=5000,φ=1% and θ=180°.

The distribution of the time-averaged velocity magnitude, $<\vec{V}>$ is presented in Figure 4.14. In general, the high-velocity region remains centered along with the centerline of the channel. The opposite occurs in wave regions along the channel, where the flow velocity is low. This behavior is directly related to that presented in Figure 4.13 for $<\psi>$, where the low-velocity region appears in the same position as the reversal flow occurs. Along the wavy channel, it is seen that $<\vec{V}>$ at the entrance section (section-1) is lower than the other sections (i.e., section-2 and section-3) of the channel. This is due to the increase in flow acceleration in the downstream direction. Further, it can be seen from this figure that by applying the pulsating flow, the values of the low-velocity region within the waves increase slightly compared to that of the reference case.

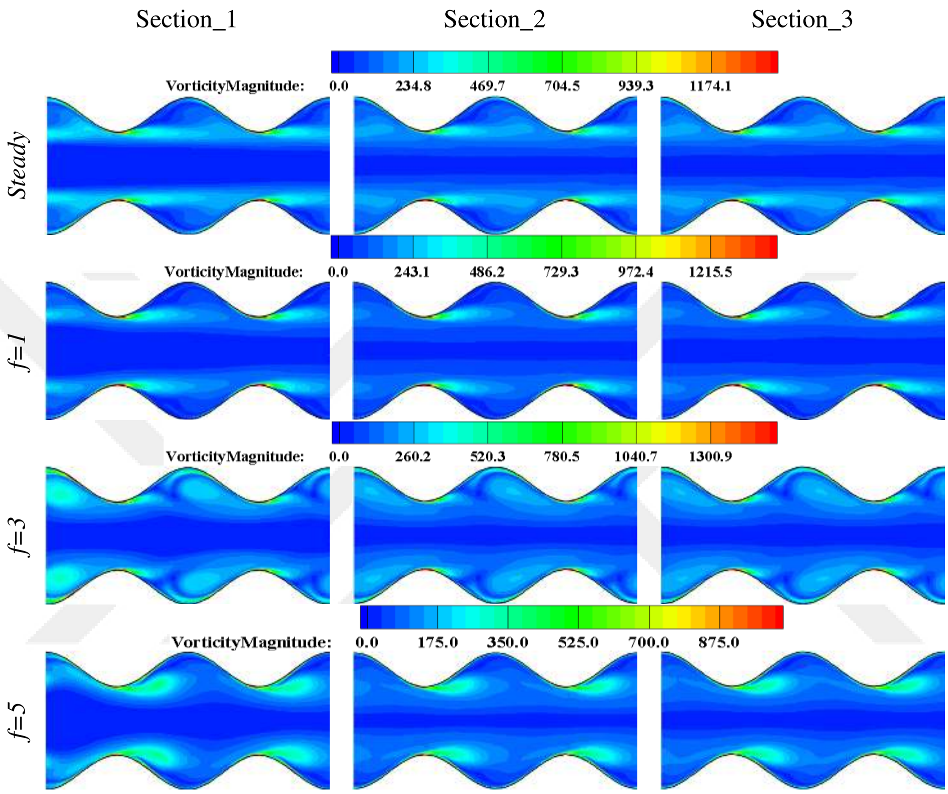

Figure 4.15. Contour lines of time-averaged vorticity magnitude, <ω> for SPM of SWCNT-water nanofluid at steady inlet flow and various pulsating frequencies, f under fixed values of Re=5000,φ=1% and θ=180^{o}.

To provide more information about the flow physics through the wavy channel, the distribution of the time-averaged vorticity, <ω> is presented in Figure 4.15. As expected, the highest vorticity levels are detected at the upper and lower walls and converging sections of the channel. Due to the high velocity gradients in the throat and wave regions, extremely unstable shear layers and consequently vorticity concentrations are developed in these regions. In the region where the flow is accelerated due to the convergence of the main stream region caused by sharp edges, the vorticity rises to a maximum value along the shear layers, while the minimum vorticity levels occur in the wake regions. The high values of vorticity with light blue color expand symmetrically along the channel and affect the main flow region, sequentially dominating the centered flow field from the upstream to the downstream direction. For pulsating flow cases, the intensity of these regions develops to cover most of the zones of diverging sections, especially at f=3. This figure shows that the impacts of pulsating frequency, f on the <ω> are more obvious than the $<\vec{V}>$. In addition, this result clearly explains why the combination of pulsating flow and corrugated channel increases the rate of heat transfer.

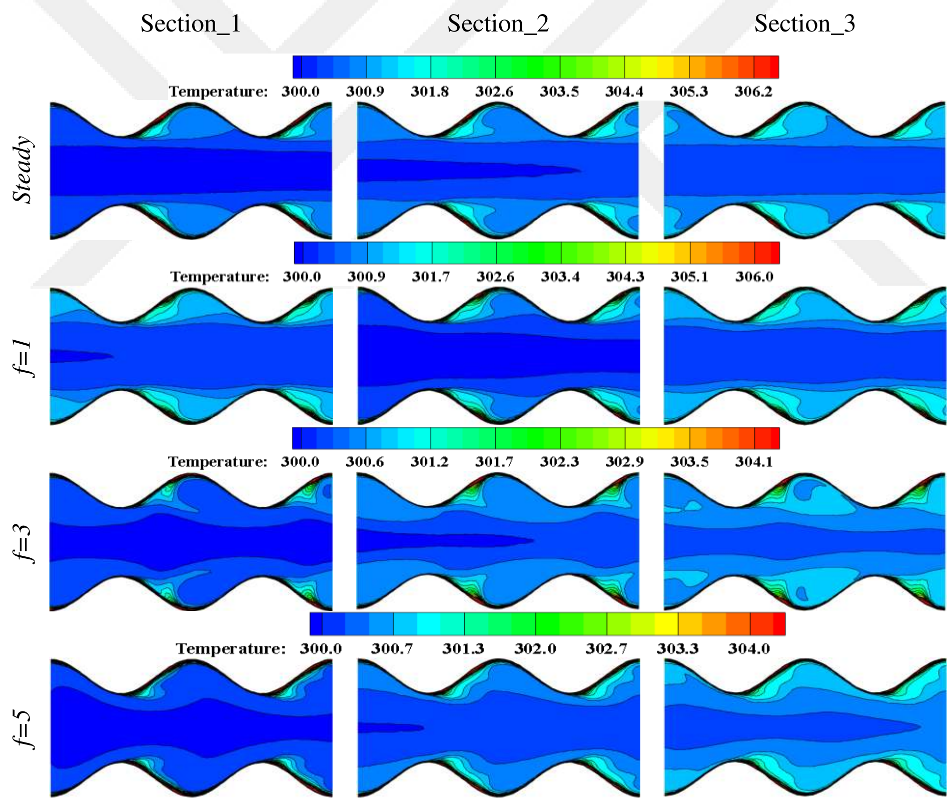

Figure 4.16. Contour lines of time-averaged temperature, $<T>$ for SPM of SWCNT-water nanofluid at steady inlet flow and various pulsating frequencies, f under fixed values of Re=5000,φ=1% and θ=180°.

The contour lines of the time-averaged temperature, <T> is shown in Figure 4.16. Generally, the temperature gradients near the heated wavy surfaces are higher than those in other areas of the channel. This occurs as a result of vortex impacts within the channel waves, which improve the mixing of flows between hot and cold regions. Similar to the <ψ>, <$\vec{V}$> and <ω> distributions, the <T> distributions also behave symmetrically about the central axis of the channel. As can be noted from these contours that the thickness of the thermal boundary layer decreases and the region of low-temperature levels occupies more area within the channel waves with an increase in pulsation frequency. For cases of pulsating flow, the maximum improvement in mixing between the hot flow zones adjacent to the solid walls and the cold flow zones in the center of the channel was recorded at f=3.

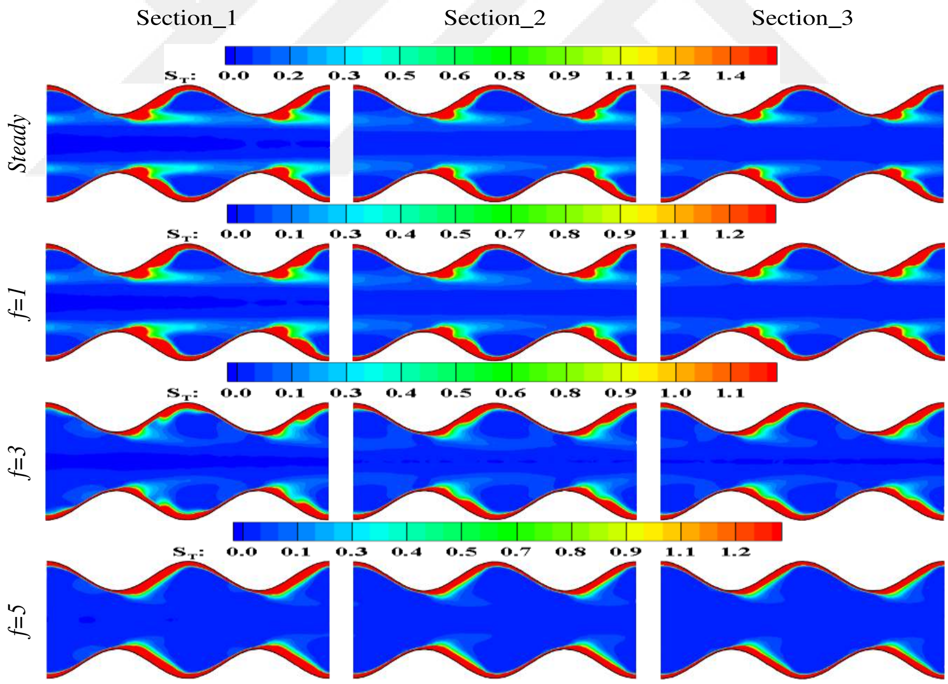

Figure 4.17. Contour lines of time-averaged total entropy generation, <S_T> for SPM of SWCNT-water nanofluid at steady inlet flow and various pulsating frequencies, f under fixed values of Re=5000,φ=1% and θ=180°.

The contour lines of the time-averaged total entropy generation, $<S_T>$ is shown in Figure 4.17. As indicated from these contours, the maximum level of the entropy generation occurs close to the solid wavy walls for all the presented cases as these walls are subjected to uniform heat flux. This is due to the high-temperature gradients at these regions, as shown from $<T>$ contours in Figure 4.18. Therefore, the high level of entropy production is dominated by thermal irreversibility.As expected, the entropy generation along the core flow region is nearly zero. Also, there is a low level of entropy inside each wave along the channel. As shown in Figure 9, vortices appear in these zones within the waves. These prevent contact between the cold liquid and the hot walls and therefore reduce the temperature gradients. Correspondingly, the thermal entropy generation drops remarkably in these zones. Due to the frictional (or viscous) impacts, entropy generation usually stacks in throat sections of the wavy channel. Here, a relatively high level of entropy with green color indicates the predominance of frictional entropy generation. As already demonstrated, these sections represent strong impedance to the main flow field and produce larger viscous irreversibility. Eventually, it can be pointed out that the maximum value of the $<S_T>$ is recorded for the wavy channel under steady flow conditions. This indicates that the use of a pulsating velocity profile reduces the generation of irreversibility in wavy channels.

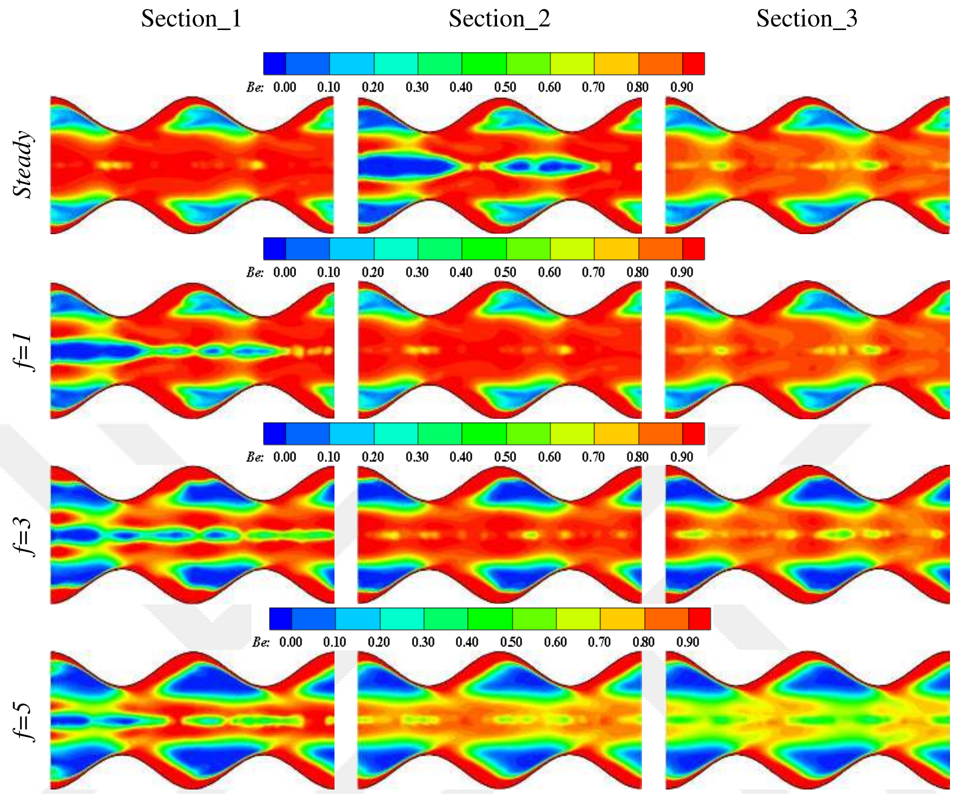

Figure 4.18. Contour lines of time-averaged Bejan number, <*Be*> for SPM of SWCNT-water nanofluid at steady inlet flow and various pulsating frequencies, *f* under fixed values of *Re*=5000,φ=1% and θ=180^{o}.

The contour lines of the time-averaged Bejan number, <*Be*> is shown in Figure 4.18. As it is defined in Equation (3.44), the Bejan number, *Be* represents the ratio of thermal entropy to the summation of thermal and friction entropies. Therefore, for <*Be*> $\geq$ 0.5, the thermal irreversibility dominates the flow process, while for <*Be*>$\leq$ 0.5, the friction irreversibility dominates. For all cases, the thermal entropy dominates in regions next to the heated wavy walls along the channel. This is due to the high differences in temperature at these regions. The high level (dark red color) of <*Be*> near the heated walls comparatively represents the thickness of the thermal boundary layer. However, the frictional entropy prevails at the inlet of the channel and the core of the waves, where the developing flow and recirculation zones occur. This is due to the high gradients in velocity at these regions. It is clearly seen that the predominance of thermal entropy generation in the core flow region and most space of waves reduces with an increase of pulsation frequency.

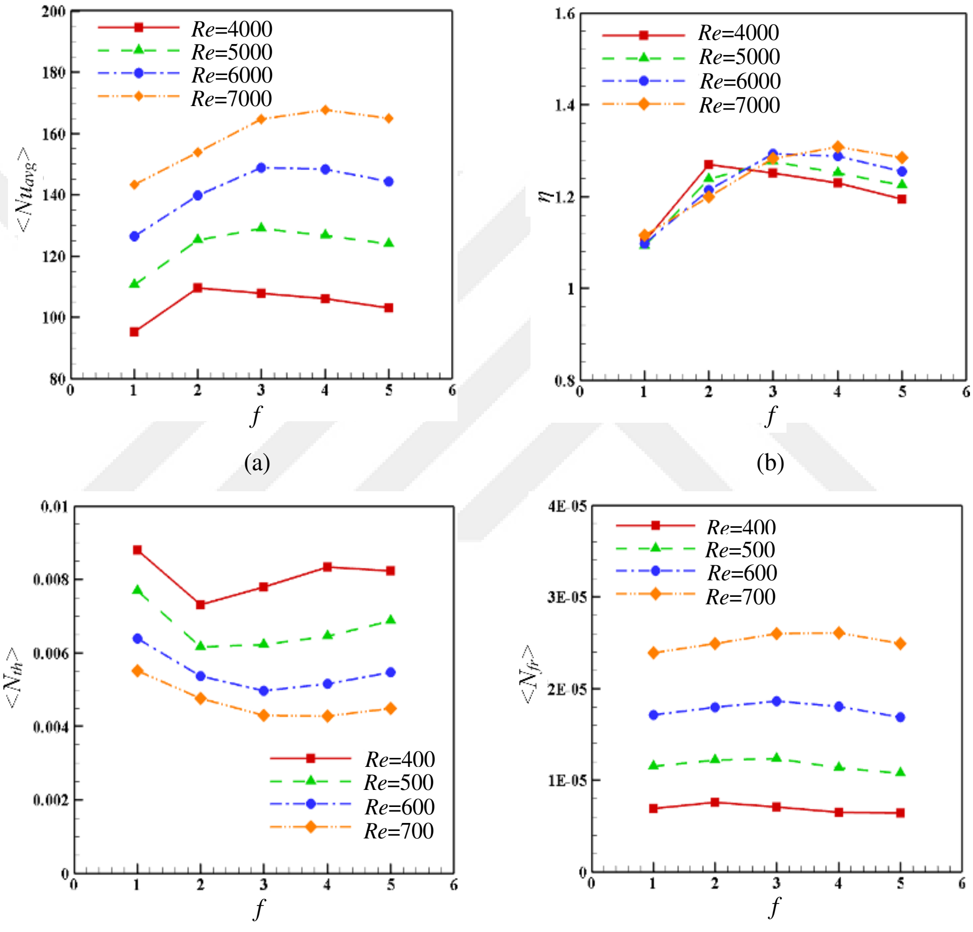

(a) (b)

(c) (d)

Figure 4.19. The influence of Reynolds number, *Re* and pulsating frequency, *f* for water (φ=0%) flow in a considered channel with a phase shift of θ=180^{o} on: (a) time-averaged Nusselt number, $<Nu_{avg}>$, (b) heat transfer rate, η(c) time-averaged thermal entropy generation, $<N_{th}>$ and (d) time-averaged frictional entropy generation, $<N_{fr}>$.

It is important to define which frequency of the pulsating inlet flow has the best influence on the thermal transmission. Further, It is essential to determine the role of implemented pulsating flow on the amount of entropy generation through the wavy channel. To achieve these requirements, Figure 4.19 investigates the impact of different Reynolds numbers, *Re* on thermal characteristics and entropy productions for water (φ=0) flow in a sinusoidal wavy channel under various pulsation frequencies, *f*. For this object, five different pulsation frequencies ($1 \leq f \leq 5$) and steady inlet flow were analyzed and compared within the turbulent flow regimes. In this figure, the phase shift between the top and bottom surfaces is fixed at θ=180°. The differences of the $<Nu_{avg}>$ against the studied ranges of the *Re* and *f* are disclosed in Figure 4.19 (a). The general view of the variance shows that the contribution of the pulsating frequency, *f* and Reynolds number, *Re* are seriously important in improving the rate of thermal transmission. At the beginning, an increase in the pulsation frequency, *f* leads to an increase in $<Nu_{avg}>$. After the $<Nu_{avg}>$ reaches its maximum value, a further increase in pulsation frequency, *f* leads to a decrease in $<Nu_{avg}>$. For the considered range of *Re*, the maximum value of $<Nu_{avg}>$ is given at f =2 for *Re* =4000, f =3 for *Re*=5000 and *Re*=6000, and f=4 for *Re*=7000. For a given pulsation frequency, *f*, this figure displays that $<Nu_{avg}>$ increases remarkably with increasing flow rate. This is due to an increase in the intensity of turbulence and, consequently, convective thermal transmission increases with an increase in *Re*. The outcomes demonstrate that the maximum value of $<Nu_{avg}>$ strongly depends on both *f* and *Re*. The variations of the heat transfer ratio, η are portrayed in Figure 4.19 (b). As given in Equation(3.37), this ratio determines the heat transfer enhancement for pulsating flow over the steady inlet flow. Since η>1, it can be announced that the pulsating inlet flow is an efficient mechanism for enhancing thermal transport in corrugated channels. As can be seen, this ratio is more sensitive for *Re* = 4000 than for other ranges of the turbulent flow regime. Moreover, the η gradually reduces with an augmentation in *f*. Finally, the maximum heat transfer ratio is given as η=1.31 for *Re*=7000 and *f* =4.

From the thermodynamic point of view, Figure 4.19 (c) presents the changes of the time-averaged thermal entropy generation, $<N_{th}>$ with both pulsation frequency, *f* and Reynolds number, *Re*. The presented results reveal that an augment in *Re* remarkably reduces the $<N_{th}>$ for all pulsation frequencies. For example, a reduction of 45.4% in the $<N_{th}>$ is detected by increasing the Reynolds number from *Re*=4000 to *Re*=7000 at *f*=5. As discussed in Figure 4.19 (a), this increment in *Re* leads to an augmentation in the thermal transmission rate. This state alters the temperature gradients through the channel and, consequently, causing a decrease in thermal entropy generation. For a given *Re*, the value of $<N_{th}>$ decreases with increasing *f* until it reaches a minimum value and then begins to increase with a further increase in *f*. For the considered range of *Re*, the minimum value of $<N_{th}>$ is given at *f*=2 for *Re*=4000 and *Re*=5000 and *f*=3 for *Re*=6000 and *Re*=7000. Figure 4.19 (d) exhibits the variations of the time-averaged frictional entropy generation, $<N_{fr}>$ with pulsation frequency, *f* for various Reynolds numbers, *Re*. In contrast to the tendency of $<N_{th}>$ that presented in Figure 4.19 (a), the $<N_{fr}>$ is directly proportional to the *Re*. For example, an increment of 287% in the $<N_{fr}>$ is found by increasing the Reynolds number from *Re*=4000 to *Re*=7000 at *f*=5. As it is known, this augment in *Re* leads to an increase in the velocity gradients through the channel flow field and, consequently, creates additional irreversibility due to the friction flow.

4.2.2. Effect of phase shifts

Many studies have shown that the performance of corrugated channels is significantly affected by changes in their phase shift. Therefore, the influences of phase shifts, θ on the patterns of time-averaged stream function, $<\psi>$, time-averaged velocity magnitude, $<\vec{V}>$, time-averaged vorticity magnitude, $<\omega>$, time-averaged temperature, <T>, time-averaged total entropy generation, <S_T> and time-averaged Bejan number, <Be> for, SPM, Re=6000, f=3 and φ=1% are displayed in Figures (4.20)-(4.25), respectively.

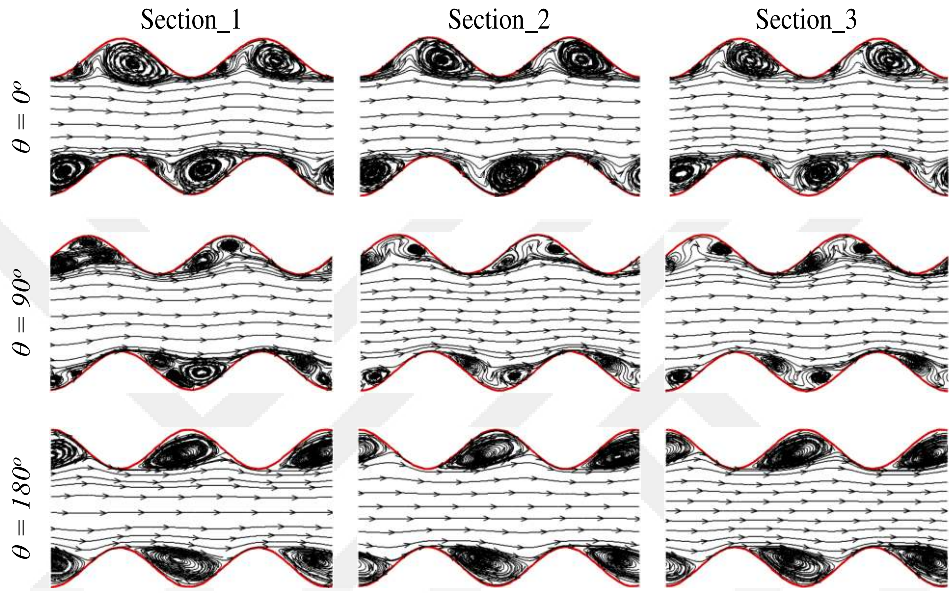

Figure 4.20. Contour lines of time-averaged stream function, <ψ> for SPM of SWCNT-water nanofluid at various phase shifts, θ under fixed values of Re=6000, f=3 and φ=1%.

For all configurations in Figure 4.20, the vortex generates within each groove as the working fluid flows through the channel. Also, it is seen from these contours that the recirculation vortexes dominate the flow within the waves. These vortexes enhance the flow mixing between the cold central region of the channel and the hot region adjacent to the channel walls. The size, position, and morphology of these vortices are different in each configuration. For example, the channel with a phase shift of θ= 0° has the largest vortex compared to other configurations. In the case of θ= 90°, this vortex is divided into two small vortices within each wave. When increasing the phase shift to θ=180°, note that the position of foci and saddle points move to the upstream direction. In addition, it can be declared that the maximum value of the <ψ> increases with increasing phase shift, θ between the channel walls.

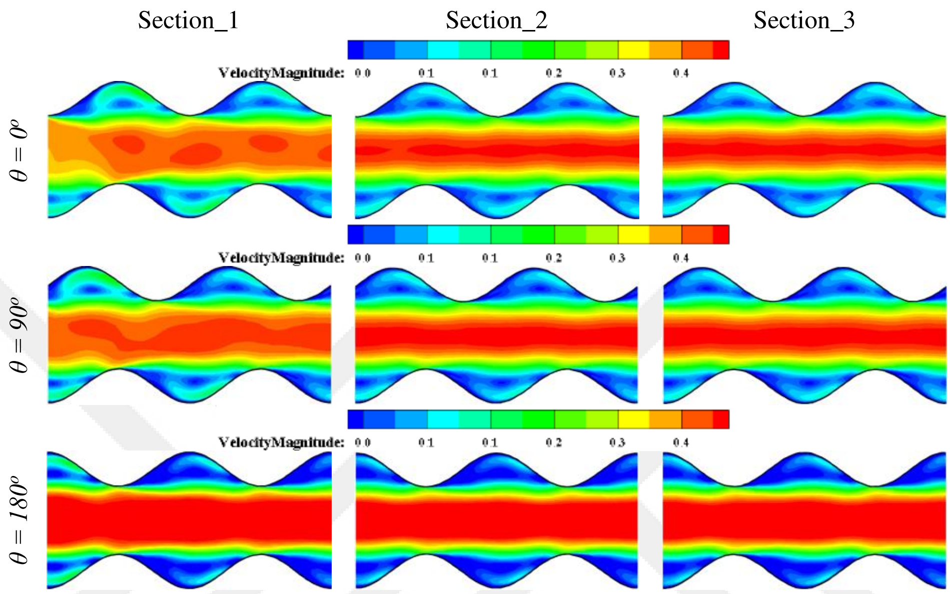

Figure 4.21. Contour lines of time-averaged velocity magnitude, <$\vec{V}$> for SPM of SWCNT-water nanofluid at various phase shifts, θ under fixed values of Re=6000, f=3 and φ=1%.

From the contours of the <$\vec{V}$> in Figure 4.21, it can be observed that the influence of the phase shift, θ strongly affects the region of the developing flow at the entrance of the channel, as clearly shown in the 1st section of these contours. For example, for θ =180^o, the mainstream flow along the channel is more uniform than other phase shifts, θ due to the consistent profile of this configuration.

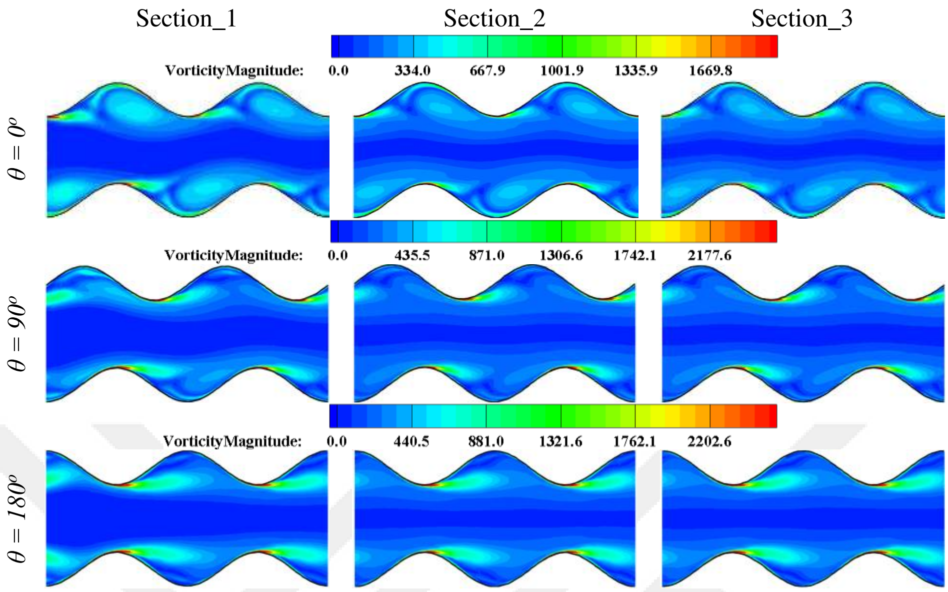

Figure 4.22. Contour lines of time-averaged vorticity magnitude, <ω> for SPM of SWCNT-water nanofluid at various phase shifts, θ under fixed values of Re=6000, f=3 and φ=1%.

From the contours of the <ω> in Figure 4.22, it can be seen that the intensity of the high-level vorticity inside the waves decreases with an increase in the phase shift between the channel walls.

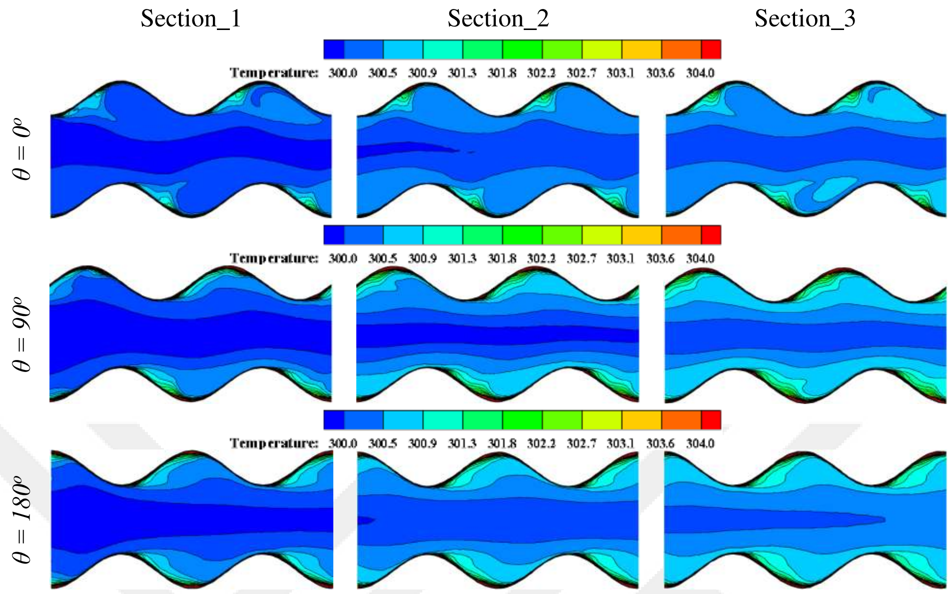

Figure 4.23. Contour lines of time-averaged temperature, <*T*> for SPM of SWCNT-water nanofluid at various phase shifts, θ under fixed values of Re=6000, f=3 and φ=1%.

From the <*T*> contours in Figure 4.23, it can be stated that the impacts of a changing phase shift on hydrodynamic flow are more evident than heat transfer.

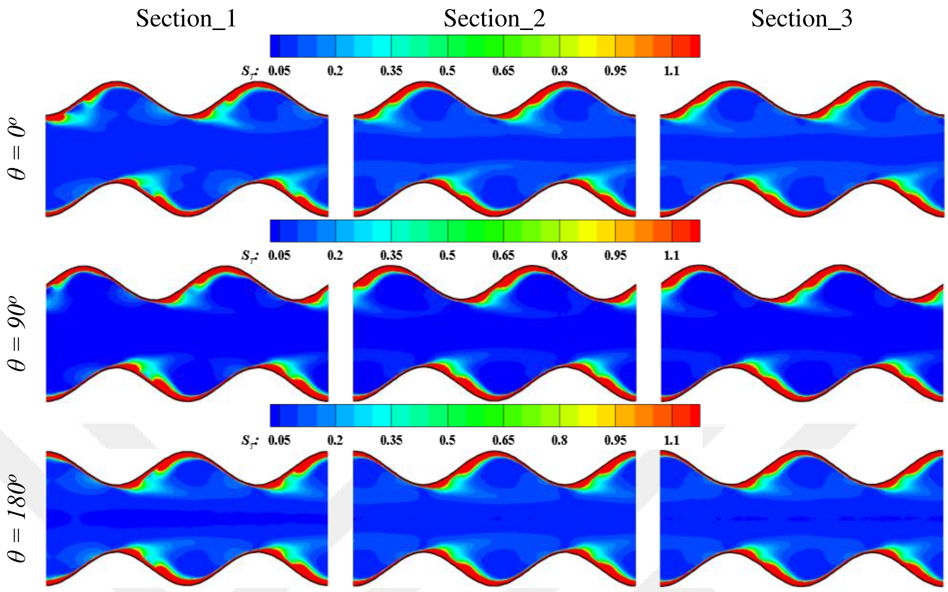

Figure 4.24. Contour lines of time-averaged total entropy generation, $<S_T>$ for SPM of SWCNT-water nanofluid at various phase shifts, θ under fixed values of Re=6000, f=3 and φ=1%.

Similar to the temperature contour lines, there are no clear differences in the $<S_T>$ contours by changing the degree of phase shift, as shown in Figure 2.24.

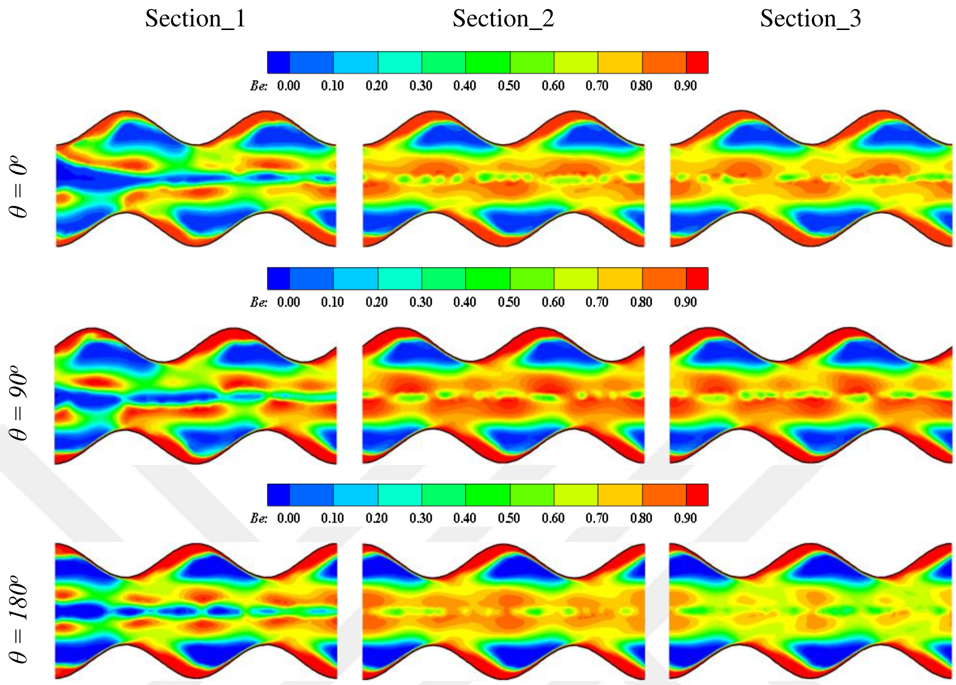

Figure 4.25. Contour lines of time-averaged Bejan number, <*Be*> for SPM of SWCNT-water nanofluid at various phase shifts, θ under fixed values of *Re*=6000, *f*=3 and φ=1%.

Further, with respect to the <*Be*> contours, Figure 4.25 shows that the predominance of thermal irreversibility is relatively reduced due to an increase in the degree of phase shift.

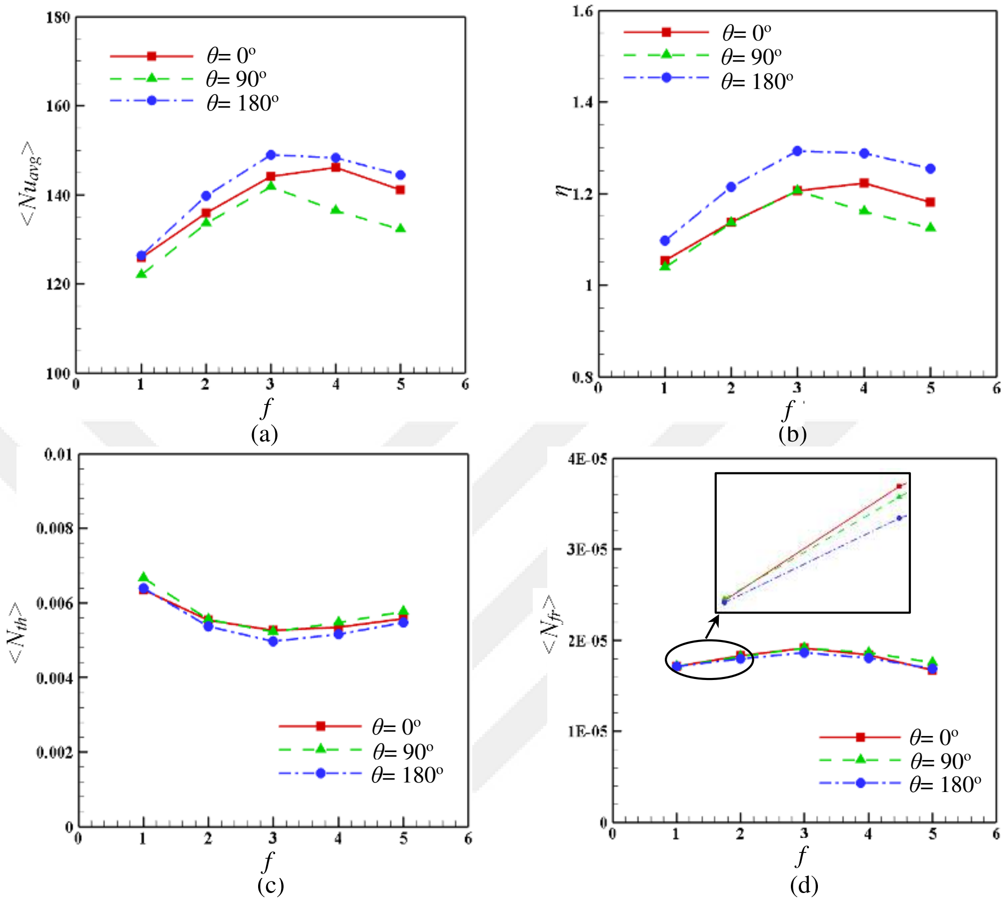

Figure 4.26. The influence of phase shift, θ and pulsating frequency, f for water (φ=0%) flow in a considered channel at Re=6000 on: (a) time-averaged Nusselt number, <Nu_{avg}>, (b) heat transfer rate, η (c) time-averaged thermal entropy generation, <N_{th}> and (d) time-averaged frictional entropy generation, <N_{fr}>.

Despite the purpose of using pulsating inlet flow is to increase thermal transport; however, it is essential to consider the effect of this flow on entropy generation in order to understand all aspects of pulsating flow in wavy channels having different configurations. Therefore, Figure 4.26 examines the influence of different phase shifts, θ on thermal transport and entropy generation for water (φ=0) flow in a sinusoidal wavy channel under various pulsation frequencies, f at Re=6000. The differences of the <Nu_{avg}> against the considered ranges of flow conditions for different wavy configurations are disclosed in Figure 4.26 (a). As can be seen in this figure, all configurations show that $<Nu_{avg}>$ increases with an increase in the pulsation frequency, f and, after reaching the maximum value, it decreases with a further increase in f. The maximum value of $<Nu_{avg}>$ is identified at f=3 for θ=90^o and θ=180^o and f=4 for θ=0^o. For a given f, the wavy channel with a phase shift of θ=180^o always has a higher $<Nu_{avg}>$ value than other configurations. This is because that the generated vortices in this geometry have a higher ability to improve the flow mixing between the hot and cold fluids compared to other geometries. Figure 4.26 (b) presents the impact of channel configuration on the heat transfer ratio, η for various flow conditions. Similar to the behavior of $<Nu_{avg}>$, the configuration of θ=180^o always has a higher enhancement ratio than other configurations for the same flow condition. Channels with phase shifts of θ=90^o and θ=0^o have an identical trend for the low pulsation frequency ($f \leq 3$), while the discrepancy between them is evident for f<4. Moreover, the maximum heat transfer ratio, η is recorded for the phase shift of θ=180^o at f=3.

With regard to the generation of entropy for different configurations, Figures 4.26 (c) and (d) display the variations in the time-averaged thermal entropy generation, $<N_{th}>$ and the time-averaged frictional entropy generation, $<N_{fr}>$, respectively, under the studied flow conditions. As it is evidently seen from these figures, there is no considerable effect of the phase shift, θ on both $<N_{th}>$ and $<N_{fr}>$ for all pulsation frequencies, f.

4.2.3. Effect of phase model and nanoparticle concentration

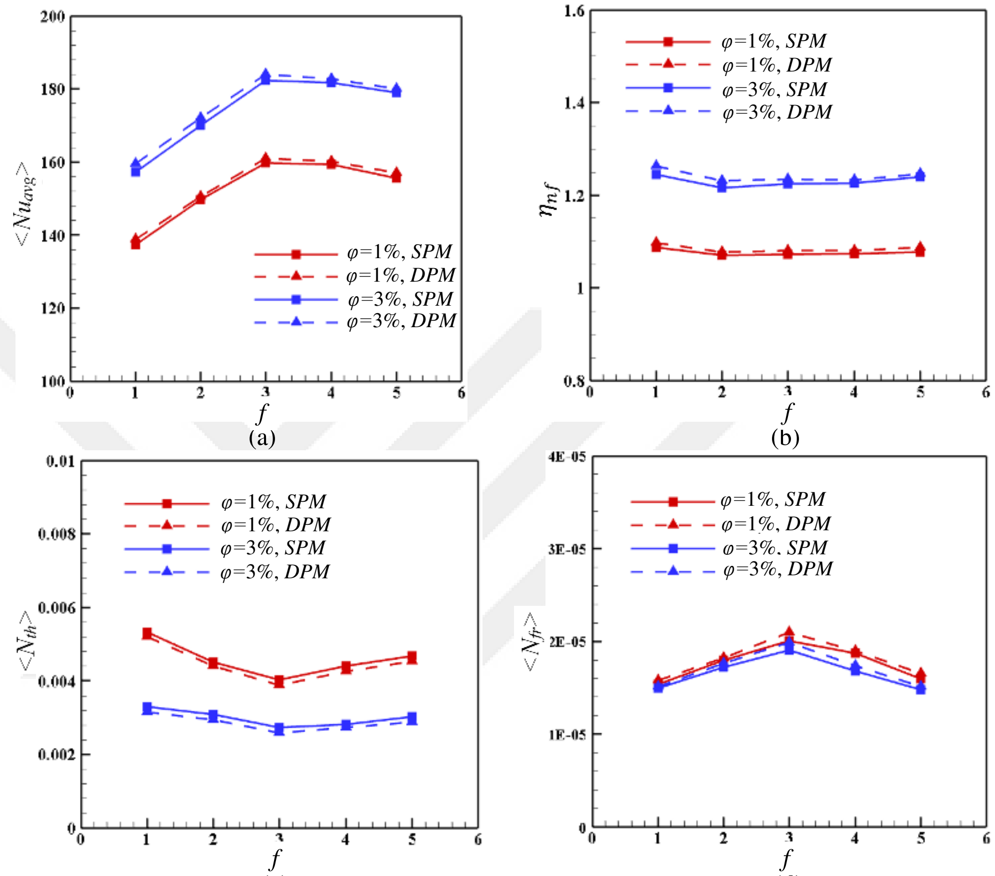

Figure 4.27. The influence of nanoparticles concentration, φ and pulsating frequency, f using both *SPM* and *DPM* for nanofluid flow in a considered channel at Re=6000 and θ=180° on: (a) time-averaged Nusselt number, $<Nu_{avg}>$, (b) heat transfer rate, η (c) time-averaged thermal entropy generation, $<N_{th}>$ and (d) time-averaged frictional entropy generation, $<N_{fr}>$.

Many studies have reported that there is not much difference in hydrothermal behavior between base liquid and nanofluid (Albojamal et al., 2017). Therefore, the corresponding quantitative figures of both SPM and DPM have been presented in this section. In this context, Figure 4.27 examines the influence of various SWCNT concentrations, φ on thermal transport and entropy generation in a sinusoidal wavy channel under various pulsation frequencies, f using both SPM and DPM at Re=6000 and θ=180°. As shown in Figure 4.27 (a), the value of $<Nu_{avg}>$ increases as the suspension of SWCNT nanoparticles in water increases for both models. This is due to the high thermophysical properties of suspended particles, as shown in Table 1. For DPM, where the momentum transfer between the nanoparticles and host liquid is considered, it can be noticed that the $<Nu_{avg}>$ is always higher than the SPM. For f=3 and DPM, the $<Nu_{avg}>$ augments 14.3% when φ rises from 1% to 3%. It was found that the deviation between SPM and DPM increases at φ=3%. Figure 4.27 (b) illustrates the heat transfer ratio, η_{nf} over the host liquid as a function of pulsation frequency, f for SPM and DPM. As expected, the ratio augments with an increment in SWCNT concentrations in water for both models. The maximum improvement over the host fluid was detected to be 24.4% for *DPM* at f=3 and φ=3%.

From the second law viewpoint, the impacts of pulsation frequency, nanoparticles concentration and phase model on the time-averaged thermal entropy generation, $<N_{th}>$ and the time-averaged frictional entropy generation, $<N_{fr}>$ are shown in Figure 4.27 (c) and (d). The results indicated that the $<N_{th}>$ diminishes with increasing SWCNT concentrations, φ for both phase models. An increase in heat transfer due to the utilize of SWCNT-water nanofluid at high values of φ is the main reason for such a decrease in $<N_{th}>$. From Fig. 23 (d), the variance in $<N_{fr}>$ is much more detectable by increasing f than by changing the phase model and φ. This is because of the stronger influence of f on the velocity gradients in comparison with the properties of nanofluid.

4.3. Special case for 3D channel

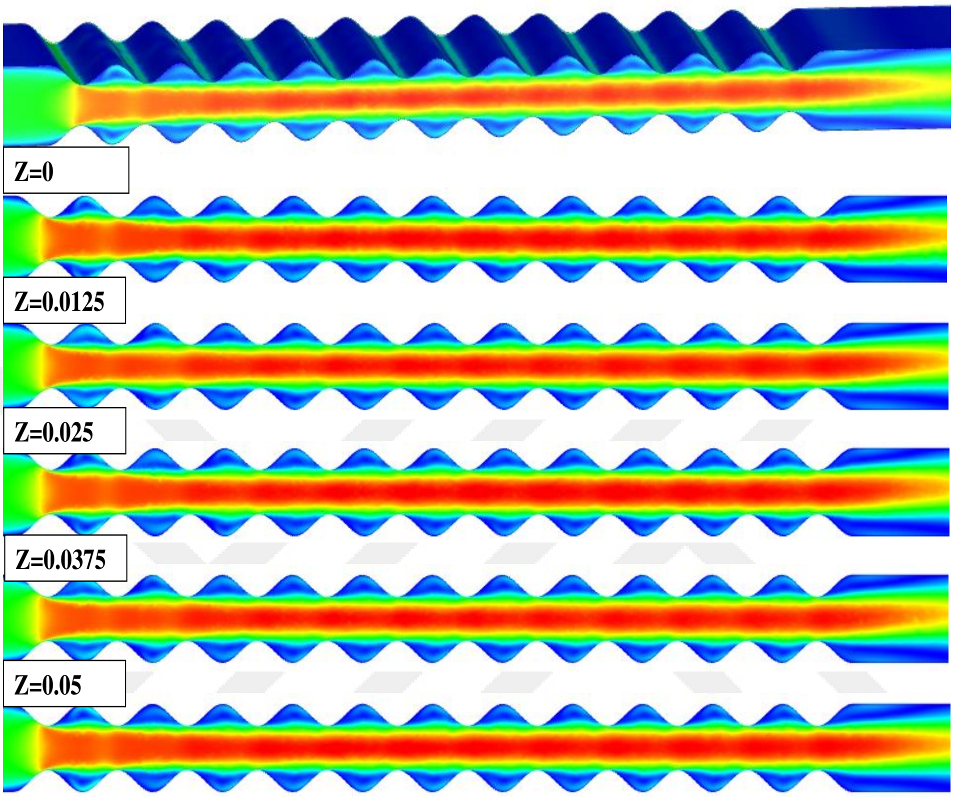

Figure 4.28. Contour lines of time-averaged velocity magnitude, $\langle \vec{V} \rangle$ at the five different cross-sections of Z-direction for SPM of SWCNT-water nanofluid under fixed values of Re=5000, f=3 and φ=1%.

Figure 4.28. exhibits velocity contours for a fully turbulent 3D behavior and helps understand the flow behavior regarding Z-direction. For internal flow, it is well known that the fluid in the central region is accelerated to compensate for the decrease in axial velocity - due to the growth of the boundary layer - near the wall; called the main area. This figure shows a shift in the position of the accelerating core from the central region towards the wall, due to change in the direction of flow in the wavy-channel. From this, it can be concluded that the flow

through the wavy channel under consideration is shown in 2D since the flow behavior does not change significantly in the Z-direction.

5. CONCLUSIONS

In this research, hydrothermal characteristics and entropy production analysis has been carried out for SWCNT-water nanofluid flow in a sinusoidal wavy channel under both steady and pulsating velocity profiles. SPM and DPM models are utilized for describing the motion of nanoparticles in a base fluid. The influences of different relevant parameters such as Reynolds number, *Re*, pulsation frequency, *f*, phase shift, θ and nanoparticle concentration, φ were examined. Therefore, the main conclusions of the current research are given for steady and pulsating flow.

5.1. Steady flow conclusions

Points stated below are the main findings of the current study for steady flow:

- The secondary flow region generated by the wavy walls has the ability to enhance the rate of heat transfer and decrease thermal irreversibility.
- Among the phase shifts, θ=0^{o} presents a limited higher thermal enhancement, *E* compared to the straight channel, but it is associated with a higher friction factor, *f*.
- Among the phase shifts, θ=180^{o} has the best *TPF* index compared to other configurations.
- Both thermal, N_{th} and frictional, N_{fr} entropy productions are a weak function of the phase shift, θ, but they are a strong function of the Reynolds number, *Re*.
- The two-phase model, *DPM* offers a reasonable prediction of the thermal and entropy characteristics of SWCNT-water nanofluid compared to the single-phase model, *SPM*.

- Nu_{avg}, E_{nf} and TPF_{nf} values significantly increase with increasing solid particle concentrations of SWCNT in the base fluid.
- The volume fraction of nanoparticles, φ has a large effect on the thermal entropy, N_{th}, while it may marginally affect the frictional entropy, N_{fr}.

5.2. Pulsating flow conclusions

Points stated below are the main findings of the current study for pulsating flow:

- The contour plots reveal that both pulsating flow and channel configuration play a significant role in hydrothermal structures and irreversibility processes through the corrugated channel.
- Using pure water as a working fluid, the maximum improvement in heat transfer of 31% compared to the case of a steady inflow was achieved at Re = 7000, f=4 and θ=180°.
- For a given pulsation frequency, the $\langle N_{th} \rangle$ is directly related to Re while $\langle N_{fr} \rangle$ is inversely related to Re.
- Among the presented configurations, the channel with θ=180° always has a higher $\langle Nu_{avg} \rangle$ and η.
- Both $\langle N_{th} \rangle$ and $\langle N_{fr} \rangle$ are a weak function of channel configurations.
- The presented results confirmed that using SWCNT-water nanofluid as the working fluid in a corrugated channel is an efficient technique to increase the rate of convective heat transfer and decrease thermal irreversibility.
- The maximum improvement in heat transfer over the base fluid was detected to be 24.4% for *DPM* at f=3 and φ=3%.

Eventually, the combination of wavy, nanofluid and pulsating flow is expected to be a hopeful strategy for improving the heat transfer ratio and controlling the irreversibility production in compact heat exchangers.

REFERENCES

Abbasian Arani, A. A., & Amani, J. (2013). Experimental investigation of diameter effect on heat transfer performance and pressure drop of TiO 2-water nanofluid. *Experimental Thermal and Fluid Science*, *44*, 520–533. https://doi.org/10.1016/j.expthermflusci.2012.08.014

Abdelaziz, E. A., Saidur, R., & Mekhilef, S. (2011). A review on energy saving strategies in industrial sector. *Renewable and Sustainable Energy Reviews*, *15*(1), 150–168. https://doi.org/10.1016/j.rser.2010.09.003

Abdelmalek, Z., Tayebi, T., Dogonchi, A. S., Chamkha, A. J., Ganji, D. D., & Tlili, I. (2020). Role of various configurations of a wavy circular heater on convective heat transfer within an enclosure filled with nanofluid. *International Communications in Heat and Mass Transfer*, *113*. https://doi.org/10.1016/j.icheatmasstransfer.2020.104525

Abdolbaqi, M. K., Azmi, W. H., Mamat, R., Sharma, K. V., & Najafi, G. (2016). Experimental investigation of thermal conductivity and electrical conductivity of BioGlycol-water mixture based Al2O3 nanofluid. *Applied Thermal Engineering*, *102*, 932–941. https://doi.org/10.1016/j.applthermaleng.2016.03.074

Abu-Nada, E., Masoud, Z., Oztop, H. F., & Campo, A. (2010). Effect of nanofluid variable properties on natural convection in enclosures. *International Journal of Thermal Sciences*, *49*(3), 479–491. https://doi.org/10.1016/j.ijthermalsci.2009.09.002

Abu-Nada, E., & Oztop, H. F. (2009). Effects of inclination angle on natural convection in enclosures filled with Cu-water nanofluid. *International Journal of Heat and Fluid Flow*, *30*(4), 669–678. https://doi.org/10.1016/j.ijheatfluidflow.2009.02.001

Adrian, B. (1984). Entropy generation through heat and fluid flow. *Solar Energy*, *33*(6), 641. https://doi.org/10.1016/0038-092x(84)90026-4

Ahmad, S., Ijaz Khan, M., Hayat, T., Imran Khan, M., & Alsaedi, A. (2018). Entropy generation optimization and unsteady squeezing flow of viscous fluid with five different shapes of nanoparticles. *Colloids and Surfaces A: Physicochemical and Engineering Aspects*, *554*, 197–210. https://doi.org/10.1016/j.colsurfa.2018.06.017

Ahmed, M. A., Shuaib, N. H., Yusoff, M. Z., & Al-Falahi, A. H. (2011). Numerical investigations of flow and heat transfer enhancement in a corrugated channel using nanofluid. *International Communications in Heat and Mass Transfer*, *38*(10), 1368–1375. https://doi.org/10.1016/j.icheatmasstransfer.2011.08.013

Ahmed, M. A., Yusoff, M. Z., Ng, K. C., & Shuaib, N. H. (2014). The effects of wavy-wall phase shift on thermal-hydraulic performance of Al2O3-water nanofluid flow in sinusoidal-wavy channel. *Case Studies in Thermal Engineering*, *4*, 153–165. https://doi.org/10.1016/j.csite.2014.09.005

Ahuja, A. S. (1975). Augmentation of heat transport in laminar flow of polystyrene suspensions. I. Experiments and results. *Journal of Applied Physics*, *46*(8), 3408–3416. https://doi.org/10.1063/1.322107

Ajeel, R. K., Salim, W. S. I. W., & Hasnan, K. (2019). Influences of geometrical parameters on the heat transfer characteristics through symmetry trapezoidal-corrugated channel using SiO 2 -water nanofluid. *International Communications in Heat and Mass Transfer*, *101*, 1–9. https://doi.org/10.1016/j.icheatmasstransfer.2018.12.016

Akbarinia, A., & Behzadmehr, A. (2007). Numerical study of laminar mixed convection of a nanofluid in horizontal curved tubes. *Applied Thermal Engineering*, *27*(8–9), 1327–1337. https://doi.org/10.1016/j.applthermaleng.2006.10.034

Akbarzadeh, M., Rashidi, S., Bovand, M., & Ellahi, R. (2016). A sensitivity analysis on thermal and pumping power for the flow of nanofluid inside a wavy channel. *Journal of Molecular Liquids*, *220*, 1–13. https://doi.org/10.1016/j.molliq.2016.04.058

Akbarzadeh, M., Rashidi, S., & Esfahani, J. A. (2017). Influences of corrugation profiles on entropy generation, heat transfer, pressure drop, and performance in a wavy channel. *Applied Thermal Engineering*, *116*, 278–291. https://doi.org/10.1016/j.applthermaleng.2017.01.076

Akbarzadeh, M., Rashidi, S., Karimi, N., & Ellahi, R. (2018). Convection of heat and thermodynamic irreversibilities in two-phase, turbulent nanofluid flows in solar heaters by corrugated absorber plates. *Advanced Powder Technology*, *29*(9), 2243–2254. https://doi.org/10.1016/j.apt.2018.06.009

Akbarzadeh, Mohsen, Rashidi, S., Keshmiri, A., & Shokri, N. (2020). The optimum position of porous insert for a double-pipe heat exchanger based on entropy generation and thermal analysis. *Journal of Thermal Analysis and Calorimetry*, *139*(1), 411–426. https://doi.org/10.1007/s10973-019-08362-x

Akdag, U. (2010). Numerical investigation of pulsating flow around a discrete heater in a channel. *International Communications in Heat and Mass Transfer*, *37*(7), 881–889. https://doi.org/10.1016/j.icheatmasstransfer.2010.04.001

Akdag, U., Akcay, S., & Demiral, D. (2014). Heat transfer enhancement with laminar pulsating nanofluid flow in a wavy channel. *International Communications in Heat and Mass Transfer*, *59*, 17–23. https://doi.org/10.1016/j.icheatmasstransfer.2014.10.008

Al-Kouz, W., Alshare, A., Kiwan, S., Al-Muhtady, A., Alkhalidi, A., & Saadeh, H. (2018). Two-dimensional analysis of low-pressure flows in an inclined square cavity with two fins attached to the hot wall. *International Journal of Thermal Sciences*, *126*, 181–193. https://doi.org/10.1016/j.ijthermalsci.2018.01.005

Albojamal, A., Hamzah, H., Haghighi, A., & Vafai, K. (2017). Analysis of nanofluid transport through a wavy channel1. Albojamal A, Hamzah H, Haghighi A, Vafai K. Analysis of nanofluid transport through a wavy channel. Numer Heat Transf Part A Appl. 2017;72. *Numerical Heat Transfer; Part A: Applications*, *72*(12). https://doi.org/10.1080/10407782.2017.1412679

Albojamal, Ahmed, Hamzah, H., Haghighi, A., & Vafai, K. (2017). Analysis of nanofluid transport through a wavy channel. *Numerical Heat Transfer; Part A: Applications*, *72*(12), 869–890. https://doi.org/10.1080/10407782.2017.1412679

Albojamal, Ahmed, & Vafai, K. (2017). Analysis of single phase, discrete and mixture models, in predicting nanofluid transport. *International Journal of Heat and Mass Transfer*, *114*, 225–237. https://doi.org/10.1016/j.ijheatmasstransfer.2017.06.030

Albojamal, Ahmed, & Vafai, K. (2020). Analysis of particle deposition of nanofluid flow through porous media. *International Journal of Heat and Mass Transfer*, *161*. https://doi.org/10.1016/j.ijheatmasstransfer.2020.120227

Ambreen, T., & Kim, M. H. (2018). Effects of variable particle sizes on hydrothermal characteristics of nanofluids in a microchannel. *International Journal of Heat and Mass Transfer*, *120*, 490–498. https://doi.org/10.1016/j.ijheatmasstransfer.2017.12.067

Amiri, A., Shanbedi, M., Yarmand, H., Arzani, H. K., Gharehkhani, S., Montazer, E., Sadri, R., Sarsam, W., Chew, B. T., & Kazi, S. N. (2015). Laminar convective heat transfer of hexylamine-treated MWCNTs-based turbine oil nanofluid. *Energy Conversion and Management*, *105*, 355–367. https://doi.org/10.1016/j.enconman.2015.07.066

Andrew, D. S., & Kirk, L. Y. (2009). Experimental investigation into the convective heat transfer and system-level effects of Al2O3-propanol nanofluid. *Journal of Nanoparticle Research*.

Anoop, K. B., Sundararajan, T., & Das, S. K. (2009). Effect of particle size on the convective heat transfer in nanofluid in the developing region. *International Journal of Heat and Mass Transfer*, *52*(9–10), 2189–2195. https://doi.org/10.1016/j.ijheatmasstransfer.2007.11.063

Arjmandi, H. R., & Amani, E. (2015). A numerical investigation of the entropy generation in and thermodynamic optimization of a combustion chamber. *Energy*, *81*, 706–718. https://doi.org/10.1016/j.energy.2014.12.077

Bahaidarah, H. M. S., & Sahin, A. Z. (2013). Thermodynamic analysis of fluid flow in channels with wavy sinusoidal walls. *Thermal Science*, *17*(3), 813–822. https://doi.org/10.2298/TSCI110403200B

Bahiraei, M. (2016). A numerical study of heat transfer characteristics of CuO-water nanofluid by Euler-Lagrange approach. *Journal of Thermal Analysis and Calorimetry*, *123*(2), 1591–1599. https://doi.org/10.1007/s10973-015-5031-0

Bahiraei, M., Jamshidmofid, M., & Heshmatian, S. (2017). Entropy generation in a heat exchanger working with a biological nanofluid considering heterogeneous particle distribution. *Advanced Powder Technology*, *28*(9), 2380–2392. https://doi.org/10.1016/j.apt.2017.06.021

Bahiraei, M., Monavari, A., Naseri, M., & Moayedi, H. (2020). Irreversibility characteristics of a modified microchannel heat sink operated with nanofluid considering different shapes of nanoparticles. *International Journal of Heat and Mass Transfer*, *151*. https://doi.org/10.1016/j.ijheatmasstransfer.2020.119359

Bai, M., Xu, Z., & Lv, J. (2008). Application of nanofluids in engine cooling system. *SAE Technical Papers*. https://doi.org/10.4271/2008-01-1821

Barbés, B., Páramo, R., Blanco, E., & Casanova, C. (2014). Thermal conductivity and specific heat capacity measurements of CuO nanofluids. *Journal of Thermal Analysis and Calorimetry*, *115*(2), 1883–1891. https://doi.org/10.1007/s10973-013-3518-0

Beck, M. P., Yuan, Y., Warrier, P., & Teja, A. S. (2009). The effect of particle size on the thermal conductivity of alumina nanofluids. *Journal of Nanoparticle Research*, *11*(5), 1129–1136. https://doi.org/10.1007/s11051-008-9500-2

Behroyan, I., Ganesan, P., He, S., & Sivasankaran, S. (2015). Turbulent forced convection of Cu-water nanofluid: CFD model comparison. *International Communications in Heat and Mass Transfer*, *67*, 163–172. https://doi.org/10.1016/j.icheatmasstransfer.2015.07.014

Behzadmehr, A., Saffar-Avval, M., & Galanis, N. (2007). Prediction of turbulent forced convection of a nanofluid in a tube with uniform heat flux using a two phase approach. *International Journal of Heat and Fluid Flow*, *28*(2), 211–219. https://doi.org/10.1016/j.ijheatfluidflow.2006.04.006

Bi, S. shan, Shi, L., & Zhang, L. li. (2008). Application of nanoparticles in domestic refrigerators. *Applied Thermal Engineering*, *28*(14–15), 1834–1843. https://doi.org/10.1016/j.applthermaleng.2007.11.018

Bianco, V., Chiacchio, F., Manca, O., & Nardini, S. (2009). Numerical investigation of nanofluids forced convection in circular tubes. *Applied Thermal Engineering*, *29*(17–18), 3632–3642. https://doi.org/10.1016/j.applthermaleng.2009.06.019

Bianco, Vincenzo, Manca, O., & Nardini, S. (2011). Numerical investigation on nanofluids turbulent convection heat transfer inside a circular tube. *International Journal of Thermal Sciences*, *50*(3), 341–349. https://doi.org/10.1016/j.ijthermalsci.2010.03.008

Bobbo, S., Colla, L., Scattolini, M., Agresti, F., Barison, S., Pagura, C., & Fedele, L. (2011). Thermal conductivity and viscosity measurements of water-based silica nanofluids. *Technical Proceedings of the 2011 NSTI Nanotechnology Conference and Expo, NSTI-Nanotech 2011*, *2*, 478–481.

Boungiorno, J., Hu, L. W., Kim, S. J., Hannink, R., Truong, B., & Forrest, E. (2008). Nanofluids for enhanced economics and safety of nuclear reactors: An evaluation of the potential features issues, and research gaps. *Nuclear Technology*, *162*(1), 80–91. https://doi.org/10.13182/nt08-a3934

Brinkman, H. C. (1952). The viscosity of concentrated suspensions and solutions. *The Journal of Chemical Physics*, *20*(4), 571. https://doi.org/10.1063/1.1700493

Choi, S. U. S. (1995). Enhancing thermal conductivity of fluids with nanoparticles. *American Society of Mechanical Engineers, Fluids Engineering Division (Publication) FED*, *231*, 99–105.

Chon, C. H., Kihm, K. D., Lee, S. P., & Choi, S. U. S. (2005). Empirical correlation finding the role of temperature and particle size for nanofluid (Al 2O 3) thermal conductivity enhancement. *Applied Physics Letters*, *87*(15), 1–3. https://doi.org/10.1063/1.2093936

Chougule, S. S., & Sahu, S. K. (2013). Comparative study on heat transfer enhancement of low volume concentration of Al2O3-water and carbon nanotube-water nanofluids in laminar regime using helical screw tape inserts. *Journal of Nanotechnology in Engineering and Medicine*, *4*(4). https://doi.org/10.1115/1.4027913

Chougule, S. S., & Sahu, S. K. (2015). Heat transfer and friction characteristics of Al2O3/water and CNT/water nanofluids in transition flow using helical screw tape inserts - a comparative study. *Chemical Engineering and Processing: Process Intensification*, *88*, 78–88. https://doi.org/10.1016/j.cep.2014.12.005

Comini, G., Nonino, C., & Savino, S. (2003). Effect of aspect ratio on convection enhancement in wavy channels. *Numerical Heat Transfer; Part A: Applications*, *44*(1), 21–37. https://doi.org/10.1080/713838173

Darr, S. R., Hu, H., Glikin, N., Hartwig, J. W., Majumdar, A. K., Leclair, A. C., & Chung, J. N. (2016). An experimental study on terrestrial cryogenic tube chilldown II. Effect of flow direction with respect to gravity and new correlation set. *International Journal of Heat and Mass Transfer*, *103*, 1243–1260. https://doi.org/10.1016/j.ijheatmasstransfer.2016.08.044

Das, S. K., Choi, S. U. S., Yu, W., & Pradeep, T. (2007). Nanofluids: Science and Technology. *Nanofluids: Science and Technology*, 1–397. https://doi.org/10.1002/9780470180693

De Robertis, E., Cosme, E. H. H., Neves, R. S., Kuznetsov, A. Y., Campos, A. P. C., Landi, S. M., & Achete, C. A. (2012). Application of the modulated temperature differential scanning calorimetry technique for the determination of the specific heat of copper nanofluids. *Applied Thermal Engineering*, *41*, 10–17. https://doi.org/10.1016/j.applthermaleng.2012.01.003

Demir, H., Dalkilic, A. S., Kürekci, N. A., Duangthongsuk, W., & Wongwises, S. (2011). Numerical investigation on the single phase forced convection heat transfer characteristics of TiO2 nanofluids in a double-tube counter flow heat exchanger. *International Communications in Heat and Mass Transfer*, *38*(2), 218–228. https://doi.org/10.1016/j.icheatmasstransfer.2010.12.009

Devendiran, D. K., & Amirtham, V. A. (2016). A review on preparation, characterization, properties and applications of nanofluids. *Renewable and Sustainable Energy Reviews*, *60*, 21–40. https://doi.org/10.1016/j.rser.2016.01.055

Dhinesh Kumar, D., & Valan Arasu, A. (2018). A comprehensive review of preparation, characterization, properties and stability of hybrid nanofluids. *Renewable and Sustainable Energy Reviews*, *81*, 1669–1689. https://doi.org/10.1016/j.rser.2017.05.257

Ding, Y., Chen, H., He, Y., Lapkin, A., Yeganeh, M., Šiller, L., & Butenko, Y. V. (2007). Forced convective heat transfer of nanofluids. *Advanced Powder Technology*, *18*(6), 813–824. https://doi.org/10.1163/156855207782515021

Dormohammadi, R., Farzaneh-Gord, M., Ebrahimi-Moghadam, A., & Ahmadi, M. H. (2018). Heat transfer and entropy generation of the nanofluid flow inside sinusoidal wavy channels. *Journal of Molecular Liquids*, *269*, 229–240. https://doi.org/10.1016/j.molliq.2018.07.119

Drew, P. (1973). Theory of Multicomponent Fluids. *The Mathematical Gazette*, *57*(399), 80. https://doi.org/10.2307/3615195

Eastman, J. A., Choi, U. S., Li, S., Soyez, G., Thompson, L. J., & DiMelfi, R. J. (1999). Novel Thermal Properties of Nanostructured Materials. *Journal of Metastable and Nanocrystalline Materials*, *2–6*, 629–634. https://doi.org/10.4028/www.scientific.net/jmnm.2-6.629

Ebrahimnia-Bajestan, E., Niazmand, H., Duangthongsuk, W., & Wongwises, S. (2011). Numerical investigation of effective parameters in convective heat transfer of nanofluids flowing under a laminar flow regime. *International Journal of Heat and Mass Transfer*, *54*(19–20), 4376–4388. https://doi.org/10.1016/j.ijheatmasstransfer.2011.05.006

El Bécaye Maïga, S., Palm, S. J., Nguyen, C. T., Roy, G., & Galanis, N. (2005). Heat transfer enhancement by using nanofluids in forced convection flows. *International Journal of Heat and Fluid Flow*, *26*(4 SPEC. ISS.), 530–546. https://doi.org/10.1016/j.ijheatfluidflow.2005.02.004

Elshafei, E. A. M., Safwat Mohamed, M., Mansour, H., & Sakr, M. (2008). Experimental study of heat transfer in pulsating turbulent flow in a pipe. *International Journal of Heat and Fluid Flow*, *29*(4), 1029–1038. https://doi.org/10.1016/j.ijheatfluidflow.2008.03.018

Esfahani, J. A., Akbarzadeh, M., Rashidi, S., Rosen, M. A., & Ellahi, R. (2017). Influences of wavy wall and nanoparticles on entropy generation over heat exchanger plat. *International Journal of Heat and Mass Transfer*, *109*, 1162–1171. https://doi.org/10.1016/j.ijheatmasstransfer.2017.03.006

Fan, X., Chen, H., Ding, Y., Plucinski, P. K., & Lapkin, A. A. (2008). Potential of "nanofluids" to further intensify microreactors. *Green Chemistry*, *10*(6), 670–677. https://doi.org/10.1039/b717943j

Fani, B., Abbassi, A., & Kalteh, M. (2013). Effect of nanoparticles size on thermal performance of nanofluid in a trapezoidal microchannel-heat-sink. *International Communications in Heat and Mass Transfer*, *45*, 155–161. https://doi.org/10.1016/j.icheatmasstransfer.2013.04.003

Feng, X. B., Liu, Q., & He, Y. L. (2020). Numerical simulations of convection heat transfer in porous media using a cascaded lattice Boltzmann method. *International Journal of Heat and Mass Transfer*, *151*. https://doi.org/10.1016/j.ijheatmasstransfer.2020.119410

Ganesan, P., Behroyan, I., He, S., Sivasankaran, S., & Sandaran, S. C. (2016). Turbulent forced convection of Cu-water nanofluid in a heated tube: Improvement of the two-phase model. *Numerical Heat Transfer; Part A: Applications*, *69*(4), 401–420. https://doi.org/10.1080/10407782.2015.1081019

Ghani, I. A., Kamaruzaman, N., & Sidik, N. A. C. (2017). Heat transfer augmentation in a microchannel heat sink with sinusoidal cavities and rectangular ribs. *International Journal of Heat and Mass Transfer*, *108*, 1969–1981. https://doi.org/10.1016/j.ijheatmasstransfer.2017.01.046

Ghani, I. A., Sidik, N. A. C., & Kamaruzaman, N. (2017). Hydrothermal performance of microchannel heat sink: The effect of channel design. *International Journal of Heat and Mass Transfer*, *107*, 21–44. https://doi.org/10.1016/j.ijheatmasstransfer.2016.11.031

Ghasemi, S. E., Ranjbar, A. A., & Hosseini, M. J. (2017). Numerical study on effect of CuO-water nanofluid on cooling performance of two different cross-sectional heat sinks. *Advanced Powder Technology*, *28*(6), 1495–1504. https://doi.org/10.1016/j.apt.2017.03.019

Gnanadason, M., Kumar, P., Jemilda, G., & Jasper, S. (2012). Effect of nanofluids in a modified vacuum single basin solar still. *Int J Sci Eng Res*, *January*, 1–7. http://www.ijser.org/researchpaper%5CEffect-of-Nanofluids-in-a-Vacuum-Single-Basin-Solar-Still.pdf

Haddad, Z., Abu-Nada, E., Oztop, H. F., & Mataoui, A. (2012). Natural convection in nanofluids: Are the thermophoresis and Brownian motion effects significant in nanofluid heat transfer enhancement? *International Journal of Thermal Sciences*, *57*, 152–162. https://doi.org/10.1016/j.ijthermalsci.2012.01.016

Haghshenas Fard, M., Esfahany, M. N., & Talaie, M. R. (2010). Numerical study of convective heat transfer of nanofluids in a circular tube two-phase model versus single-phase model. *International Communications in Heat and Mass Transfer*, *37*(1), 91–97. https://doi.org/10.1016/j.icheatmasstransfer.2009.08.003

Hamzah, H., Hasan, S. I., & Küçüka, S. (2020). Numerical study of thermal transport in a flat-plate solar collector using novel absorber plate. In *Green Energy and Technology*. https://doi.org/10.1007/978-3-030-20637-6_32

Hamzah, Hudhaifa, Albojamal, A., Sahin, B., & Vafai, K. (2020). Thermal management of transverse magnetic source effects on nanofluid natural convection in a wavy porous enclosure. *Journal of Thermal Analysis and Calorimetry*. https://doi.org/10.1007/s10973-020-10246-4

Hamzah, Hudhaifa, Canpolat, C., Jasim, L. M., & Sahin, B. (2021). Hydrothermal index and entropy generation of a heated cylinder placed between two oppositely rotating cylinders in a vented cavity. *International Journal of Mechanical Sciences*, *201*. https://doi.org/10.1016/j.ijmecsci.2021.106465

Hassani, S., Saidur, R., Mekhilef, S., & Hepbasli, A. (2015). A new correlation for predicting the thermal conductivity of nanofluids; using dimensional analysis. *International Journal of Heat and Mass Transfer*, *90*, 121–130. https://doi.org/10.1016/j.ijheatmasstransfer.2015.06.040

Hatami, M., & Jing, D. (2017). Optimization of wavy direct absorber solar collector (WDASC) using Al2O3-water nanofluid and RSM analysis. *Applied Thermal Engineering*, *121*, 1040–1050. https://doi.org/10.1016/j.applthermaleng.2017.04.137

Hazeri-Mahmel, N., Shekari, Y., & Tayebi, A. (2021). Three-dimensional analysis of forced convection of Newtonian and non-Newtonian nanofluids through a horizontal pipe using single- and two-phase models. *International Communications in Heat and Mass Transfer*, *121*. https://doi.org/10.1016/j.icheatmasstransfer.2021.105119

He, Y., Men, Y., Zhao, Y., Lu, H., & Ding, Y. (2009). Numerical investigation into the convective heat transfer of TiO2 nanofluids flowing through a straight tube under the laminar flow conditions. *Applied Thermal Engineering*, *29*(10), 1965–1972. https://doi.org/10.1016/j.applthermaleng.2008.09.020

Heidary, H., & Kermani, M. J. (2010). Effect of nano-particles on forced convection in sinusoidal-wall channel. *International Communications in Heat and Mass Transfer*, *37*(10), 1520–1527. https://doi.org/10.1016/j.icheatmasstransfer.2010.08.018

Hejazian, M., & Moraveji, M. K. (2013). A comparative analysis of single and two-phase models of turbulent convective heat transfer in a tube for TiO2 nanofluid with CFD. *Numerical Heat Transfer; Part A: Applications*, *63*(10), 795–806. https://doi.org/10.1080/10407782.2013.756759

Hemmat Esfe, M., Bahiraei, M., Torabi, A., & Valadkhani, M. (2021). A critical review on pulsating flow in conventional fluids and nanofluids: Thermo-hydraulic characteristics. *International Communications in Heat and Mass Transfer*, *120*. https://doi.org/10.1016/j.icheatmasstransfer.2020.104859

Hemmat Esfe, M., & Saedodin, S. (2015). Turbulent forced convection heat transfer and thermophysical properties of Mgo-water nanofluid with consideration of different nanoparticles diameter, an empirical study. *Journal of Thermal Analysis and Calorimetry*, *119*(2), 1205–1213. https://doi.org/10.1007/s10973-014-4197-1

Ho, C. J., Liu, W. K., Chang, Y. S., & Lin, C. C. (2010). Natural convection heat transfer of alumina-water nanofluid in vertical square enclosures: An experimental study. *International Journal of Thermal Sciences*, *49*(8), 1345–1353. https://doi.org/10.1016/j.ijthermalsci.2010.02.013

Hoang, V. Q., Hoang, T. T., Dinh, C. T., & Plourde, F. (2021). Large eddy simulation of the turbulence heat and mass transfer of pulsating flow in a V-sharp corrugated channel. *International Journal of Heat and Mass Transfer*, *166*. https://doi.org/10.1016/j.ijheatmasstransfer.2020.120720

Hu, P., & Li, Q. (2020). Effect of heat source on forced convection in a partially-filled porous channel under LTNE condition. *International Communications in Heat and Mass Transfer*, *114*. https://doi.org/10.1016/j.icheatmasstransfer.2020.104578

Hu, Y., Li, H., He, Y., Liu, Z., & Zhao, Y. (2017). Effect of nanoparticle size and concentration on boiling performance of SiO2nanofluid. *International Journal of Heat and Mass Transfer*, *107*, 820–828. https://doi.org/10.1016/j.ijheatmasstransfer.2016.11.090

Huang, D., Wu, Z., & Sunden, B. (2016). Effects of hybrid nanofluid mixture in plate heat exchangers. *Experimental Thermal and Fluid Science*, *72*, 190–196. https://doi.org/10.1016/j.expthermflusci.2015.11.009

Hwang, Y., Park, H. S., Lee, J. K., & Jung, W. H. (2006). Thermal conductivity and lubrication characteristics of nanofluids. *Current Applied Physics*, *6*(SUPPL. 1). https://doi.org/10.1016/j.cap.2006.01.014

Iijima, S., & Ichihashi, T. (1993). Single-shell carbon nanotubes of 1-nm diameter. *Nature*, *363*(6430), 603–605. https://doi.org/10.1038/363603a0

Islamoglu, Y., & Parmaksizoglu, C. (2003). The effect of channel height on the enhanced heat transfer characteristics in a corrugated heat exchanger channel. *Applied Thermal Engineering*, *23*(8), 979–987. https://doi.org/10.1016/S1359-4311(03)00029-2

J.C., M. (1873). A Treatise on Electricity and Magnetism. *Nature*, *7*(182), 478–480. https://doi.org/10.1038/007478a0

Jafari, M., Farhadi, M., & Sedighi, K. (2015). Convection heat transfer of SWCNT-nanofluid in a corrugated channel under pulsating velocity profile. *International Communications in Heat and Mass Transfer*, *67*, 137–146. https://doi.org/10.1016/j.icheatmasstransfer.2015.07.008

Jafari, M., Farhadi, M., & Sedighi, K. (2017). An experimental study on the effects of a new swirl generator on thermal performance of a circular tube. *International Communications in Heat and Mass Transfer*, *87*, 277–287. https://doi.org/10.1016/j.icheatmasstransfer.2017.07.016

Jalal, R., Goharshadi, E. K., Abareshi, M., Moosavi, M., Yousefi, A., & Nancarrow, P. (2010). ZnO nanofluids: Green synthesis, characterization, and antibacterial activity. *Materials Chemistry and Physics*, *121*(1–2), 198–201. https://doi.org/10.1016/j.matchemphys.2010.01.020

James Clerk, M. (2010). A treatise on electricity and magnetism. *A Treatise on Electricity and Magnetism*, *9781108014*, 1–442. https://doi.org/10.1017/CBO9780511709333

Janssen, L. A. M., & Hoogendoorn, C. J. (1978). Laminar convective heat transfer in helical coiled tubes. *International Journal of Heat and Mass Transfer*, *21*(9), 1197–1206. https://doi.org/10.1016/0017-9310(78)90138-2

Jasim, L. M., Hamzah, H., Canpolat, C., & Sahin, B. (2021). Mixed convection flow of hybrid nanofluid through a vented enclosure with an inner rotating cylinder. *International Communications in Heat and Mass Transfer*, *121*. https://doi.org/10.1016/j.icheatmasstransfer.2020.105086

Jin, D. X., Lee, Y. P., & Lee, D. Y. (2007). Effects of the pulsating flow agitation on the heat transfer in a triangular grooved channel. *International Journal of Heat and Mass Transfer*, *50*(15–16), 3062–3071. https://doi.org/10.1016/j.ijheatmasstransfer.2006.12.001

Kalteh, M., Abbassi, A., Saffar-Avval, M., Frijns, A., Darhuber, A., & Harting, J. (2012). Experimental and numerical investigation of nanofluid forced convection inside a wide microchannel heat sink. *Applied Thermal Engineering*, *36*(1), 260–268. https://doi.org/10.1016/j.applthermaleng.2011.10.023

Kalteh, M., Abbassi, A., Saffar-Avval, M., & Harting, J. (2011). Eulerian-Eulerian two-phase numerical simulation of nanofluid laminar forced convection in a microchannel. *International Journal of Heat and Fluid Flow*, *32*(1), 107–116. https://doi.org/10.1016/j.ijheatfluidflow.2010.08.001

Kao, M. J., Lo, C. H., Tsung, T. T., Wu, Y. Y., Jwo, C. S., & Lin, H. M. (2007). Copper-oxide brake nanofluid manufactured using arc-submerged nanoparticle synthesis system. *Journal of Alloys and Compounds*, *434–435*(SPEC. ISS.), 672–674. https://doi.org/10.1016/j.jallcom.2006.08.305

Keshavarz Moraveji, M., & Esmaeili, E. (2012). Comparison between single-phase and two-phases CFD modeling of laminar forced convection flow of nanofluids in a circular tube under constant heat flux. *International Communications in Heat and Mass Transfer*, *39*(8), 1297–1302. https://doi.org/10.1016/j.icheatmasstransfer.2012.07.012

Keshavarz Moraveji, M., & Mohammadi Ardehali, R. (2013). CFD modeling (comparing single and two-phase approaches) on thermal performance of Al2o3/water nanofluid in mini-channel heat sink. *International Communications in Heat and Mass Transfer*, *44*, 157–164. https://www.sciencedirect.com/science/article/pii/S0735193313000407

Khaleduzzaman, S. S., Mahbubul, I. M., Shahrul, I. M., & Saidur, R. (2013). Effect of particle concentration, temperature and surfactant on surface tension of nanofluids. *International Communications in Heat and Mass Transfer*, *49*, 110–114. https://doi.org/10.1016/j.icheatmasstransfer.2013.10.010

Khanafer, K., Vafai, K., & Lightstone, M. (2003). Buoyancy-driven heat transfer enhancement in a two-dimensional enclosure utilizing nanofluids. *International Journal of Heat and Mass Transfer*, *46*(19), 3639–3653. https://doi.org/10.1016/S0017-9310(03)00156-X

Kim, Y. S., & Kim, Y. H. (2003). Application of ferro-cobalt magnetic fluid for oil sealing. *Journal of Magnetism and Magnetic Materials*, *267*(1), 105–110. https://doi.org/10.1016/S0304-8853(03)00342-1

Kleinstreuer, C., & Feng, Y. (2011). Erratum to: Experimental and theoretical studies of nanofluid thermal conductivity enhancement: a review. *Nanoscale Research Letters*, *6*(1). https://doi.org/10.1186/1556-276x-6-439

Kulkarni, D. P., Das, D. K., & Vajjha, R. S. (2009). Application of nanofluids in heating buildings and reducing pollution. *Applied Energy*, *86*(12), 2566–2573. https://doi.org/10.1016/j.apenergy.2009.03.021

Kumar, K., Kumar, R., Bharj, R. S., & Mondal, P. K. (2021). Irreversibility analysis of the convective flow through corrugated channels: a comprehensive review. *European Physical Journal Plus*, *136*(4). https://doi.org/10.1140/epjp/s13360-021-01388-x

Kumar, V., Tiwari, A. K., & Ghosh, S. K. (2016). Effect of variable spacing on performance of plate heat exchanger using nanofluids. *Energy*, *114*, 1107–1119. https://doi.org/10.1016/j.energy.2016.08.091

Kurtulmuş, N., & Sahin, B. (2019). A review of hydrodynamics and heat transfer through corrugated channels. *International Communications in Heat and Mass Transfer*, *108*. https://doi.org/10.1016/j.icheatmasstransfer.2019.104307

Kurtulmuş, N., & Sahin, B. (2020). Experimental investigation of pulsating flow structures and heat transfer characteristics in sinusoidal channels. *International Journal of Mechanical Sciences*, *167*. https://doi.org/10.1016/j.ijmecsci.2019.105268

Kurtulmuş, N., Zontul, H., & Sahin, B. (2020). Heat transfer and flow characteristics in a sinusoidally curved converging-diverging channel. *International Journal of Thermal Sciences*, *148*. https://doi.org/10.1016/j.ijthermalsci.2019.106163

Leong, K. Y., Ku Ahmad, K. Z., Ong, H. C., Ghazali, M. J., & Baharum, A. (2017). Synthesis and thermal conductivity characteristic of hybrid nanofluids – A review. *Renewable and Sustainable Energy Reviews*, *75*, 868–878. https://doi.org/10.1016/j.rser.2016.11.068

Li, Q., & Xuan, Y. (2003). Investigation on Convective Heat Transfer and Flow Features of Nanofluids. *Journal of Heat Transfer*, *125*(1), 151–155. http://link.aip.org/link/?JHR/125/151/1

Lotfi, R., Saboohi, Y., & Rashidi, A. M. (2010). Numerical study of forced convective heat transfer of Nanofluids: Comparison of different approaches. *International Communications in Heat and Mass Transfer*, *37*(1), 74–78. https://doi.org/10.1016/j.icheatmasstransfer.2009.07.013

M'hamed, B., Che Sidik, N. A., Akhbar, M. F. A., Mamat, R., & Najafi, G. (2016). Experimental study on thermal performance of MWCNT nanocoolant in Perodua Kelisa 1000cc radiator system. *International Communications in Heat and Mass Transfer*, *76*, 156–161. https://doi.org/10.1016/j.icheatmasstransfer.2016.05.024

Mahian, O., Kolsi, L., Amani, M., Estellé, P., Ahmadi, G., Kleinstreuer, C., Marshall, J. S., Siavashi, M., Taylor, R. A., Niazmand, H., Wongwises, S., Hayat, T., Kolanjiyil, A., Kasaeian, A., & Pop, I. (2019). Recent advances in modeling and simulation of nanofluid flows-Part I: Fundamentals and theory. *Physics Reports*, *790*, 1–48. https://doi.org/10.1016/j.physrep.2018.11.004

Maïga, S. E. B., Nguyen, C. T., Galanis, N., & Roy, G. (2004). Heat transfer behaviours of nanofluids in a uniformly heated tube. *Superlattices and Microstructures*, *35*(3–6), 543–557. https://doi.org/10.1016/j.spmi.2003.09.012

Menter, F. R. (1994). Two-equation eddy-viscosity turbulence models for engineering applications. *AIAA Journal*, *32*(8), 1598–1605. https://doi.org/10.2514/3.12149

Minea, A. A. (2014). Uncertainties in modeling thermal conductivity of laminar forced convection heat transfer with water alumina nanofluids. *International Journal of Heat and Mass Transfer*, *68*, 78–84. https://doi.org/10.1016/j.ijheatmasstransfer.2013.09.018

Minea, A. A. (2017). Hybrid nanofluids based on Al2O3, TiO2 and SiO2: Numerical evaluation of different approaches. *International Journal of Heat and Mass Transfer*, *104*, 852–860. https://doi.org/10.1016/j.ijheatmasstransfer.2016.09.012

Mintsa, H. A., Roy, G., Nguyen, C. T., & Doucet, D. (2009). New temperature dependent thermal conductivity data for water-based nanofluids. *International Journal of Thermal Sciences*, *48*(2), 363–371. https://doi.org/10.1016/j.ijthermalsci.2008.03.009

Mirmasoumi, S., & Behzadmehr, A. (2008). Effect of nanoparticles mean diameter on mixed convection heat transfer of a nanofluid in a horizontal tube. *International Journal of Heat and Fluid Flow*, *29*(2), 557–566. https://doi.org/10.1016/j.ijheatfluidflow.2007.11.007

Miroshnichenko, I. V., Sheremet, M. A., Pop, I., & Ishak, A. (2017). Convective heat transfer of micropolar fluid in a horizontal wavy channel under the local heating. *International Journal of Mechanical Sciences*, *128–129*, 541–549. https://doi.org/10.1016/j.ijmecsci.2017.05.013

Mirzaei, M., Saffar-Avval, M., & Naderan, H. (2014). Heat transfer investigation of laminar developing flow of nanofluids in a microchannel based on Eulerian-Lagrangian approach. *Canadian Journal of Chemical Engineering*, *92*(6), 1139–1149. https://doi.org/10.1002/cjce.21962

Mitsuishi, A., Sakoh, M., Shimura, T., Iwamoto, K., Murata, A., & Mamori, H. (2020). Direct numerical simulation of convective heat transfer in a pipe with transverse vibration. *International Journal of Heat and Mass Transfer*, *148*. https://doi.org/10.1016/j.ijheatmasstransfer.2019.119048

Mojarrad, M. S., Keshavarz, A., & Shokouhi, A. (2013). Nanofluids thermal behavior analysis using a new dispersion model along with single-phase. *Heat and Mass Transfer/Waerme- Und Stoffuebertragung*, *49*(9), 1333–1343. https://doi.org/10.1007/s00231-013-1182-3

Moraveji, M. K., Darabi, M., Haddad, S. M. H., & Davarnejad, R. (2011). Modeling of convective heat transfer of a nanofluid in the developing region of tube flow with computational fluid dynamics. *International Communications in Heat and Mass Transfer*, *38*(9), 1291–1295. https://doi.org/10.1016/j.icheatmasstransfer.2011.06.011

Murshed, S. M. S., Leong, K. C., & Yang, C. (2008). Investigations of thermal conductivity and viscosity of nanofluids. *International Journal of Thermal Sciences*, *47*(5), 560–568. https://doi.org/10.1016/j.ijthermalsci.2007.05.004

Nada, E. A.-. (2009). Effects of variable viscosity and thermal conductivity of Al2O3- water nanofluid on heat transfer enhancement in natural convection. *International Journal of Heat and Fluid Flow*, *30*(4), 679–690.

Naphon, P., & Wiriyasart, S. (2018). Pulsating flow and magnetic field effects on the convective heat transfer of TiO2-water nanofluids in helically corrugated tube. *International Journal of Heat and Mass Transfer*, *125*, 1054–1060. https://doi.org/10.1016/j.ijheatmasstransfer.2018.05.015

Naphon, P., & Wongwises, S. (2006). A review of flow and heat transfer characteristics in curved tubes. *Renewable and Sustainable Energy Reviews*, *10*(5), 463–490. https://doi.org/10.1016/j.rser.2004.09.014

Nield, D. A., & Kuznetsov, A. V. (2007). Forced convection with laminar pulsating flow in a channel or tube. *International Journal of Thermal Sciences*, *46*(6), 551–560. https://doi.org/10.1016/j.ijthermalsci.2006.07.011

Nóbrega, C. E. L., & Brum, N. C. L. (2009). Modeling and simulation of heat and enthalpy recovery wheels. *Energy*, *34*(12), 2063–2068. https://doi.org/10.1016/j.energy.2008.08.016

Nuim Labib, M., Nine, M. J., Afrianto, H., Chung, H., & Jeong, H. (2013). Numerical investigation on effect of base fluids and hybrid nanofluid in forced convective heat transfer. *International Journal of Thermal Sciences*, *71*, 163–171. https://doi.org/10.1016/j.ijthermalsci.2013.04.003

O'Hanley, H., Buongiorno, J., McKrell, T., & Hu, L. W. (2011). Measurement and model correlation of specific heat capacity of water-based nanofluids with silica, alumina and copper oxide nanoparticles. *ASME 2011 International Mechanical Engineering Congress and Exposition, IMECE 2011*, *10*(PARTS A AND B), 1209–1214. https://doi.org/10.1115/imece2011-62054

Oh, D. W., Jain, A., Eaton, J. K., Goodson, K. E., & Lee, J. S. (2008). Thermal conductivity measurement and sedimentation detection of aluminum oxide nanofluids by using the 3ω method. *International Journal of Heat and Fluid Flow*, *29*(5), 1456–1461. https://doi.org/10.1016/j.ijheatfluidflow.2008.04.007

Onyiriuka, E. J., Obanor, A. I., Mahdavi, M., & Ewim, D. R. E. (2018). Evaluation of single-phase, discrete, mixture and combined model of discrete and mixture phases in predicting nanofluid heat transfer characteristics for laminar and turbulent flow regimes. *Advanced Powder Technology*, *29*(11), 2644–2657. https://doi.org/10.1016/j.apt.2018.07.013

Ooi, E. H., & Popov, V. (2013). Numerical study of influence of nanoparticle shape on the natural convection in Cu-water nanofluid. *International Journal of Thermal Sciences*, *65*, 178–188. https://doi.org/10.1016/j.ijthermalsci.2012.10.020

Oosthuizen, P. H., & Carscallen, W. E. (2013). Introduction to Compressible Fluid Flow. *Introduction to Compressible Fluid Flow*. https://doi.org/10.1201/b15414

Oztop, H. F., & Abu-Nada, E. (2008). Numerical study of natural convection in partially heated rectangular enclosures filled with nanofluids. *International Journal of Heat and Fluid Flow*, *29*(5), 1326–1336. https://doi.org/10.1016/j.ijheatfluidflow.2008.04.009

Pak, B. C., & Cho, Y. I. (1998). Hydrodynamic and heat transfer study of dispersed fluids with submicron metallic oxide particles. *Experimental Heat Transfer*, *11*(2), 151–170. https://doi.org/10.1080/08916159808946559

Palm, S. J., Roy, G., & Nguyen, C. T. (2006). Heat transfer enhancement with the use of nanofluids in radial flow cooling systems considering temperature-dependent properties. *Applied Thermal Engineering*, *26*(17–18), 2209–2218. https://doi.org/10.1016/j.applthermaleng.2006.03.014

Pandey, S. D., & Nema, V. K. (2012). Experimental analysis of heat transfer and friction factor of nanofluid as a coolant in a corrugated plate heat exchanger. *Experimental Thermal and Fluid Science*, *38*, 248–256. https://doi.org/10.1016/j.expthermflusci.2011.12.013

Pastoriza-Gallego, M. J., Casanova, C., Páramo, R., Barbś, B., Legido, J. L., & Piñeiro, M. M. (2009). A study on stability and thermophysical properties (density and viscosity) of Al2 O3 in water nanofluid. *Journal of Applied Physics*, *106*(6). https://doi.org/10.1063/1.3187732

Peng, W., Minli, B., Jizu, L., Chengzhi, H., & Yuyan, W. (2014). Numerical investigation on the turbulent flow characteristic of nanofluids in a horizontal circular tube. *Numerical Heat Transfer; Part A: Applications*, *66*(6), 646–668. https://doi.org/10.1080/10407782.2014.894389

Philip, J., Jaykumar, T., Kalyanasundaram, P., & Raj, B. (2003). A tunable optical filter. *Measurement Science and Technology*, *14*(8), 1289–1294. https://doi.org/10.1088/0957-0233/14/8/314

Pitla, S. S., Groll, E. A., & Ramadhyani, S. (2002). New correlation to predict the heat transfer coefficient during in-tube cooling of turbulent supercritical CO2. *International Journal of Refrigeration*, *25*(7), 887–895. https://doi.org/10.1016/S0140-7007(01)00098-6

Popa, I., Gillies, G., Papastavrou, G., & Borkovec, M. (2010). Attractive and repulsive electrostatic forces between positively charged latex particles in the presence of anionic linear polyelectrolytes. *Journal of Physical Chemistry B*, *114*(9), 3170–3177. https://doi.org/10.1021/jp911482a

Prasher, R., Phelan, P. E., & Bhattacharya, P. (2006). Effect of aggregation kinetics on the thermal conductivity of nanoscale colloidal solutions (nanofluid). *Nano Letters*, *6*(7), 1529–1534. https://doi.org/10.1021/nl060992s

Rahgoshay, M., Ranjbar, A. A., & Ramiar, A. (2012). Laminar pulsating flow of nanofluids in a circular tube with isothermal wall. *International Communications in Heat and Mass Transfer*, *39*(3), 463–469. https://doi.org/10.1016/j.icheatmasstransfer.2011.12.008

Ramgadia, A. G., & Saha, A. K. (2014). Characteristics of fully developed flow and heat transfer in channels with varying wall geometry. *Journal of Heat Transfer*, *136*(2). https://doi.org/10.1115/1.4024552

Rashidi, S., Akbarzadeh, M., Masoodi, R., & Languri, E. M. (2017). Thermal-hydraulic and entropy generation analysis for turbulent flow inside a corrugated channel. *International Journal of Heat and Mass Transfer*, *109*, 812–823. https://doi.org/10.1016/j.ijheatmasstransfer.2017.02.033

Rashidi, S., Bovand, M., & Esfahani, J. A. (2017). Sensitivity analysis for entropy generation in porous solar heat exchangers by RSM. *Journal of Thermophysics and Heat Transfer*, *31*(2), 390–402. https://doi.org/10.2514/1.T5003

Rashidi, Saman, Akar, S., Bovand, M., & Ellahi, R. (2018). Volume of fluid model to simulate the nanofluid flow and entropy generation in a single slope solar still. *Renewable Energy*, *115*, 400–410. https://doi.org/10.1016/j.renene.2017.08.059

Roslan, R., Saleh, H., & Hashim, I. (2012). Effect of rotating cylinder on heat transfer in a square enclosure filled with nanofluids. *International Journal of Heat and Mass Transfer*, *55*(23–24), 7247–7256. https://doi.org/10.1016/j.ijheatmasstransfer.2012.07.051

S M S Murshed, K C Long, & C Yang. (2005). Enhanced Thermal Conductivity of TiO2-Water Based Nanofluids. *International Journal of Thermal Sciences*, *44*, 367–373.

Saeedinia, M., Akhavan-Behabadi, M. A., & Razi, P. (2012). Thermal and rheological characteristics of CuO-Base oil nanofluid flow inside a circular tube. *International Communications in Heat and Mass Transfer*, *39*(1), 152–159. https://doi.org/10.1016/j.icheatmasstransfer.2011.08.001

Said, Z., Sajid H, M., Kamyar, A., & Saidur, R. (2013). Experimental investigation on the stability and density of TiO2, Al2O3, SiO2 and TiSiO4. *IOP Conference Series: Earth and Environmental Science*, *16*(1). https://doi.org/10.1088/1755-1315/16/1/012002

Said, Zafar, El Haj Assad, M., Hachicha, A. A., Bellos, E., Abdelkareem, M. A., Alazaizeh, D. Z., & Yousef, B. A. A. (2019). Enhancing the performance of automotive radiators using nanofluids. *Renewable and Sustainable Energy Reviews*, *112*, 183–194. https://doi.org/10.1016/j.rser.2019.05.052

Saidur, R., Leong, K. Y., & Mohammed, H. A. (2011). A review on applications and challenges of nanofluids. *Renewable and Sustainable Energy Reviews*, *15*(3), 1646–1668. https://doi.org/10.1016/j.rser.2010.11.035

Sajadi, A. R., & Kazemi, M. H. (2011). Investigation of turbulent convective heat transfer and pressure drop of TiO2/water nanofluid in circular tube. *International Communications in Heat and Mass Transfer*, *38*(10), 1474–1478. https://doi.org/10.1016/j.icheatmasstransfer.2011.07.007

Saleh, H., Roslan, R., & Hashim, I. (2011). Natural convection heat transfer in a nanofluid-filled trapezoidal enclosure. *International Journal of Heat and Mass Transfer*, *54*(1–3), 194–201. https://doi.org/10.1016/j.ijheatmasstransfer.2010.09.053

Sarafraz, M. M., & Hormozi, F. (2016). Heat transfer, pressure drop and fouling studies of multi-walled carbon nanotube nano-fluids inside a plate heat exchanger. *Experimental Thermal and Fluid Science*, *72*, 1–11. https://doi.org/10.1016/j.expthermflusci.2015.11.004

Sekhar, Y. R., & Sharma, K. V. (2015). Study of viscosity and specific heat capacity characteristics of water-based Al2O3nanofluids at low particle concentrations. *Journal of Experimental Nanoscience*, *10*(2), 86–102. https://doi.org/10.1080/17458080.2013.796595

Selimefendigil, F., & Öztop, H. F. (2018). Numerical analysis and ANFIS modeling for mixed convection of CNT-water nanofluid filled branching channel with an annulus and a rotating inner surface at the junction. *International J"ournal of Heat and Mass Transfer*, *127*, 583–599. https://doi.org/10.1016/j.ijheatmasstransfer.2018.07.038

Selimefendigil, F., Öztop, H. F., & Özgul, R. (2019). Turbulent forced convection of nanofluid in an elliptic cross-sectional pipe. *International Communications in Heat and Mass Transfer*, *109*. https://doi.org/10.1016/j.icheatmasstransfer.2019.104384

Shah, R. K., & Sekuli, D. P. (2003). Fundamentals of Heat Exchanger Design. *Fundamentals of Heat Exchanger Design*. https://doi.org/10.1002/9780470172605

Shahrul, I. M., Mahbubul, I. M., Khaleduzzaman, S. S., Saidur, R., & Sabri, M. F. M. (2014). A comparative review on the specific heat of nanofluids for energy perspective. *Renewable and Sustainable Energy Reviews*, *38*, 88–98. https://doi.org/10.1016/j.rser.2014.05.081

Shahsavar, A., Alimohammadi, S. S., Askari, I. B., & Ali, H. M. (2021). Numerical investigation of the effect of corrugation profile on the hydrothermal characteristics and entropy generation behavior of laminar forced convection of non-Newtonian water/CMC-CuO nanofluid flow inside a wavy channel. *International Communications in Heat and Mass Transfer*, *121*. https://doi.org/10.1016/j.icheatmasstransfer.2021.105117

Shariat, M., Moghari, R. M., Akbarinia, A., Rafee, R., & Sajjadi, S. M. (2014). Impact of nanoparticle mean diameter and the buoyancy force on laminar mixed convection nanofluid flow in an elliptic duct employing two phase mixture model. *International Communications in Heat and Mass Transfer*, *50*, 15–24. https://doi.org/10.1016/j.icheatmasstransfer.2013.11.003

Sheikholeslami, M., & Ellahi, R. (2015). Three dimensional mesoscopic simulation of magnetic field effect on natural convection of nanofluid. *International Journal of Heat and Mass Transfer*, *89*, 799–808. https://doi.org/10.1016/j.ijheatmasstransfer.2015.05.110

Sheikholeslami, Mohsen. (2017). Magnetic field influence on CuO–H2O nanofluid convective flow in a permeable cavity considering various shapes for nanoparticles. *International Journal of Hydrogen Energy*, *42*(31), 19611–19621. https://doi.org/10.1016/j.ijhydene.2017.06.121

Shen, B., Shih, A. J., & Tung, S. C. (2008). Application of nanofluids in minimum quantity lubrication grinding. *Tribology Transactions*, *51*(6), 730–737. https://doi.org/10.1080/10402000802071277

Siavashi, M., Yousofvand, R., & Rezanejad, S. (2018). Nanofluid and porous fins effect on natural convection and entro[1] B. Ghasemi, S.M. Aminossadati, A. Raisi, Magnetic field effect on natural convection in a nanofluid-filled square enclosure, Int. J. Therm. Sci. 50 (2011) 1748–1756. https://doi.org/10.10. *Advanced Powder Technology*, *29*(1), 142–156. https://doi.org/10.1016/j.apt.2017.10.021

Sidik, N. A. C., Muhamad, M. N. A. W., Japar, W. M. A. A., & Rasid, Z. A. (2017). An overview of passive techniques for heat transfer augmentation in microchannel heat sink. *International Communications in Heat and Mass Transfer*, *88*, 74–83. https://doi.org/10.1016/j.icheatmasstransfer.2017.08.009

Sivakumar, A., Alagumurthi, N., & Senthilvelan, T. (2016). Experimental investigation of forced convective heat transfer performance in nanofluids of Al2O3/water and CuO/water in a serpentine shaped micro channel heat sink. *Heat and Mass Transfer/Waerme- Und Stoffuebertragung*, *52*(7), 1265–1274. https://doi.org/10.1007/s00231-015-1649-5

Sparrow, E. M., & Hossfeld, L. M. (1984). Effect of rounding of protruding edges on heat transfer and pressure drop in a duct. *International Journal of Heat and Mass Transfer*, *27*(10), 1715–1723. https://doi.org/10.1016/0017-9310(84)90154-6

Stephen U. S. Choi and J. A. Eastman. (1995). Enhancing thermal conductivity of fluids with nanoparticles. *American Society of Mechanical Engineers, Fluids Engineering Division (Publication) FED*, *231*, 99–105.

Sun, B., Zhang, Z., Yang, D., & Li, H. (2015). Heat transfer and flow resistance characteristics with drag reducing nanofluids in circular tube. *Huagong Xuebao/CIESC Journal*, *66*(11). https://doi.org/10.11949/j.issn.0438-1157.20150496

Tahir, S., & Mital, M. (2012). Numerical investigation of laminar nanofluid developing flow and heat transfer in a circular channel. *Applied Thermal Engineering*, *39*, 8–14. https://doi.org/10.1016/j.applthermaleng.2012.01.035

Tashtoush, B., & Al-Odat, M. (2004). Magnetic field effect on heat and fluid flow over a wavy surface with a variable heat flux. *Journal of Magnetism and Magnetic Materials*, *268*(3), 357–363. https://doi.org/10.1016/S0304-8853(03)00547-X

Taylor, R. A., Phelan, P. E., Otanicar, T. P., Walker, C. A., Nguyen, M., Trimble, S., & Prasher, R. (2011). Applicability of nanofluids in high flux solar collectors. *Journal of Renewable and Sustainable Energy*, *3*(2). https://doi.org/10.1063/1.3571565

Teng, T. P., & Hung, Y. H. (2014). Estimation and experimental study of the density and specific heat for alumina nanofluid. *Journal of Experimental Nanoscience*, *9*(7), 707–718. https://doi.org/10.1080/17458080.2012.696219

Thirugnanasambandam, M., Iniyan, S., & Goic, R. (2010). A review of solar thermal technologies. *Renewable and Sustainable Energy Reviews*, *14*(1), 312–322. https://doi.org/10.1016/j.rser.2009.07.014

Thostenson, E. T., Ren, Z., & Chou, T. W. (2001). Advances in the science and technology of carbon nanotubes and their composites: A review. *Composites Science and Technology*, *61*(13), 1899–1912. https://doi.org/10.1016/S0266-3538(01)00094-X

Timofeeva, E. V., Routbort, J. L., & Singh, D. (2009). Particle shape effects on thermophysical properties of alumina nanofluids. *Journal of Applied Physics*, *106*(1). https://doi.org/10.1063/1.3155999

Tsai, C. Y., Chien, H. T., Ding, P. P., Chan, B., Luh, T. Y., & Chen, P. H. (2004). Effect of structural character of gold nanoparticles in nanofluid on heat pipe thermal performance. *Materials Letters*, *58*(9), 1461–1465. https://doi.org/10.1016/j.matlet.2003.10.009

Tzeng, S. C., Lin, C. W., & Huang, K. D. (2005). Heat transfer enhancement of nanofluids in rotary blade coupling of four-wheel-drive vehicles. *Acta Mechanica*, *179*(1–2), 11–23. https://doi.org/10.1007/s00707-005-0248-9

Vajjha, R. S., & Das, D. K. (2009). Specific heat measurement of three nanofluids and development of new correlations. *Journal of Heat Transfer*, *131*(7), 1–7. https://doi.org/10.1115/1.3090813

Vanaki, S. M., Ganesan, P., & Mohammed, H. A. (2016). Numerical study of convective heat transfer of nanofluids: A review. *Renewable and Sustainable Energy Reviews*, *54*, 1212–1239. https://doi.org/10.1016/j.rser.2015.10.042

Vanaki, S. M., Mohammed, H. A., Abdollahi, A., & Wahid, M. A. (2014). Effect of nanoparticle shapes on the heat transfer enhancement in a wavy channel with different phase shifts. *Journal of Molecular Liquids*, *196*, 32–42. https://doi.org/10.1016/j.molliq.2014.03.001

Wang, B. X., Zhou, L. P., & Peng, X. F. (2006). Surface and size effects on the specific heat capacity of nanoparticles. *International Journal of Thermophysics*, *27*(1), 139–151. https://doi.org/10.1007/s10765-006-0022-9

Wang, C. C., & Chen, C. K. (2002). Forced convection in a wavy-wall channel. *International Journal of Heat and Mass Transfer*, *45*(12), 2587–2595. https://doi.org/10.1016/S0017-9310(01)00335-0

Wang, G., & Vanka, S. P. (1995). Convective heat transfer in periodic wavy passages. *International Journal of Heat and Mass Transfer*, *38*(17), 3219–3230. https://doi.org/10.1016/0017-9310(95)00051-A

Wang, J., Zhu, J., Zhang, X., & Chen, Y. (2013). Heat transfer and pressure drop of nanofluids containing carbon nanotubes in laminar flows. *Experimental Thermal and Fluid Science*, *44*, 716–721. https://doi.org/10.1016/j.expthermflusci.2012.09.013

Wang, Yun, Fisher, T. S., Davidson, J. L., & Jiang, L. (2002). Thermal conductivity of nanoparticle suspensions. *8th AIAA/ASME Joint Thermophysics and Heat Transfer Conference*. https://doi.org/10.2514/6.2002-3345

Wang, Yuyan, Wang, P., Yoon, S., Yu, Y., & Bai, M. (2018). Characteristics of flow and heat transfer of nanofluids under laminar states. *Numerical Heat Transfer; Part A: Applications*, *73*(1), 1–16. https://doi.org/10.1080/10407782.2017.1420298

Webb, R. L. (1994). *Principles of enhanced heat transfer*. https://doi.org/10.1016/0301-9322(95)90005-5

Wen, D., & Ding, Y. (2004). Experimental investigation into convective heat transfer of nanofluids at the entrance region under laminar flow conditions. *International Journal of Heat and Mass Transfer*, *47*(24), 5181–5188. https://doi.org/10.1016/j.ijheatmasstransfer.2004.07.012

Wen, D., & Ding, Y. (2005). Formulation of nanofluids for natural convective heat transfer applications. *International Journal of Heat and Fluid Flow*, *26*(6), 855–864. https://doi.org/10.1016/j.ijheatfluidflow.2005.10.005

Wen, D., & Ding, Y. (2006). Natural convective heat transfer of suspensions of titanium dioxide nanoparticles (nanofluids). *IEEE Transactions on Nanotechnology*, *5*(3), 220–227. https://doi.org/10.1109/TNANO.2006.874045

Wong, K. V., Khanafer, K., & Vafai, K. (2018). A Critical Synthesis of Thermophysical Characteristics of Nanofluids. *Nanotechnology and Energy*, 279–332. https://doi.org/10.1201/9781315163574-12

Xie, H., Wang, J., Xi, T., & Liu, Y. (2002). Thermal Conductivity of Suspensions Containing Nanosized SiC Particles. *International Journal of Thermophysics*, *23*(2), 571–580. https://doi.org/10.1023/A:1015121805842

Xuan, Y., & Roetzel, W. (2000). Conceptions for heat transfer correlation of nanofluids. *International Journal of Heat and Mass Transfer*, *43*(19), 3701–3707. https://doi.org/10.1016/S0017-9310(99)00369-5

Xue, Q. Z. (2005). Model for thermal conductivity of carbon nanotube-based composites. *Physica B: Condensed Matter*, *368*(1–4), 302–307. https://doi.org/10.1016/j.physb.2005.07.024

Yang, F., Qiu, X. M., Li, Y., Yin, Y., & Fan, Q. (2008). Specific heat of super carbon nanotube and its chirality independence. *Physics Letters, Section A: General, Atomic and Solid State Physics*, *372*(46), 6960–6964. https://doi.org/10.1016/j.physleta.2008.09.048

Yang, L., Du, K., & Zhang, Z. (2020). Heat transfer and flow optimization of a novel sinusoidal minitube filled with non-Newtonian SiC/EG-water nanofluids. *International Journal of Mechanical Sciences*, *168*. https://doi.org/10.1016/j.ijmecsci.2019.105310

Yang, Y. T., Tang, H. W., Zeng, B. Y., & Jian, M. H. (2016). Numerical simulation and optimization of turbulent nanofluids in a three-dimensional arc rib-grooved channel. *Numerical Heat Transfer; Part A: Applications*, *70*(8), 831–846. https://doi.org/10.1080/10407782.2016.1214513

Yang, Y. T., Wang, Y. H., & Tseng, P. K. (2014). Numerical optimization of heat transfer enhancement in a wavy channel using nanofluids. *International Communications in Heat and Mass Transfer*, *51*, 9–17. https://doi.org/10.1016/j.icheatmasstransfer.2013.12.002

Yarmand, H., Gharehkhani, S., Kazi, S. N., Sadeghinezhad, E., & Safaei, M. R. (2014). Numerical investigation of heat transfer enhancement in a rectangular heated pipe for turbulent nanofluid. *Scientific World Journal*, *2014*. https://doi.org/10.1155/2014/369593

Yazid, M. N. A. W. M., Sidik, N. A. C., & Yahya, W. J. (2017). Heat and mass transfer characteristics of carbon nanotube nanofluids: A review. *Renewable and Sustainable Energy Reviews*, *80*, 914–941. https://doi.org/10.1016/j.rser.2017.05.192

Yiamsawasd, T., S. Dalkilic, A., & Wongwises, S. (2012). Measurement of Specific Heat of Nanofluids. *Current Nanoscience*, *8*(6), 939–944. https://doi.org/10.2174/157341312803989132

Yin, J., Yang, G., & Lib, Y. (2012). The effects of wavy plate phase shift on flow and heat transfer characteristics in corrugated channel. *Energy Procedia*, *14*, 1566–1573. https://doi.org/10.1016/j.egypro.2011.12.1134

Yu, W., & Choi, S. U. S. (2003). The role of interfacial layers in the enhanced thermal conductivity of nanofluids: A renovated Maxwell model. *Journal of Nanoparticle Research*, *5*(1–2), 167–171. https://doi.org/10.1023/A:1024438603801

Zhang, H., Li, S., Cheng, J., Zheng, Z., Li, X., & Li, F. (2018). Numerical study on the pulsating effect on heat transfer performance of pseudo-plastic fluid flow in a manifold microchannel heat sink. *Applied Thermal Engineering*, *129*, 1092–1105. https://doi.org/10.1016/j.applthermaleng.2017.10.124

Zhou, J., Wu, Z., Zhang, Z., Liu, W., & Xue, Q. (2000). Tribological behavior and lubricating mechanism of Cu nanoparticles in oil. *Tribology Letters*, *8*(4), 213–218. https://doi.org/10.1023/A:1019151721801

Zhou, S. Q., & Ni, R. (2008). Measurement of the specific heat capacity of water-based Al2 O3 nanofluid. *Applied Physics Letters*, *92*(9). https://doi.org/10.1063/1.2890431

Zontul, H., Hamzah, H., & Sahin, B. (2021). Impact of periodic magnetic source on natural convection and entropy generation of ferrofluids in a baffled cavity. *International Journal of Numerical Methods for Heat and Fluid Flow*. https://doi.org/10.1108/HFF-10-2020-0671

BIOGRAPHY

He received his Bachelor of Science degree from the Faculty of Mechanical Engineering of Mosul University in 2010 and his Master's degree from the same university in 2014. His research interests are fluid mechanics, heat transfer, numerical analysis, nanofluids and entropy generation.